Title
Neuromorphic hardware: the investigation of atomic switch networks as complex physical systems

Author
Sillin, Henry Outhwaite

Publication Date
2014

Peer reviewed|Thesis/dissertation

UNIVERSITY OF CALIFORNIA

Los Angeles

Neuromorphic hardware:

the investigation of atomic switch networks

as complex physical systems

A dissertation submitted in partial satisfaction of the requirements for the degree Doctor of Philosophy in Chemistry

By

Henry Outhwaite Sillin

2015

ABSTRACT OF THE DISSERTATION

Neuromorphic hardware:

the investigation of atomic switch networks

as complex physical systems

by

Henry Outhwaite Sillin

Doctor of Philosophy in Chemistry

University of California, Los Angeles, 2015

Professor James Gimzewski, Chair

The emergent dynamical behaviors of biological neuronal networks and other natural, complex systems point towards new computing paradigms which can overcome limitations of digital computers. This work catalogues the development and characterization of an electronic circuit purpose built to exhibit emergent behaviors intended for use in neuromorphic computation. These circuits, atomic switch networks (ASNs), are fabricated through a self-assembly process that yields a highly interconnected network of silver nanowires with embedded

inorganic synapses known as atomic switches. When stimulated with external bias voltage, ASNs are shown to possess the synaptic and memory properties of individual atomic switches, as well as network-specific behavior consisting of distributed, system wide switching events. These emergent behaviors exhibit striking similarity to those observed in many natural systems, including biological neural networks. Experiment and numerical simulations have provided proof of principle that ASNs are complex systems whose emergent behaviors may be used in implementations of neuromorphic computing paradigms such as reservoir computing. Furthermore, they demonstrate the utility of ASNs as a uniquely scalable physical platform useful for exploring complexity, neuroscience, and engineering.

The Dissertation of Henry Outhwaite Sillin is approved.

Chi On Chui

Xiangfeng Duan

James Gimzewski, Committee Chair

University of California, Los Angeles

2015

Table of Contents

List of Tables

List of Figures

Acknowledgements

To my parents Liz and Will, and my brother Jeff for, well, everything. To Gamma, Gampa, Gram, and Grandad for…also everything, but especially their support of my education. To Dave and Jess, Faye and Breen, Em and Jane, Ryan, Larsson, and Trevor for reminding me of the outside world and how nice it is out of lab.

To my chemistry cohort Jon, Mike, Angela, Ben, Jordan, Tristan, Liz, Ilya, Nanette, Stephan, Blanton, Matt, and honorary member Chun-Mei for getting me through classes and being such super pals.

To James Gimzewski for providing the inspiration, resources, and encouragement to pursue my degree. To Adam Stieg for being an endlessly helpful mentor in all areas of science, writing, career development. To Delroy Baugh for inspiring me to come to LA and work on resistive switches. To the former GimGroup members, Brian, Greg, Cristina, Carlin, Haider, Paul, Paul, Paul, Nik, Jason, and current GimGroup members Shivani, Renato, Eric, Ellie, Kelsey, Dayan, Jung-Reem, and Huanqi for being wonderful, enriching influences on my career, I am so grateful and lucky to have had such terrific colleagues. To Audrius "Odo" Avizienis for being the brave soul to begin work on the ASN and welcoming me onto the project. Also for Honky, the Robot Restaurant, and delicious, delicious sausage.

To Lindy for keeping the machine running, you're the best!

To our research collaborators Masakazu Aono, Dante Chialvo, Robert Kozma, Walter Freeman, and Juan Pablo Carbajal, for your invaluable perspectives on our work and for having conducted so much research that enabled us to find our way.

To the Defense Advanced Research Projects Agency (DARPA) Physical Intelligence project (BAA-09-63), and the WPI International Center for Materials Nanoarchitectonics (MANA) for providing financial support necessary to conduct this research.

Chapter 2 is a version of Sillin, H. O., Sandouk, E. J., Avizienis, A. V., Aono, M., Stieg, A. Z., & Gimzewski, J. K. (2013). Benchtop Fabrication of Memristive Atomic Switch Networks. *Journal of nanoscience and nanotechnology, 14(4)*.2792-2798, and carries the following acknowledgements: This work was partially supported by the Ministry of Education, Culture, Sports, Science, and Technology (MEXT) World Premier International (WPI) Research Center for Materials Nanoarchitectonics (MANA), HRL Laboratories, and the Defense Advanced Research Projects Agency (DARPA) - Physical Intelligence Program (BAA-09-63), US Department of Defense. The authors acknowledge use of The Nanoelectronics Research Facility (NRF) and Nano and Pico Characterization Laboratory (NPC) at the University of California, Los Angeles.

Chapter 3 is a version of Avizienis, A. V., Martin-Olmos, C., Sillin, H. O., Aono, M., Gimzewski, J. K., & Stieg, A. Z. (2013). Morphological Transitions from Dendrites to Nanowires in the Electroless Deposition of Silver. *Crystal Growth & Design*, *13*(2), 465-469. and carries the following acknowledgements: The authors acknowledge Hsien Hang Shieh and Makoto Sakurai for their helpful assistance as well as the use of the Molecular Instrumentation Center in the Department of Chemistry and Biochemistry at the University of California, Los Angeles. This research was partially supported by the Defense Advanced Research Projects Agency (DARPA) Physical Intelligence project (BAA-09-63) and by the WPI International Center for Materials Nanoarchitectonics (MANA).

Chapter 4 is a version of Stieg, A. Z., Avizienis, A. V., Sillin, H.O., Martin-Olmos, C., Aono, M., Gimzewski, J. K. (2013) Self-Organized Atomic Switch Networks. *Japanese Journal of Applied Physics. 53(1)*. and carries the following acknowledgements: This work was supported by the Defense Advanced Research Projects Agency (DARPA)—Physical Intelligence Program (BAA-09-63), US Department of Defense and the Ministry of Education, Culture, Sports, Science and Technology (MEXT) World Premier International (WPI) Research Center for Materials Nanoarchitectonics (MANA).

Chapter 5 is a version of Sillin, H. O., Avizienis, A. V., Martin-Olmos, C., Shieh, H. H., Aono, M., Stieg, A. Z., & Gimzewski, J. K. (2012). Neuromorphic atomic switch networks. *PloS one*, *7*(8), e42772. and carries the following acknowledgements: The authors acknowledge Dr. Igor Ovchinnikov for his helpful comments.

Chapter 6 is a version of Stieg, A. Z., Avizienis, A. V., Sillin, H. O., Martin-Olmos, C., Aono, M., & Gimzewski, J. K. (2012). Emergent Criticality in Complex Turing B-Type Atomic Switch Networks. *Advanced Materials*, *24*(2), 286-293. and carries the following acknowledgements: A.Z.S. and A.V.A. contributed equally to this work. The authors gratefully acknowledge Dante Chialvo, Kang Wang, Bob Schwartz, Igor Ovchinnikov and Brian Shieh for their input and assistance. This work was partially supported by the Ministry of Education, Culture, Sports, Science, and Technology (MEXT) World Premier International (WPI) Research Center for Materials Nanoarchitectonics (MANA) and the Defense Advanced Research Projects Agency (DARPA) - Physical Intelligence Program (BAA-09-63), US Department of Defense.

Chapter 7 is a version of Sillin, H. O., Aguilera, R., Shieh, H. H., Avizienis, A. V., Aono, M., Stieg, A. Z., & Gimzewski, J. K. (2013). A theoretical and experimental study of neuromorphic atomic switch networks for reservoir computing. *Nanotechnology*,*24*(38), 384004. and carries the following acknowledgements: The authors gratefully acknowledge Cristina Martin-Olmos, Walter Freeman, Robert Kozma and Narayan Srinivasa for their helpful assistance. Physical ASN chips were fabricated in the Integrated Systems Nanofabrication Cleanroom (ISNC) at the California Nanosystems Institute (CNSI) and simulations utilized resources at the Nano & Pico Characterization Lab (NPC) of CNSI. This work was partially supported by the Japanese Ministry of Education, Culture, Sports, Science, and Technology (MEXT) World Premier International (WPI) Research Center for Materials Nanoarchitectonics (MANA), HRL Laboratories, and the Defense Advanced Research Projects Agency (DARPA)— Physical Intelligence Program (BAA-09-63), US Department of Defense.

Chapter 8 is a version of Sillin, H. O., Aguilera, R. A., Stieg, A. Z., Gimzewski, J. K. (2015) Programmable short- and long-term memory in atomic switch networks using a reinforcement learning scheme. *IEEE Transactions on Nanotechnology*. In Press.

Vita

2005-2009	B.S. (Chemistry), *Cum Laude* The Colorado College, Colorado Springs, CO
2008	Research Experience for Undergraduates Fellowship The University of Colorado, Boulder, CO
2009-2011	M.S. (Chemistry) University of California, Los Angeles, CA
2010-2014	Research Assistant Department of Chemistry and Biochemistry University of California, Los Angeles

Publications

[1] Sillin, H. O., Avizienis, A. V., Martin-Olmos, C., Shieh, H. H., Aono, M., Stieg, A. Z., & Gimzewski, J. K. (2012). Neuromorphic atomic switch networks. *PloS one*, *7*(8), e42772.

[2] Sillin, H. O., Aguilera, R., Shieh, H. H., Avizienis, A. V., Aono, M., Stieg, A. Z., & Gimzewski, J. K. (2013). A theoretical and experimental study of neuromorphic atomic switch networks for reservoir computing. *Nanotechnology*,*24*(38), 384004.

[3] Sillin, H. O., Sandouk, E. J., Avizienis, A. V., Aono, M., Stieg, A. Z., & Gimzewski, J. K. (2013). Benchtop Fabrication of Memristive Atomic Switch Networks. *Journal of nanoscience and nanotechnology*, *14(4).*2792-2798

[4] Stieg, A. Z., Avizienis, A. V., Sillin, H. O., Martin-Olmos, C., Aono, M., & Gimzewski, J. K. (2012). Emergent Criticality in Complex Turing B-Type Atomic Switch Networks. *Advanced Materials*, *24*(2), 286-293.

[5] Avizienis, A. V., Martin-Olmos, C., Sillin, H. O., Aono, M., Gimzewski, J. K., & Stieg, A. Z. (2013). Morphological Transitions from Dendrites to Nanowires in the Electroless Deposition of Silver. *Crystal Growth & Design*, *13*(2), 465-469.

[6] Stieg, A. Z., Avizienis, A. V., Sillin, H.O., Martin-Olmos, C., Aono, M., Gimzewski, J. K. (2013) Self-Organized Atomic Switch Networks. *Japanese Journal of Applied Physics. 53(1).*

[7] Sillin, H. O., Aguilera, R. A., Stieg, A. Z., Gimzewski, J. K. (2015) Programmable short- and long-term memory in atomic switch networks using a reinforcement learning scheme. *IEEE Transactions on Nanotechnology.* In Press

Chapter 1. Introduction.

It is a beautiful and powerful fact that so many diverse phenomena in the universe emerge out of simple interactions between atoms. Fundamentally new behaviors emerging out of a system of interacting components is a counterpoint to the notion that some set of laws that underlie the universe can predict or explain everything else [1, 2]. The work described herein resulted from the desire to replicate this process of emergence in an electronic circuit designed to elicit such behaviors. But what constitutes emergence? What features of a physical system permit such behavior? And how could such an electronic circuit contribute to human knowledge? This introduction attempts to answer these questions and provide context for more detailed discussions of the system itself in later chapters.

To better understand the phenomenon of emergence, an instructive example of a physical system which displays emergent behaviors is a container of air at uniform temperature and pressure. At standard temperature and pressure, the gaseous particles in air can be reasonably approximated as a collection of hard spheres which repel each other when brought very close together, but exert negligible forces on each other once any separation exists between two particles. At the nanometer scale, this container of air would appear as particles moving and colliding at random, but as system size is increased, these two interactions lead to progressively more extraordinary effects. To begin, the distribution of speeds at which the particles move can be described by a single measurable quantity called temperature. The rate at which collisions occur directly results in another measurable quantity called pressure. These quantities are simple emergent properties – they exist when large numbers of particles are considered, but are meaningless or even nonexistent in the context of few particles. Now, consider gentle heating applied to the bottom of the container. Gradients are induced in the simple emergent behaviors of temperature and pressure, resulting in non-trivial patterns of turbulent flow comprised of warm regions rising, and cool, dense regions falling under the influence of gravity. Under the right conditions, turbulent flow can spontaneously organize into discrete convection cells, which can pack together to form periodic patterns

such as hexagonal honeycomb arrays [3, 4]. Easily identifiable, measurable behaviors emerge out of the system's dynamics - behaviors which simply do not exist in small system sizes. Taken to global scales, the interactions of gaseous particles result in an enormous range of emergent weather patterns: cold fronts, hurricanes, tornadoes, and dozens of cloud formations. Many examples throughout nature can be found interacting systems in which emergent behaviors become essential aspects of the system, where larger system sizes result in progressively larger hierarchies of emergent behaviors [5, 6].

Complex, emergent behaviors arise in a wide range natural systems such as weather, social networks, and animal metabolisms, but the essential qualities of such systems are non-equilibrium dynamics and complex architecture [6, 7]. Non-equilibrium dynamics means simply that when supplied with an external energy source, the system is able to evolve in time. The descriptor 'complex' requires a more detailed explanation, and it will take on a couple different definitions in this work – one to describe system architecture, and the other which is used to describe system dynamics. Structurally, a complex system is comprised of many individual units that are often structurally and functionally identical, and readily interact with each other in a non-trivial manner [6]. A notable quality of complex systems is that its operational characteristics are consistent even if individual units are removed. This is not always the case in systems which many interacting parts such as a Swiss watch. This is an admittedly complicated system, but the interaction of its parts are fixed – imposed by the physical design, where removal of any one part will compromise or catastrophically ruin the system's behavior. Returning to the example of a container of air, it is dynamical in that gas particles are continually moving, it is non-equilibrium when gentle heating is applied asymmetrically, and it is complex in that it is comprised of many functionally identical gas particles that freely interact, and removing particles will not change the nature of emergent behaviors [8].

While some emergent behaviors can be predicted easily from first principles, while others are far more difficult to characterize rigorously. A conceptually essential description of what qualifies as emergent behavior is based on the minimum effort required to completely describe the behavior. Simple

emergence such as temperature and pressure may be fully described by reducing the system to state equations such as the ideal gas law or Maxwell's relations. Minute details of system state are not required for accurate predictions and calculations. By contrast, complex emergence, or complexity (here 'complex' takes on its second meaning) is by definition most efficiently reproduced and predicted by simulating the system. In other words, the simplest descriptor of the system is the system itself [9-11]. This presents a significant challenge for those wishing to study or utilize complex emergent behaviors from complex, non-equilibrium dynamical systems. Despite any state equations which may prove useful, thorough analysis is not possible without simulations or direct observation of the physical system.

While complexity generally refers to the generation of complex emergent patterns, complexity observed at second order phase transitions draws particular attention because of the prevalence of critical dynamics, or criticality. What makes criticality unique is that it cannot be described as existing in either an ordered or disordered regime, but rather poised somewhere in the middle [5, 12-15]. A common example of a critical dynamics at a phase transition is that of a ferromagnetic material becoming paramagnetic at the Curie temperature. Below the Curie temperature, individual magnetic domains are strongly coupled with neighboring cells, such that macroscopic portions of the material are aligned, and reconfigurations are infrequent. Above the Curie temperature, thermal energy causes magnetc domains to rapidly change orientation with little or no coupling with neighboring domains. At the critical point, however, ordered magnetic domains of all sizes exist in concert with stochastic reconfigurations. The combination of ordered coupling between adjacent units and dynamical rearrangements reaches an optimum combination such that the correlation length reaches a maximum. At the critical point, the action of a single unit of may influence the entire system, part of it, or none of it, meaning that the system has a maximum possible dynamic range in response to external perturbations [16]. As both criticality contains aspects of both order and disorder, an accurate description of the degree of complexity exhibited by a system is the length of a concise description of a set of the systems regularities [17]. A perfectly ordered crystal lattice requires a very short description, while the aforementioned container of unheated gas is

purely stochastic and therefore contains no regularities. The reason, then, that criticality is particularly interesting is that complex emergent dynamics reach their maximum possible diversity: emergent, ordered patterns exist on all possible size scales extending from ordered clusters of a few individual units to ordered patterns that encompass significant portions of the entire system. Systems exhibiting criticality both fascinate and confound researchers due to their richness and diversity of behaviors that cannot be easily summarized.

In addition to complexity and criticality, a third descriptor often associated with these systems is self-organization. Self-organization describes the tendency of some non-equilibrium, dissipative systems to spontaneously generate order on macroscopic scales as a result of interactions between a multitude of microscopic units [9, 18]. As seen in the example of the asymmetrically heated gas container, the stochastic interactions of gas particles at microscopic scales gives way to macroscopic order in the form of regular arrays of convection cells. An important distinction is that self-organization of a non-equilibrium system is not associated with a gradual tendency towards equilibrium. In other words, ordered states are not achieved because they are the most thermodynamically stable state, rather steady energy input enables the system to maintain order.

At this point the structure and operation of the proposed electronic circuit should be clear: it must be comprised of a collection of functionally identical units whose autonomous, non-trivial interactions result in complex emergent behaviors when an external energy source is applied to the system in such a way as to perturb it from equilibrium, ideally pushing system dynamics towards a critical state. Aside from serving as a microcosm or toy complex system, what could such a device contribute to human knowledge?

The answer should be clearer when we consider in the context of one of, if not the single most complex system known to modern science: the workings of the human brain. The human brain comprises an extraordinarily intricate network of neurons, whose autonomous electrical activity enables an animal to

act and react to environmental stimuli, experience emotions, and even possess consciousness – behaviors which epitomize the very definition of emergence [19, 20]. The essence of brain activity is action potentials – voltage pulses with duration and magnitude on the order of 10^{-3} s and 10^{-1} V, respectively. Neurons intermittently emit action potentials, while simultaneously detecting action potentials emitted by neurons to which they are connected. When an action potential is detected from a neighbor, a neuron may or may not emit an action potential in response – an all or nothing reaction that forms the basis of non-linear interaction between neurons. Action potential transmission is mediated by the connecting interfaces between neurons known as synapses, which are able to adjust the probability that an action potential from one neuron will trigger an action potential in the other, based on past behaviors of action potentials [21, 22] . The end result is that while the physical structure of the neuronal network remains fairly constant, chain reactions of action potentials known as 'avalanches' traverse the neuronal network resulting in complex dynamics [19, 23]. The brain's ability to process information is in no small way due to the abundant evidence that these neuronal avalanches exist in a critical state with complex emergent patterns. At the critical state, the increased correlation length allows distant neurons to communicate most effectively, while the maximal dynamic range inherent of critical systems means that a tiny subset of neurons firing, as when a small sound is heard, can trigger a system-wide event such as a fight or flight response [8, 16].

Information processing occurs when input signals flow through the brain as avalanches of activity, while changes in synaptic transmission result in long-term changes in the patterns of brain activity, forming the basis of memory. The existence of parallel pathways in the neuronal network allows the brain to receive countless simultaneous, multisensory inputs while feedforward and recurrent structures allow it to handle noisy, imperfect input data with ease. Many details of how the brain actually processes information are unknown, but the astounding information processing abilities of the brain are a direct result of emergent behaviors in a complex dynamical system. It is from this observation that researchers have been striving to fabricate physical electronic circuitry which incorporates both complex

structure and intrinsic complex emergent behaviors with the hypothesis that similar information processing capabilities may be realized [24-28].

The value in creating a complex physical system can be further appreciated by understanding how traditional computers operate, and why there are fundamental physical limitations that prohibit them from achieving the information processing capabilities of the brain with similar size and energy efficiency.

Modern computers are overwhelmingly based on the operation of a Universal Turing Machine using von Neumann architecture [29, 30]. Data is input serially into memory banks where it is then shuttled to a central processing unit (CPU). The CPU performs computations on the data as prescribed by software, which has also been input from memory. The processed data is once again sent back to memory, forming an endless cycle occurs in which data is manipulated one bit at a time, billions of times per second. When compared to the brain, operations are nearly flawless in terms of precision and reproducibility - computers excel at manipulating clearly defined data with strict rules of how it must be interpreted, while brains specialize in dealing with noisy, multisensory data.

Although computers are physically comprised of many interacting units (complementary metal-oxide semiconductor transistors), their architecture does not qualify as ‘complex’. Firstly, they lack the fault tolerance of complex architectures – a single faulty transistor can render an entire CPU useless. Secondly, they are assembled in such a way that autonomous interactions between units are strictly eliminated. Interactions can be simulated as when software dictates, but the difference between simulated interactions between units on a digital computer and intrinsic, autonomous interactions in a complex system are profound. This is best illustrated when computers are used to simulate emergent activity in the brain: In 2013, the K supercomputer in Japan simulated 1 second of 1% of typical human brain activity, requiring 82,944 multi-core processors, 1.4 petabytes of RAM (requiring the space of a large warehouse), 9 MW of power, and 40 minutes of processing time [31]. Meanwhile, a human brain possessing actual complex architecture is roughly 1 dm^3 and consumes only 20 W. As previously discussed, the emergent

properties of the brain are the essence of its operation, and as with all complex emergent behaviors, the simplest descriptor is the system itself. Therefore, if a von Neumann computer cannot perform the same tasks as a brain, and simulations are prohibitively inefficient, the only solution is to build an electronic circuit which physically resembles the brain in structure and function.

Even during the surge in traditional digital computing, a great deal of research has been conducted with the goal of creating brain-inspired hardware. The project detailed in this work utilizes recent developments in materials engineering of nano-scale, synaptic electronics – devices commonly known as 'memristors' [32-37]. Considered to be the fourth fundamental circuit element (next to resistors, capacitors, and inductors), memristors are devices which maintain a linear relationship between electronic flux and charge. Applying a sinusoidal bias results in non-linear I-V behavior caused by the memristor reversibly switching between resistive and conductive states. Both the frequency and magnitude of input bias affect the ratio of the two resistance states, with high frequency low magnitude bias resulting in nearly linear, ohmic I-V behavior, and low frequency high magnitude bias yielding the greatest contrast between resistive and conductive states. The physical composition of a memristor consists of a metal-insulator-metal interface, where the insulator is typically on the order of 10^{-9} m thick. Bias applied across the interface results in a physical or chemical change in the insulating layer, forming a conductive pathway between the two metal layers which can be destroyed by reversing the bias. Chemical composition and physical dimensions of this interface can influence device operational properties such as volatility of the different resistance states, number of possible resistance states, and the voltages required for regular operation. The ability for the circuit element to modify conductance based on previous I-V history is strikingly similar to the characteristics of a synapse, creating opportunities for memristors to be incorporated into brain-inspired hardware.

A memristor with particularly suitable characteristics for use as a synthetic synapse is the silver sulfide atomic switch. An MIM interface comprised of $Ag|Ag_2S|X$ (where X is a metal such as Pt, W, or Ag) forms the basis of the switch [38, 39]. When bias is applied across the junction, the ionically and

electrically insulating Ag_2S layer undergoes a phase transition from monoclinic acanthite to body centered cubic argentite. Argentite is electrically semiconducting, resulting in a slight increase in conductance. Additionally, it is ionically conducting, such that Ag^+ cations dissolved in the insulator are able to migrate to the cathode where they are reduced to Ag^0. Eventually, a continuous Ag^0 filament extends across the insulator, significantly decreasing resistance of the interface. If bias is discontinued, the recently formed cation vacancies in the insulator serve as a thermodynamic driving force for the Ag^0 filament to redissolve, returning the interface to the high resistance state [40]. This process enables the interface to serve as a short term memory resistance switch, with a decay time on the order of milliseconds. Continued application of bias across a formed filament causes more cations to reduce, thickening the filament. Thicker filaments are more robust against thermodynamically driven dissolution, resulting in a long term memory characteristic with decay times on the order of hours or days. The high resistance state may be accessed again by reversing polarity of the bias, forcing Ag^0 to reduce once more. Since the atomic switch has intrinsic long and short term memory resistance switching based on applied bias, it is an ideal synaptic electronic element to serve as the basis of brain-inspired hardware systems [41-43].

Typically, atomic switches and memristors in general are fabricated using 'crossbar' architecture, in which a series of parallel metal nanowires are lithographically patterned with an insulator coating, followed by a second series of parallel nanowires that are orthogonal to the first layer, creating an MIM interface at each nanowire crosspoint [36, 44-47]. Electrodes positioned outside the array allow voltage to be applied to each nanowire individually, such that each combination of nanowires has a unique memristor junction which controls the resistance between the two nanowires. This architecture offers precise control over memristors, and a high density of units with promising applications to logic and memory storage. But from a brain-inspired computing standpoint, the architecture does not provide a complex structure or allow intrinsic system interactions to form complex emergent behaviors. Furthermore, crossbar architecture is subject to scaling limitations – a principle known as Rent's Rule

stipulates a power law relationship between the number of functional elements on a chip and the number of input and output wires [48, 49]. Biological neuronal networks obey this relationship and optimize structure through modular, self similar design while the implications for von Neumann architecture are prohibitively expensive wiring costs [50].

Fortunately, because complex systems have inherent fault tolerance, memristor networks serving as complex systems can be fabricated used less precise methods. Self-assembly offers a divergent approach to the fabrication of complex device architecture through the use of thermodynamically driven chemical processes. In particular, the galvanic displacement reaction:

$$2Ag_{(aq)}^{-} + Cu_{(s)}^{0} \rightarrow 2Ag_{(s)}^{0} + Cu_{(aq)}^{2+}$$

is known to create a wide variety micro- and nano-scale silver morphologies [51, 52]. The work detailed in this thesis is based on the idea that this reaction can be used to create a brain-inspired electronic device with a simple 3 step process. First, copper particles on an insulating substrate are used as nucleation sites for the galvanic displacement reaction. Second, aqueous silver nitrate is deposited on the substrate, allowing the reaction to proceed, producing a densely interconnected network of micro- and nano- scale silver structures. In the last fabrication step, the network is rinsed, dried, and exposed to gaseous sulfur [53]. This coats the silver structures with sulfur, reacting to form silver sulfide, such that locations where silver structures intersect or overlap create $Ag|Ag_2S|Ag$ interfaces at a density of up to 10^8 cm^{-2}, forming the basis of atomic switches embedded in an interconnected network. In theory, the end result is a structure referred as an Atomic Switch Network (ASN), an electrical device which bears resemblance to the complex network architecture found in the brain, and is capable of producing complex emergent behaviors.

Characterizations of ASNs revealed that the self-assembly fabrication process was successful, yielding fully functional atomic switches which display both long- and short-term memory properties. Furthermore, under steady DC bias and square wave pulse bias, fluctuations in current and resistance are

observed caused by spatially distributed avalanches of switching events in subsets of atomic switches. These fluctuations have not been reported as occurring in single switches, and confirm that the network architecture allows for complex emergent behaviors. These findings are shown to be relevant in the implementation of brain-inspired computing paradigms.

The chapters that follow catalogue the findings of this project, each one a self-contained article with introductions and conclusions to frame the different experimental results. Chapter 2 outlines the experimental procedure in the most simple and straightforward device architecture, produced using simple benchtop chemistry, and focusing on individual atomic switch and memristor behaviors manifested in the network architecture. Chapter 3 details the silver network fabrication step: the physical dimensions of copper nucleation sites affect the resulting silver morphology, adding a control parameter to the self-assembly process. Large (> 10 μm) copper seeds result in self-similar fractal structures, while small (<10 μm) seeds result in nanowires. Chapter 4 is a survey of different ASN behaviors observed in fractal device architectures, while chapter 5 surveys ASN behaviors in nanowire network architectures. Chapter 6 explores the evidence that the emergent resistance fluctuations in the device occur in a critical state, and what implications that has in the device towards brain-inspired computing paradigms. Chapter 7 further explores the ASN in the context of brain-inspired computing, using a simulated network as a model to check hypotheses made about how individual atomic switches behave in the network setting – measurements that cannot be made in a physical ASNs. Chapter 8 explores interactive control over the network's resistance state, and the potential uses this has in the framework of brain-inspired hardware applications. Finally, chapter 9 provides outlook on the future directions the project can take.

2. Benchtop fabrication of atomic switch networks

Abstract

Recent advances in nanoscale science and technology provide possibilities to directly self-assemble and integrate functional circuit elements within the wiring scheme of devices with potentially unique architectures. Electroionic resistive switching circuits comprising highly interconnected fractal electrodes and metal-insulator-metal interfaces, known as atomic switch networks, have been fabricated using simple benchtop techniques including solution-phase electroless deposition. These devices are shown to activate through a bias-induced forming step that produces the frequency dependent, nonlinear hysteretic switching expected for gapless-type atomic switches and memristors. By eliminating the need for complex lithographic methods, such an approach toward device fabrication provides a more accessible platform for the study of ionic resistive switches and memristive systems.

2.1 Introduction

As ongoing trends in device technology continue on a path toward operation at increasingly reduced spatiotemporal and energetic scales, the perpetual demand for increased density in solid-state electronics and integrated circuits requires new approaches in device fabrication. Modern approaches to advanced computation commonly involve solid-state very-large-scale integration (VLSI) circuits which increase the density of functional elements at reduced dimensionality through a merger of complementary metal–oxide–semiconductor (CMOS) technologies with nanoscale architectures known as CMOS-Molecular (CMOL) [54]. As a result, the fabrication of nanoelectronic devices has typically been consigned to advanced techniques and sophisticated equipment.

Realization of the nanoscale memristor [34, 36], an exciting class of two-terminal circuit elements whose behavior can be defined as a relationship between charge and flux [33, 34, 55], has shown great promise in circumventing the challenges of CMOS-based electronics. The memristor is in theory as fundamental to electronic circuit design as are the resistor, capacitor, and inductor [56]. Functional memristive devices show both volatile and non-volatile memory capacity, while current fabrication methods allow for nanoscale memristive elements to be integrated in ultra-high dense topographies [44, 47, 57]. In practice, nanoscale memristive devices generally exist as a metal-insulator-metal (MIM) junction consisting of two conductive electrodes separated by an insulating gap of width *D*. Application of an external bias voltage alters the conductance of the insulator by various mechanisms including but not limited to charge carrier migration, phase changes and magnetic domain rearrangements [36, 37, 39, 58-60]. In the case of a charge carrier based device, devices operate in an ionic drift model whose state equation modifies the constant parameter of resistance, *R*, in Ohm's law $V(t) = R\,I(t)$, with the charge (q) dependent memristance, $M(q)$

$$M(q) = \left[\frac{\mu_v R_{ON}{}^2}{D^2} q(t) + R_{OFF}\left(1 - \frac{\mu_v R_{ON}}{D^2} q(t)\right)\right] \qquad (1)$$

where μ_v is the charge carrier mobility, R_{ON} and R_{OFF} are the resistance states for the maximal and minimally doped states, respectively, and *D* is the gap width [36]. Through variation of the gap width, memristive systems act similarly to leaky transistors that can be controllably set to different resistance states in a continuum between high and low resistance states (R_{OFF} and R_{ON}, respectively) as a function of applied voltage.

Atomic switches are a class of nanoscale electroionic circuit elements that exhibit memristive switching under applied AC bias [39, 41, 43]. In the specific case of a silver sulfide atomic switch, the MIM junction is composed of conductors (Pt, W, or Ag) and an insulator

(Ag_2S). The resistance switching arises from two distinct mechanisms – a phase transition of Ag_2S, and the creation and dissolution of a Ag filament. Silver sulfide and has two distinct phases – insulating α-phase acanthite (2.5×10^{-3} Ωcm^{-1}) at room temperature and conductive β-phase argentite (1.6×10^{3} Ωcm^{-1}) above 178° C. External bias voltage causes the α-Ag_2S insulator to transition into the electronically and ionically conducting high temperature β-phase [53]. Silver cations are more mobile in the β-phase, so this phase transition facilitates a migration of Ag^+ ions towards the cathode where they are reduced, forming a highly conductive Ag filament [40, 61, 62]. When negative bias is applied, the Ag filament oxidizes, β-Ag_2S reverts to α-Ag_2S and Ag^+ ions re-dissolve into the insulator. Thus the conducting channel is broken and the junction returns to the high resistance state. Under repeated bipolar voltage, the filaments continually reform and re-dissolve, resulting in repeatable resistive switching.

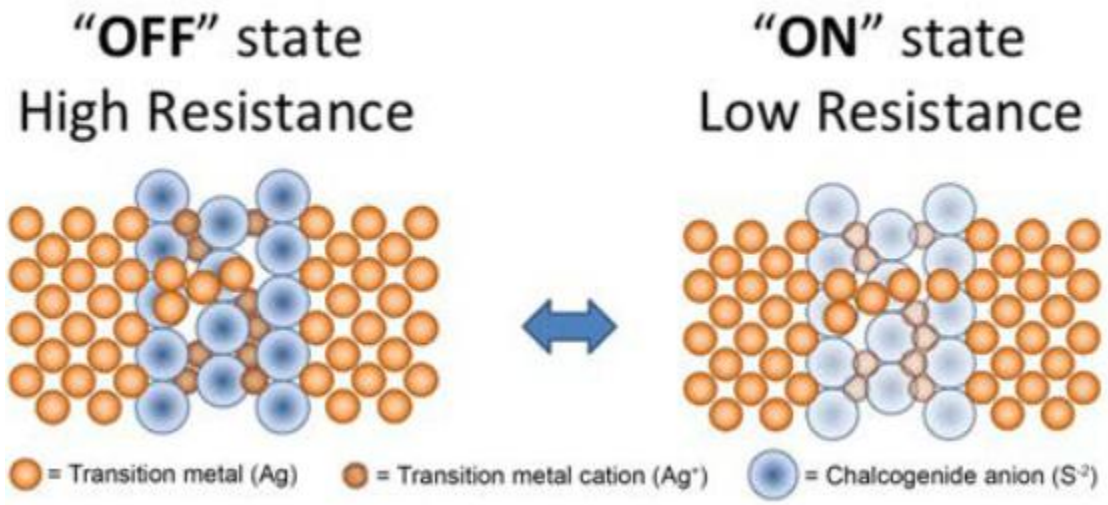

Figure 2-1. Operational schematic of a Ag|Ag_2S|Ag atomic switch. Changes in device resistance result from the formation of a conductive Ag filament across the insulator. In the OFF state the Ag channel is incomplete as it is separated by the insulating Ag_2S layer. Applied voltage stimulates the migration of Ag^+ cations to the end of the filament, extending it and completing the channel, which characterizes the ON state.

Due to their small size, low power consumption, and nonlinear characteristics memristive circuit elements are rapidly emerging as a complementary technology to CMOS-based

computation and memory storage. The development of commercial devices based on memristive elements, however, remains limited due to the factor of $1/D^2$ in eqn. (1) which causes the nonlinear memristive behavior to be dramatically stronger at small values of D. Devices which display nonlinear resistance at the voltage, current, and time scales of conventional CMOS transistors typically require an insulator gap size at the nanometer scale. As a result, precision nanofabrication techniques [36, 47], scanning probe microscopes [39], pulsed laser [63] and atomic layer deposition [64] are employed to achieve such gap widths.

In contrast to complex lithographic methods, solution-phase approaches have been shown to produce functional memristive devices using spin-coated solgel films alongside anodic electrochemical deposition [65-72]. Electrochemistry in particular offers a divergent approach for the fabrication of metallic structures. Specifically, electroless deposition of various metals through the spontaneous reduction of soluble metal cations is a mature technology that has been employed extensively in macroscopic plating applications and the manufacture of printed circuit boards. Under diffusion-limited conditions [73], the reaction has been shown to generate a diversity of self-assembled structures including nanowires, dendrites, and fractals at the micro- and nanometer scales [52, 74-76]. Such assemblies present an opportunity to readily achieve MIM interfaces with sufficiently small gap sizes to enable memristive operation.

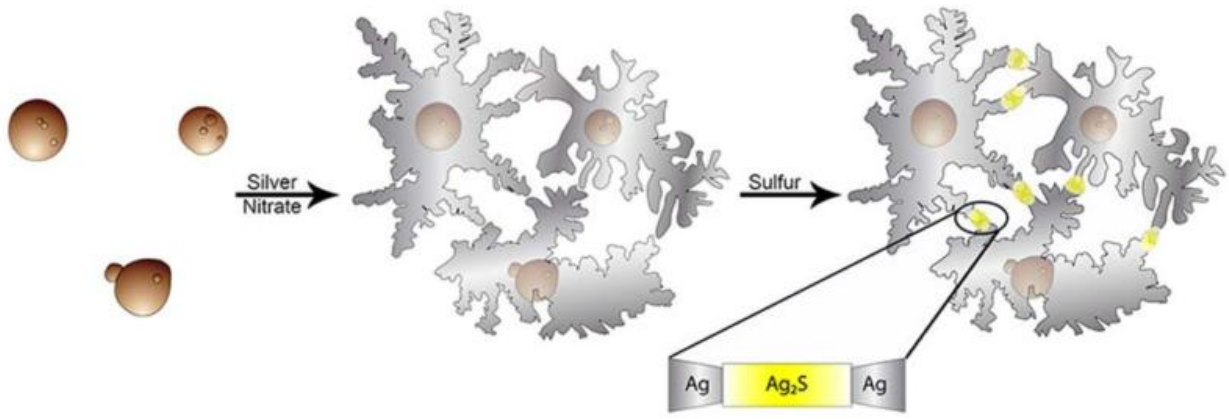

Figure 2-2. Schematic for fabrication of fractal ASN by electroless deposition. Copper microsphere seeds serve as nucleation sites for the spontaneous reduction of soluble silver ions and formation of dendritic silver structures which are subsequently converted to Ag_2S through gas phase sulfurization. The Ag_2S layer creates the MIM interfaces required for resistive switching.

Here we present the fabrication of functional memristive devices based on a self-assembled network of highly-interconnected Ag|Ag_2S|Ag atomic switches using entirely inexpensive materials and techniques following the scheme shown in Figure 2-2. These atomic switch networks (ASN) rely on the electroless deposition of silver from copper seeds to form an intricate fractal wiring architecture suitable for creating a network of nanoscale MIM junctions. Applied bias converts these junctions into atomic switches and the entire network demonstrates the frequency-dependent, nonlinear hysteretic switching requisite for applications in data storage and computation. Our approach drastically reduces the need for precision fabrication or placement of the switching junctions as compared to typical lithographic methods. This demonstrates the utility of alternative fabrication techniques, and provides a unique approach toward the production of functional memristive devices. The process described here has further implications for the fabrication of large memristive devices and networks, opens future development to a wider field of investigation, and facilitates the study of memristive devices in educational environments.

2.2 Experimental methods

Atomic switch network devices were fabricated using inexpensive and commonly available materials, and followed by self assembly processes to create an interconnected network of nanoscale MIM junctions. Two silver coated copper wires were fixed to a glass microscope slide with kapton tape with a 2-4 mm separation between wires (Figure 2-3a). Next, a solution of copper microspheres (d = 10 μm, 99.995% purity, Alfa-Aesar) was prepared in isopropyl alcohol (5 mg/mL). A small droplet (20 μL) of this solution was transferred via pipette between the wires, allowing the Cu spheres to disperse uniformly across the region (Figure 2-3b). Following solvent evaporation, a droplet of 50 mM aqueous $AgNO_3$ was dropcast onto the Cu treated areas. With the Cu spheres serving as seed sites for the galvanic displacement of Ag^+, the reaction (2):

$$2\,Ag^{+}_{(aq)} + Cu_{(s)} \leftrightarrow 2\,Ag_{(s)} + Cu^{2+}_{(aq)} \qquad \varepsilon_0 = 1.2573V \qquad (2)$$

occurred gradually over 5-8 minutes. The choice of concentration of soluble cations (50 mM) caused reaction (2) to occur under diffusion-limited conditions, producing complex networks of silver fractals [76].

Upon completion, the silver fractal networks were rinsed of any remaining reagents by dilution with a droplet (20 μL) of deionized water (18 MΩ). One half (20 μL) of the diluted solution was removed by pipette, and the process was repeated an additional five times. The solution remaining on the device was carefully removed with an absorbent wipe and then evaporated by placing the device on a hot plate at 70° C for 10 minutes. The entire rinsing process was completed with minimal destruction of the network. As the networks dried, three-dimensional silver fractal structures flattened to a quasi-2D shape in which overlapping structures came into contact with each other, forming an interconnected network [75]. Electrical resistance of the silver fractal network ranged from 40-60 Ω.

To convert interconnections among Ag fractal structures into the MIM junction requisite for atomic switch operation, the networks were functionalized by exposure to sulfur gas. This sulfurization step was conducted by heating a crucible of sulfur (Sigma, 99.98%) to 140° C on a hot plate. The device was mounted onto a wire stand (10 cm) placed on the hot plate to ensure that the device remained close to room temperature during sulfurization. The sample, sulfur and wire stand were then covered with a large beaker for 10 minutes. The confined evaporated sulfur gas then deposited onto the cooler fractal network. The resulting thin film of sulfur reacted with the Ag fractal structures to form an insulating Ag_2S surface layer while leaving the bulk internal structures as metallic Ag, creating an assemblage of $Ag|Ag_2S|Ag$ MIM junctions. Electrical resistance of the across the ASN device was measured periodically to assess the degree of sulfurization. Devices with negligible resistance change from the initial state (40-60 Ω) were re-sulfurized to achieve appropriate values for memristive operation (0.5 - 1.5 MΩ).

Structural characterization was carried out using the optical (Nikon Eclipse TE2000-U) and scanning electron (FEI Nova600 NanoLab) microscopes. Electrical characterization employed current-voltage (*I-V*) spectroscopy using a precision source measure unit (National Instruments 4132) for resistance measurements, while timeseries IV data was collected using an analog voltage input/output module (National Instruments 6368) in conjunction with a current-to-voltage preamplifier (Stanford Research Systems SR570). Resistance measurements were conducted using a 2-electrode configuration with a 100 ms, 200 mV pulse. Timeseries data was collected at 10 kHz. Subsequent data analyses were carried out using MATLAB 2010b (MathWorks) and Origin 8.1 (OriginLab Corporation).

2.3 Results and discussion

In order to maximize both the number and proximity of MIM switching junctions, substrate coverage of dispersed copper microspheres was optimized in order to achieve a dense 2-D silver fractal network. Modelling and simulation of the resultant network topology was carried out using a tesselation method based on Voronoi diagrams in combination with a diffusion-limited model of electroless deposition. By partitioning a plane of *n* points into convex polygons (called Voronoi Cells) such that each polygon contains exactly one nucleation site and every point in a given polygon is closer to its generating point than to any other, the resulting simulations provided direct insight into the design of fractal-based networks with respect to optimal surface coverage of microsphere seeds. As seen in Figure 2-3, metallic silver fractals generated by electroless deposition resulted in self-similar structures with fractal dimensions 1.72.

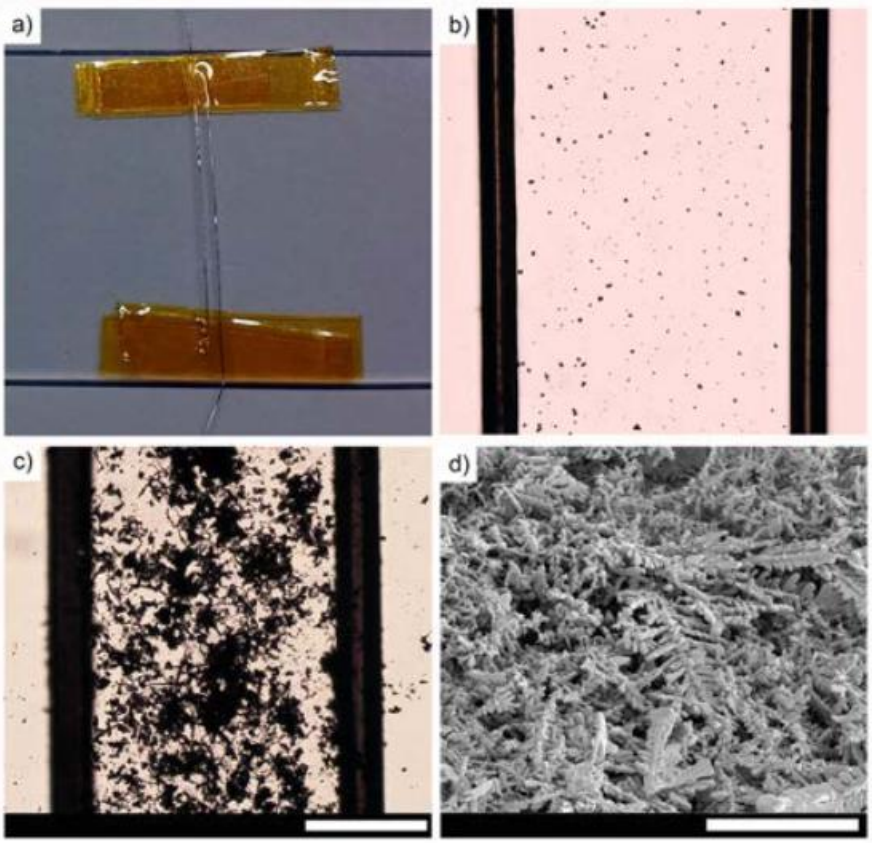

Figure 2-3. Device Fabrication – Illustrative representation of a device. **(a)** Initial state of devices with both wires fastened to the glass slide. The possible sites of contact on the wires are insulated. **(b)** Copper spheres applied to the area between electrodes react with $AgNO_3$, **(c)** resulting in electroless deposition of complex silver nanofilament and fractal networks (scale bar = 1mm). **(d)** SEM image of silver fractals (scale bar = 30 µm).

As-fabricated ASNs are initially collections of interconnected ohmic resistors. In common with many memristive devices, ASNs require an initial forming step to create a high conductivity 'ON' state through application of a sufficiently large bias voltage [73, 77]. Upon application of an appropriate activation bias voltage, subsequent sweeps produced an increased current output caused by the bias-induced phase transition (α/β-Ag_2S), alongside concurrent formation of conductive metal (Ag) filaments. This formed a distributed assembly of weakly memristive junctions in which electronic conduction occurred through the β-Ag_sS across a gap of decreased width due to the forming metallic filaments. Continued application of bias voltage

induced filament growth across the gap, reducing the gap widths and increasing the measured current. The network then comprised resistive junctions with a growing number of completed memristive elements (atomic switches) and increasingly non-linear *I-V* behavior. The formation of a complete percolative path of memristive junctions from one electrode to the other resulted in a sharp increase in network conductivity and defined the completion of this activation process.

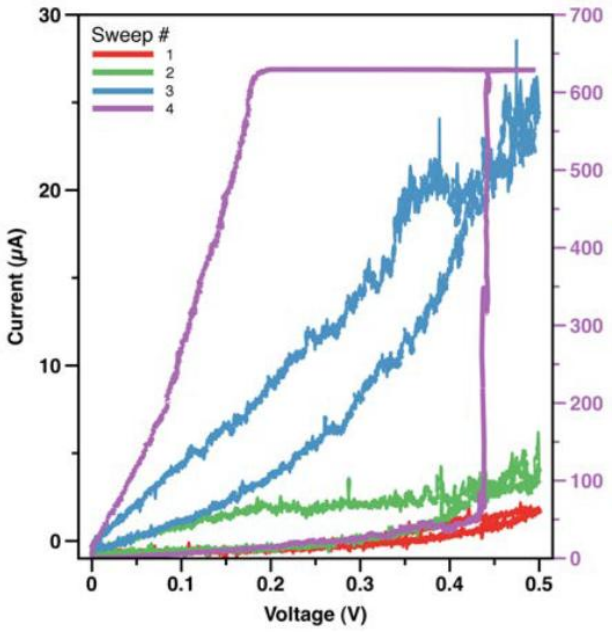

Figure 2-4. ASN device activation by applied bias voltage sweeps. With each successive sweep (0-500 mV, 1 Hz) the resistance appeared to decrease quickly while voltage increased linearly and increase slowly while voltage decreased linearly. Continual increases in conductance (3.86 μS, 10.94 μS, 50.2 μS, 1.248 mS at peak voltage) are typical in initial forming steps for memristive devices as conducting channels through the ASNs lengthen and increase in number.

The entire forming step of an ASN device is shown in Figure 2-4 as a series of consecutive 0-500 mV sweeps, where an initially gradual increase in conductance was followed by an abrupt transition to the activated 'ON' state. Here, successive positive bias voltage sweeps of increasing amplitude were applied to initiate the forming step until measureable current began to flow through the ASN device. The minimum voltage required for activation ranged from 0.3 to 2 V. Following activation, ASN devices were stimulated with symmetric (±300 mV, 1-50 Hz)

triangle wave voltage inputs. As Figure 2-5 shows, ASNs displayed repeatable switching between distinct resistance states, resulting in the pinched hysteresis *I-V* behavior typical of memristive systems. During consecutive sweeps, the threshold voltage for the low resistance state steadily decreased. Observed in individual switches, this behavior is due to a steady decrease in gap width where the theoretical minimum threshold is due to the oxidation and reduction of a single Ag atom which breaks and completes the filament [78]. In the network setting, reduction in threshold voltage is more likely due to a decrease in the ensemble average of gap widths in the ASN.

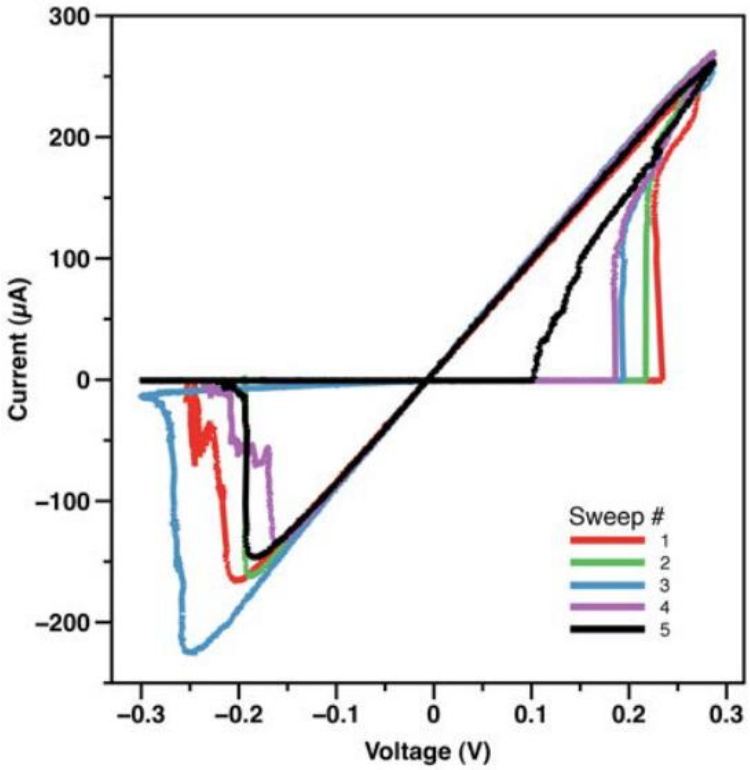

Figure 2-5. Robust hysteretic switching. Five consecutive hysteresis curves show that each sweep is associated with a lower threshold voltage, due to decreasing insulator gap sizes. This data was produced directly after the network activation step. Voltage stimulus was a symmetric triangle wave (10 Hz, 300mV).

A known fundamental property of memristive systems is that stimulation at increased

frequency diminishes the degree of resistance change, resulting in more linear, ohmic *I-V* behavior [36, 56, 79]. As shown in Figure 2-6, this behavior was observed in ASN devices over an input bias frequency range of 1-20 Hz, where conductance decreased from 1.01 mS at 1 Hz to 0.57 mS at 20 Hz. Given constant input bias amplitude, a higher input frequency permits less net flux to pass through the junction during each half-sweep (i.e. 0 to +300 mV to 0). Charge carriers therefore have less time to migrate and are forced to reverse direction more often, causing them to instead fluctuate about their equilibrium point, resulting in larger gap widths and higher resistance. In contrast, slower sweeps allow enough cations to migrate not only to complete a conductive filament but to thicken it, which further increases conductance.

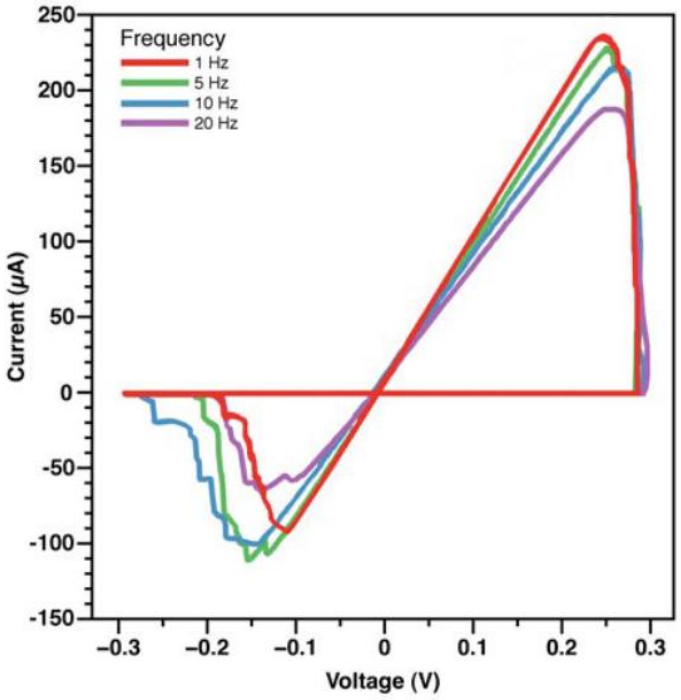

Figure 2-6. Frequency dependent hysteresis. Representative average output of 10 sweeps with a given threshold voltage of 300 ±10 mV at 1 Hz, 5 Hz, 10 Hz and 20 Hz. Greater *I-V* hysteresis is associated with lower frequency sweeps. The amplitude of the current near the threshold value is typically greater for lower frequency sweeps. Conductances in increasing order of frequency were 1.01 mS, 0.94 mS, 0.72 mS and 0.57 mS.

Additional evidence of frequency dependent behavior was observed alongside changes in the R_{ON}/R_{OFF} ratio. Devices would occasionally fail to switch ON during application of AC bias voltage, remaining in the OFF state for the duration of a complete triangle wave voltage sweep. A minimum current output threshold (I_t = 20 µA) was defined such that a complete sweep which failed to produce a current above I_t, and thus displayed no memristive properties, was deemed as lacking a switching event. Sweeps that displayed clear hysteresis and current output above I_t were labeled as having a switching event. The device was then stimulated repeatedly for 60 second trials at 1, 5, 10, 20, or 50 Hz. The frequency for each trial was randomly selected in order to minimize the potential effects that a trial at a particular frequency would have on subsequent trials at different frequencies. As shown in Figure 2-7, the percentage of sweeps containing switching events was seen to decrease with increasing frequency of applied bias. This is qualitatively in agreement with the expected trend of *I-V* nonlinearity versus input frequency.

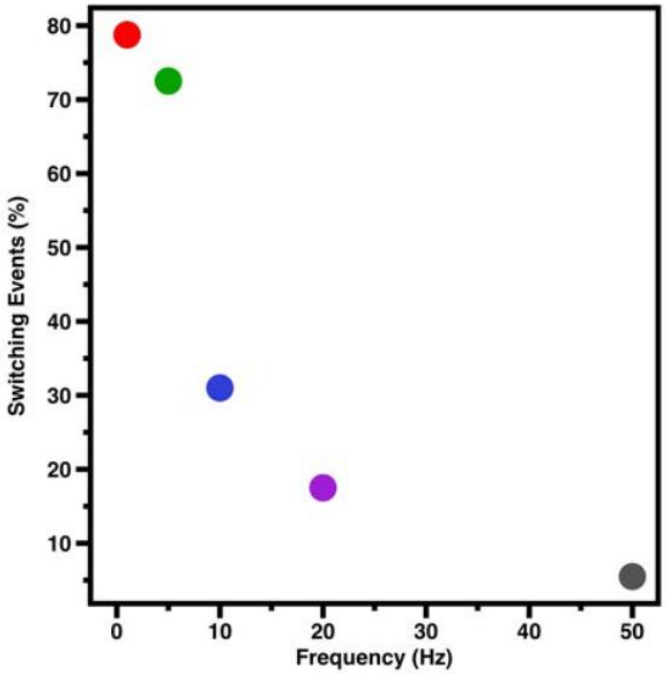

Figure 2-7. Ratio of switching events to total voltage sweeps as a function of frequencies. Networks were stimulated with a symmetric triangle wave bias voltage (300 mV) at 1, 5, 10, 20, and 50 Hz. During a sweep, the device may display a switching event (pinched hysteresis) or it may remain in the high resistance state. The percentage of sweeps which contained a switching event was measured from an aggregate of over 10^3 sweeps.

As compared to isolated atomic switches, ASNs require that gap widths be considered in the context of a network setting where filament creation and annihilation can result in complex interactions of many individual MIM junctions [73, 77]. At relatively low frequencies, repeatable switching between two primary distinguishable states shown in Figures 2-5 and 2-6 was dominated by the rapid transition to and from a low resistance state occurring immediately upon the completion or breakage of a completed percolative pathway across the network.

Based on prior studies of frequency dependence in memristive systems and the results presented in Figures 2-6 and 2-7, we infer that at higher frequencies the amount of flux per cycle becomes progressively insufficient to allow for the completion of Ag filament formation [32, 36, 56, 79]. From these results, we attribute the observed frequency dependent behavior in a network of Ag-Ag_2S atomic switches not only to variations in filament thickness in individual switches, but also whether or not a percolative pathway of completed filaments is able to extend continuously across the entire network.

2.4 Conclusion and outlook

Using accessible materials and benchtop synthetic techniques we have prepared memristive atomic switch networks which display fundamental properties of memristive systems such as frequency-dependent, pinched hysteretic switching. The behavior of these devices is comparable to both theoretical predictions and previously reported properties of ASNs and memristive networks. The method of fabrication demonstrated here veers away from the top-down approach of complex lithographic techniques and instead utilizes a simplified, cost-effective method for the creation and study of memristive devices through bottom-up self-assembly. Memristors will undoubtedly find many uses as memory or logic elements in both

conventional and neuro-inspired computing and new fabrication approaches such as this will aid in realizing their potential.

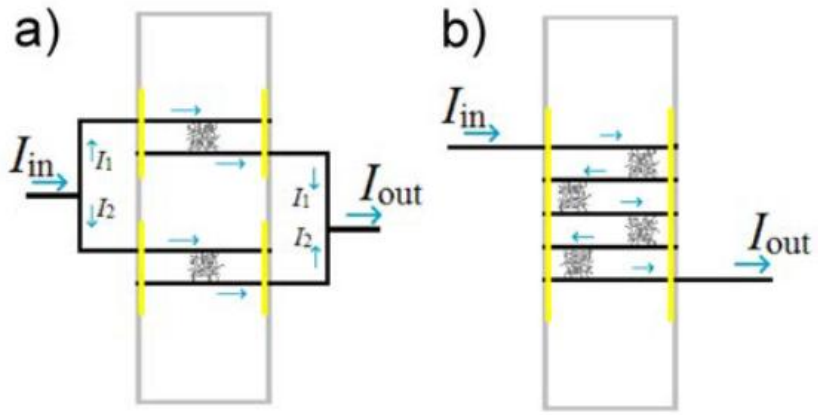

Figure 2-8. Schematic of parallel and series ASNs in benchtop devices. The bottom-up fabrication approach allows for very flexible arrangements of networks. Additional networks may be connected in parallel (a) on an existing device by joining corresponding wires to the input and output nodes. Similarly, additional networks may be connected in series (b) by affixing wires to an existing device in the manner shown.

The simplicity of this benchtop approach to ASN fabrication also provides an accessible platform for further investigations of complex systems and an educational tool to introduce memristive systems. Because this method can produce easily reconfigurable networks, it provides an opportunity to investigate the properties of ASNs in various arrangements without requiring the development of unique designs or complex fabrication protocols. Recently it has been suggested that memristors or ASNs connected in parallel or series be studied [77]. A few proposed configurations for benchtop ASN devices which connect multiple networks in either series or parallel are provided in Figure 2-8. Redistribution of current in parallel configurations could allow for memristive elements with increased current output and power dissipation. Series configurations would produce larger functional networks, which may reveal advantages not seen in single ASNs including tunable threshold voltages and recurrent feedback [73]. This work represents a step forward in facilitation of such explorations by reducing the technical demands

and monetary expense of current research in memristive systems, making it more readily accessible to a broader population of investigators.

3. Morphological transitions from dendrites to nanowires in the electroless deposition of silver

Abstract

A morphological transition from dendrites to nanowires in the electroless deposition of silver by galvanic displacement of copper seeds is investigated as a function of seed size. The transition to dendritic growth is interpreted as arising from local reaction anisotropies interacting with the global solute concentration distribution. Reactions were performed on substrates bearing lithographically patterned grids of copper posts with sizes ranging from 1 to 50 μm. When copper seed size exceeds 10 μm, the deposition reaction consumes silver cations at a sufficient rate to create ripple-like Mullins-Sekerka instabilities in their distribution. The resulting concave growth fronts produce branched, dendritic structures. For copper posts smaller than 3.5 μm, cation consumption is balanced by diffusion and the growth front's advance toward the bulk, leading to networks of nanowires formed as the local reaction anisotropy favors growth by stacking along Ag(111) planes.

3.1 Introduction

Morphological transitions in nonequilibrium growth processes arise from interactions between microscopic interfacial dynamics and macroscopic driving forces [80, 81]. Such transitions occur when variation of a process parameter alters the expression of local anisotropy in the global growth mechanism [82]. Determining which parameters are responsible presents a challenge, as intuition derived from classical thermodynamics may become misleading far from

equilibrium [83]. Reliable selection of morphology requires parameters that control the interplay of temporal and spatial scales, functioning as nonequilibrium analogues to thermodynamic state variables [84]. Experimental investigations can identify these control parameters for specific growth processes and enable their use in directing the morphology of self-assembling structures.

Electroless deposition (ELD), a general term encompassing processes also referred to as galvanic displacement or cementation, involves the reduction of metal ions in solution without the application of an external bias voltage. The technique is primarily used for depositing metal coatings and differs from simple homogeneous redox reactions in that deposition occurs at a specific interface and not in the bulk of the solution [85]. The utility of ELD as a fabrication strategy arises from its capacity to combine surface patterning with chemical self-assembly, gaining the flexibility of solution-phase synthesis while retaining the control of top-down design processes. This work focuses on the ELD of silver from copper seeds in silver nitrate solution, according to the reaction: $Cu^{0}_{(s)} + 2Ag^{+}_{(aq)} \rightarrow 2Ag^{0}_{(s)} + Cu^{2+}_{(aq)}$

Controlled synthesis of silver nanostructures is of particular interest, as bulk silver has the highest electrical and thermal conductivity of all metals [86]. Extensive studies of silver nanostructures have also demonstrated strong antimicrobial characteristics [87] as well as size-/shape-dependent surface plasmonic effects, with particular implications for sensing and optical spectroscopies [75, 88, 89]. The wiring of interconnects has become the most important factor in electronic chip design and performance [90], motivating the development of biologically inspired, self-assembled complex nanowire network architectures [91], and devices [77]. Higher dimensional, dendritic silver nanostructures have additional advantages in surface enhancement for catalysis [86], detection [75], and as electrodes for electrochemical devices such as batteries, which harness the efficiency of branching geometries to optimize transport processes [92].

3.2 Results and discussion

We present a study on the morphology of ELD silver structures where the size of the copper seeds used to grow them under nonequilibrium conditions serves as a control parameter. Lithographically patterned Cu posts with edge lengths ranging from 1 to 50 μm and heights of 200–790 nm were reacted with 50 mM silver nitrate solutions. This concentration was selected to investigate diffusion-limited deposition mechanisms [52, 93]. ELD occurred simultaneously at all Cu-solution interfaces upon immersing the substrate in $AgNO_3$, keeping all reaction parameters (temperature, concentration, reaction time) identical except for the dimensions of the Cu seeds (Figure 3-1).

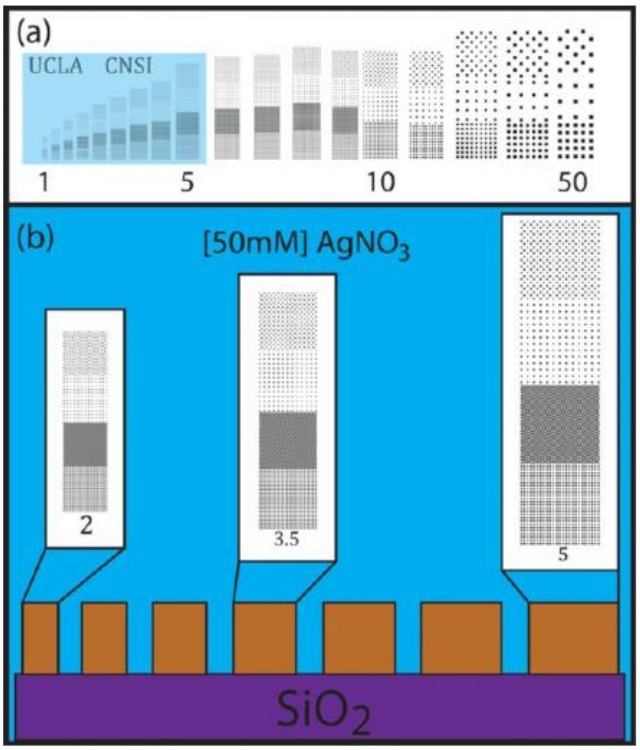

Figure 3-1. Experimental schematic. (a) Representation of the lithographic mask used for patterning Cu seeds of various size and pitch. Two distinct patterns, square and chessboard, are deposited onto SiO2 substrates for each seed size with pitch equal to and double that of the respective seed edge length (1−50 μm). (b) Schematic of a SiO2

substrate with Cu seeds immersed in a 50 mM AgNO3 solution, where individual blocks represent a grid of given size. ELD reactions occur simultaneously under identical reaction conditions (temperature, concentration, time) with the exception of Cu seed size. Post heights ranging from 200 to 790 nm were used.

Deposit morphology was observed to depend on seed size, with edge dimensions on the order of 1 μm producing extended wires (Figure 3-2a), while above 10 μm the deposits have a branched, dendritic structure (Figure 3-2b). This emergent length scale can be used to bridge the gap between top-down and bottom-up fabrication techniques in directing the self-assembly of functional nanostructured devices [73].

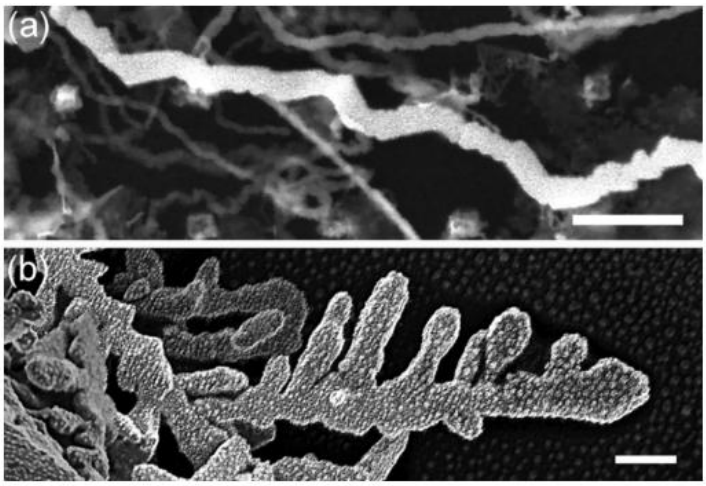

Figure 3-2. Branching of Ag structures increasing with the decreasing strength of anisotropic forces. Preferential orientations for crystal growth lead to the formation of nanowires (a) until the growth front is sufficiently large to interact with the concentration field and produce branched dendrites (b). Scale bars = 1 μm.

Morphological transitions in nonequilibrium growth processes such as diffusion-limited ELD result from changes in the nature of the solid–solution interface at the growth front [94]. The pure diffusion-limited aggregation (DLA) model of Witten and Sander has proven a powerful tool for understanding a range of fractal growth phenomena [51]. In the DLA model,

solid growth occurs as random walkers (in our case, Ag^+ cations) diffuse into contact with the solid and attach (e.g., are reduced to Ag metal), becoming part of the growing aggregate [95]. Good agreement has been seen between DLA model predictions and Ag structures grown using diffusion-limited ELD from Cu at seed sizes larger than a millimeter [52, 96]. However, there is no size scale inherent in the DLA model, which approximates an idealized case of a solution approaching zero density [97], and it is therefore unable to predict a morphological transition based on the size of the aggregate interacting with the solute distribution as a whole.

Size scales can be introduced by turning to mean-field models of diffusion-limited growth [98]. They begin by defining a field controlling the growth process, in our case, the concentration distribution of diffusing Ag^+ cations, which has a maximum value of the bulk concentration and is zero at the solid–solution interface. Growth is most likely to occur at protruding tips, as they extend furthest toward the bulk concentration. However, the interaction between the consumption of ions and the restoring forces resulting from concentration gradients at the interface is known to lead to instabilities in the distribution of ions around the growth front. The formation of such instabilities was analyzed by Mullins and Sekerka, who determined conditions for the propagation of perturbations at growth fronts [99], which have been used to explain the nonequilibrium formation of dendritic patterns [100]. We investigate these conditions experimentally, by simultaneously performing silver ELD reactions identical except for the size of the copper seeds.

Experiments were performed using microscale copper posts lithographically patterned on thermally oxidized (500 nm SiO_2) silicon. Electron beam lithography was used to prepare 1 μm^2Cu seeds, while UV lithography was used to deposit Cu grids with edges dimensions ranging

from 2 to 50 μm and thicknesses of 200–790 nm. Microfluidic wells were fabricated around the Cu to facilitate the ELD reaction with aqueous $AgNO_3$. A thick layer of SU-8 (approximately 500 μm) was deposited by spin coating, then UV exposed and baked at 95 °C before developing in propylene glycol methyl ether acetate and a final hard baking at 130 °C under nitrogen. Silver nitrate (99.98%, Fischer) was dissolved in 18.2 MΩ deionized water to prepare 50 mM solutions. Samples were characterized using optical and scanning electron microscopy.

Small Cu posts (<3.5 μm, Figure 3-4) were observed to exclusively grow nanowires when reacted with 50 mM $AgNO_3$. At larger seed dimensions, branched structures were produced. The transition from wires to dendrites occurred for edge lengths near 10 μm (see typical images shown in Figure 3-4). Extended wires were not observed at edge lengths greater than 15 μm. No morphological dependence on the height of the posts was noted over the range examined.

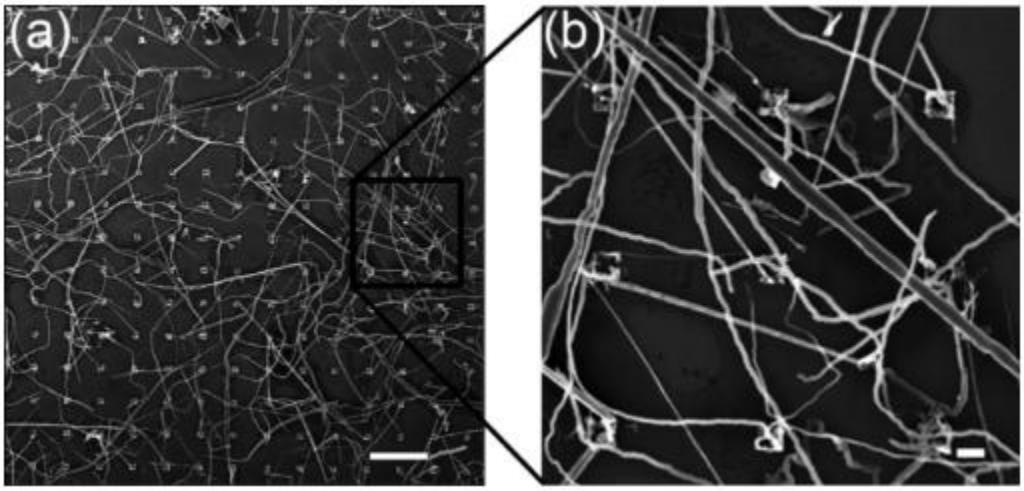

Figure 3-3. SEM images of Ag nanowires formed by ELD from lithographic Cu grids (1 × 1 μm, 300 nm thickness, 5 μm pitch). The interpenetration of simultaneously grown wires highlights the predominance of local forces in the reaction at this seed size. Structures do not branch but may thicken. Scale bars: (a) 10 μm, (b) 1 μm.

In order to investigate the possible influence of the substrate on the morphological transition, we reacted Cu microspheres (99.995%, Alfa-Aesar, average diameters of 1 and 10 μm) in stirred 50 mM $AgNO_3$ solutions. These solution-grown Ag deposits were compared to structures produced from identical Cu seeds initially drop cast onto a supporting substrate. Optical images of each preparation showed no appreciable variation in structural morphology for a given seed size. However, comparison of XRD spectra for the deposits evoked distinctions, as collected using a Panalytical X'Pert Pro X-ray powder diffractometer using Cu Kα radiation (Figure 3-5).

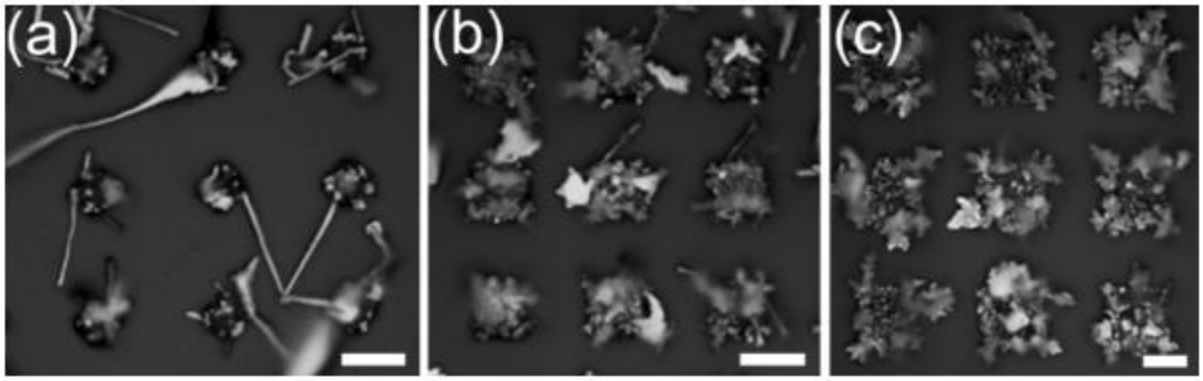

Figure 3-4. Optical micrographs illustrating the transition from wire to dendrite growth as a function of Cu seed size. At 7 μm (a) wires predominate, with branched structures appearing as (b) seed size is increased to 9 μm. (c) Wires were not observed for deposits from 15 μm seeds. Scale bars = 10 μm.

Diffraction peaks near 38° and 44° were assigned to the (111) and (200) planes of fcc silver, respectively, according to standard values (Joint Committee on Powder Diffraction Standards file 04-0783). The shoulders on the (111) peaks are attributed to an Ag–Cu solid solution. Ag and Cu do not typically form alloys, despite both metals having fcc structures with a size mismatch satisfying the Hume–Rothery criterion for the formation of solid solutions (<15%), but they have been observed in nonequilibrium deposition processes such as sputtering

[101]. While the ELD mechanism is driven by simultaneous reduction and oxidation half-reactions at the metal–solution interfaces, the potential is transferred from the dissolving Cu seed to the Ag plating growth front through the metal–metal interface inside the deposit. The resultant local electric field is of sufficient strength to form an Ag–Cu solid solution at this interface.

The influence of size and substrate was taken from the XRD spectra by comparing the ratios of (111) and (200) peak intensities. This ratio gives a metric for the relative strength of anisotropic forces in the crystal growth process, where higher ratios are correlated to the preferential stacking of (111) planes associated with wire growth [102]. In aqueous solution, the (111) and (100) facets of fcc Ag are the most stable, with water molecules interacting more strongly with the (100) surface, making (111) the preferred growth orientation [103]. The observed trend in Figure 3-5 indicates that both smaller size and restricted volume (surface-based) growth serve to increase the anisotropy, with (111):(200) ratios increasing above the 10:4 standard for fcc silver crystals. This indicates that slower [Ag^+] depletion rates are associated with increased expression of oriented growth.

Given these observations, we find the transition between growth modes to be a feature of the nonequilibrium nature of the ELD process. Recent investigation into the effect of the size of Cu microspheres in a similar Cu/Ag^+ ELD reaction attributed the observed morphological transitions from plates to belts and branched structures to changes in the electrochemical potential as a function of the concentration of reactants, calculated using the Nernst equation [104]. However, the Nernst equation is derived to estimate the reactivity of an electrode–solution interface at equilibrium and is not applicable to the ELD process that occurs far from it. We propose that the formation of dendrites does not occur due to the reaction potential increasing

with seed size, but rather because of Mullins-Sekerka (MS) instabilities appearing when the rate of depletion of reactants in the vicinity of the growth front critically outpaces restoring forces. Past this critical point, the growth mode changes because of nonequilibrium patterns in the solute concentration distribution caused by MS instabilities.

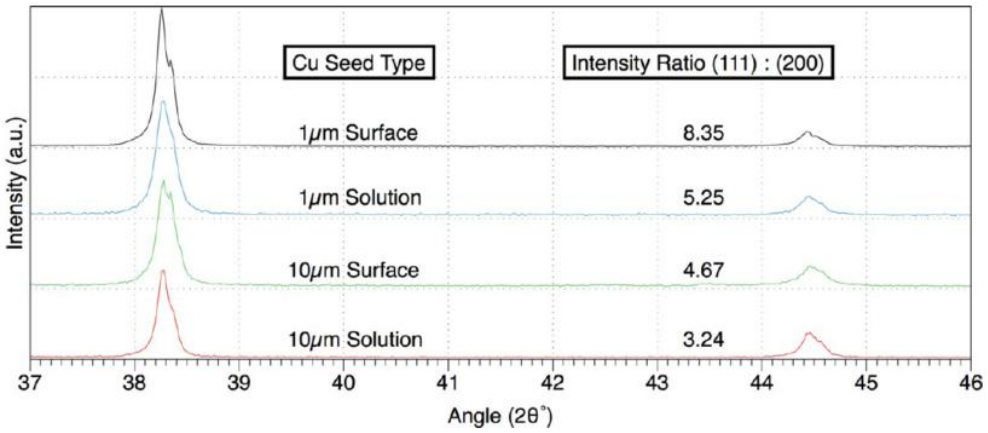

Figure 3-5. Comparing X-ray diffractograms of Ag structures grown from 1 and 10 μm Cu microspheres in solution and on a glass surface shows that both seed size and surface proximity influence the preference for the (111) orientation associated with crystal growth anisotropy.

At a growing solid–liquid interface, the presence of a perturbation in the concentration field that is not stabilized by damping influences will propagate to form ripples in the distribution of solution-phase components. This tendency for an initially infinitesimal perturbation in a concentration distribution to increase and spread is the essence of the MS instability analysis. Above the emergent size scale (~10 μm Cu seeds for the reaction conditions used in this experiment), the consumption of Ag^+ at the growth front is sufficiently rapid to form MS instabilities, which create variations in the concentration distribution (Figure 3-6). Local regions of high [Ag^+] reach sufficient chemical potential to nucleate branches, which can in turn form new MS instabilities. As the principal growth front advances at a constant velocity *v*, the

instability-related branches grow at a rate proportional to $v^{1/2}$, creating a dendritic structure with a preferred axis of orientation through otherwise self-similar branches [96].

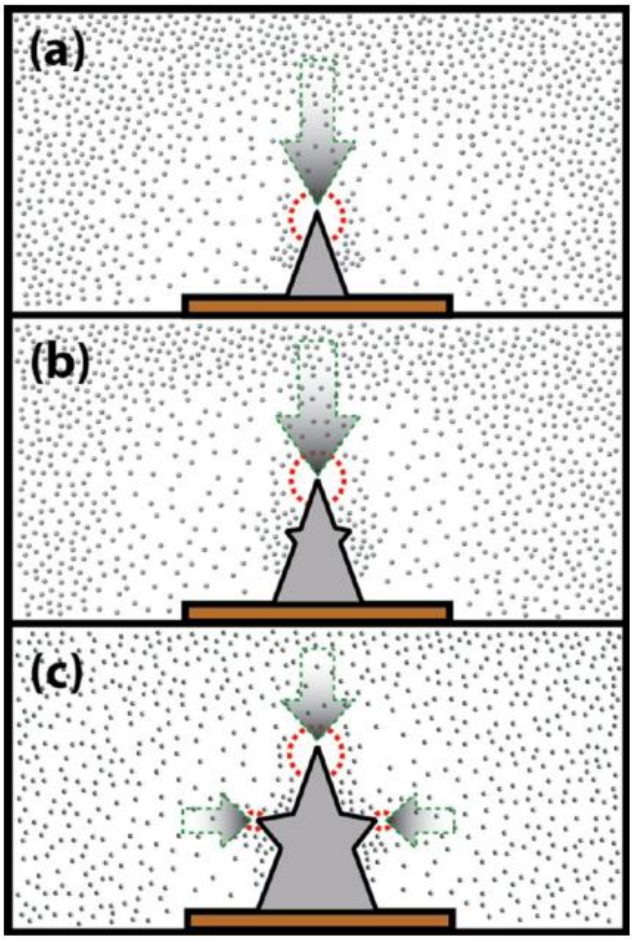

Figure 3-6. Dendritic growth due to Mullins-Sekerka instabilities. (a) For growth fronts of sufficient size, the consumption of Ag+ outpaces the rate of replenishment, creating an instability in the concentration distribution. Diffusion gradients (represented as green arrows) are largest between the bulk and depleted regions, but the MS instability perturbs the flux of incoming cations to create a concave growth front. (b) The concave growth front leads to regions of increased Ag+ concentration near the surface of the growing deposit with sufficient electrochemical potential to nucleate new growth sites. (c) As the branches grow, additional MS instabilities form, repeating the process and leading to the self-similar dendritic morphology

Below the transitional Cu seed edge length, local forces sufficiently dampen the perturbations caused by the consumption of Ag^+ at the growth front, and no large-scale

disruptions of the concentration field occur. The tip of the growing deposit moves smoothly toward higher concentration areas, such that local crystal growth anisotropy dominates the process and produces wires preferentially oriented along the (111) surface. The advancing growth front functions similarly to a directed drift term in diffusion-driven aggregation models, which predict needle-like growth when the flow of reactants toward the interface is sufficient to dampen instability [105].

The localized nature of the wire growth mechanism is illustrated by the formation of interpenetrating wire networks (Figure 3-3). Since there is no disruption of the concentration field, each growth process is effectively independent, so the wires can grow past each other. Conversely, during dendritic growth, MS instabilities alter the distribution of available Ag^+ at a more global scale. As dendritic growth fronts approach, the depletion effects compound, and growth halts before deposits come into contact (Figure 3-4c). These observations support the notion that the transition in deposition morphology is associated with a change in the scope of the growth front's interaction with the solute concentration distribution. The specific magnitude of the critical parameters for inducing the transition are sensitive to many factors, from the bulk concentration of silver cations to the presence of hydroxide and nitrate anions, which have been found to promote nanowire formation in other Ag reduction processes [106, 107]. While the observed ~10 μm transition length is particular to our choice of reaction parameters, this investigation is of general interest because of the mechanistic insight gained by experimentally isolating a single parameter—the seed size—and observing its influence on the emergence of global nonequilibrium patterns from local anisotropy.

In conclusion, we have developed a flexible ELD technique using lithographically patterned copper seeds reacted with silver nitrate solutions to controllably produce either wires or dendrites by utilizing an emergent length scale in the nonequilibrium deposition process. We propose that at seed sizes on the order of 1 μm, the process is controlled by local crystal growth anisotropy and produces wires, while above 10 μm the growth front depletes reactive solute species at a rate sufficient to create MS instabilities in the concentration field and forms dendritic deposits. This combination of patterning and self-assembly is an effective means for constructing biomorphic electroionic devices and is a useful blueprint for connecting bottom-up and top-down methodologies to efficiently produce complex nanotechnology [77].

Chapter 4. Self-organized atomic switch networks

Abstract

The spontaneous emergence of complex behavior in dynamical systems occurs through the collective interaction of nonlinear elements toward a highly correlated, non-equilibrium critical state. Criticality has been proposed as a model for understanding complexity in systems whose behavior can be approximated as a state lying somewhere between order and chaos. Here we present unique, purpose-built devices, known as atomic switch networks (ASN), specifically designed to generate the class of emergent properties which underlie critical dynamics in complex systems. The network is an open, dissipative system comprised of highly interconnected ($\sim 10^9/cm^2$) atomic switch interfaces wired through the spontaneous electroless deposition of metallic silver fractal architectures. The functional topology of ASN architectures self-organizes to produce persistent critical dynamics without fine-tuning, indicating a capacity for memory and learning via persistent critical states toward potential utility in real-time, neuromorphic computation.

4.1 Introduction

Complex systems are ubiquitous in the natural world. Studies of their structure and functional connectivity have revealed underlying network topologies that are both adaptive and evolutionary as a consequence of self-organization [108-110]. Biological neural networks are intrinsically complex and utilize self-configuring, hardware-based architectures capable of dynamic topological alteration. These intrinsically nonlinear, complex systems demonstrate extraordinarily efficient transmission of information, function without the need for pre-

programming or an underlying software algorithm [111], and exhibit emergent behaviors commonly associated with intelligence such as associative memory, learning and predictive capacity in non-deterministic environments [112].

Despite substantial effort to date, there remain relatively few theoretical constructs capable of providing fundamental insight into the occurrence of complex phenomena. One such construct, known as criticality, attributes spontaneous emergence of complex behaviors to the collective interactions of simple, nonlinear elements [14]. It is associated with the critical point of second-order phase transitions, whereby the system correlation length diverges in both space and time. Consideration of non-equilibrium critical states in the underlying dynamics of complex systems has provided substantial insight into possible mechanisms for the emergence of collective behavior in a wide variety of phenomena ranging from earthquakes, forest fires, avalanches, traffic patterns to economic trends [5, 113].

Recent findings have shown biological neural networks operate in a critical regime, where "avalanches" drive internal system dynamics independent of initial system conditions and without the need for fine-tuning [23]. Their collective properties have led researchers in the field of complexity and neuroscience to further examine the fundamental nature of intelligence in terms of criticality [19]. Concomitantly, interest in correlations between neural activity, cognition, associative memory and intelligence has also promulgated proposals for bio-mimetic neural network-based computing devices [25]. Practical implementation of such concepts has been limited by their complicated fabrication requirements, reliance on sequential operations of logical processing and memory, or dependence on innovative software algorithms.

In contrast, criticality presents a framework for computation that leverages system-wide spatiotemporal correlations to provide maximal information capacity and signal propagation.

Despite the discernible advantages offered by criticality as the basis for an optimal computational paradigm, this construct has received limited attention as a operational mode for the design and operation of purpose-built devices capable of doing useful work such as signal processing. Here, we discuss the design, fabrication and operation of a self-organized fractal version of the previously reported atomic switch network (ASN) [73, 77, 114-116] and demonstrate its capacity to function in a persistent critical state. This system is shown to emulate many relevant features of biological neural networks and provides a novel way to explore the utility of criticality as a basic framework for hardware implementations of a new paradigm in neuromorphic computation.

4.2 Self-organizing networks

Complex systems are commonly described as networks with hierarchical topologies composed of highly interconnected functional units. In many cases, these networks are scale-free and involve sparsely connected "small world" regions [108, 117, 118]. Fabrication of such complex architectures in synthetic systems and devices, especially those including random structural topology, cannot be readily achieved through traditional methods due to formidable challenges in forming robust intra- and inter-device connections in a cost-efficient manner [49]. Whereas biological networks realize a compromised balance of cost and complexity through self-organization, structural self-similarity, and hierarchical modularity [119], artificial network architectures remain at the mercy of the so-called "cost of wiring" limit [90, 91].

To overcome these limitations, we set out to design and fabricate complex, hierarchical device architectures by exploiting self-organization of nanoscale building blocks as functional device components. In contrast to complex lithographic methods, solution phase

electrochemistry offers an alternative approach for the unconventional fabrication of complex metallic structures. In particular, the electroless deposition of various metals through the spontaneous reduction of soluble metal cations has been shown to form structures that exhibit scale-invariant fractal-like geometry and dimensionality via diffusion limited aggregation (DLA) [52]. This process can be exploited to present a new method for fabricating self-similar, small-world networks optimized for maximum interconnect density. As shown schematically in Figure 4-1(a) , this concept involves the growth of sparsely interconnected fractal nodes randomly positioned in quasi-two dimensional space to form an extended network on top of an underlying conventional electrode array enabling direct electrical characterization and excitation of the network.

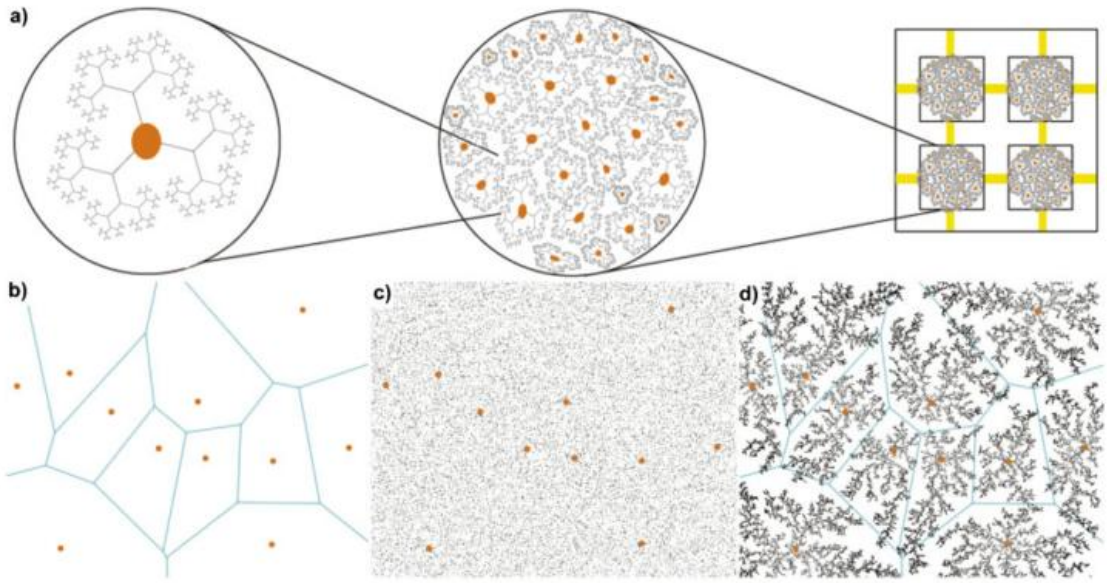

Figure 4-1. Hierarchical network device concept of the fractal atomic switch network composed of "small world" regions of densely interconnected nodes and integrated with a macroscopic electrical I/O platform (a). Voronoi diagram-based simulation of metallic fractal growth by electroless deposition of a randomly distributed network of self-similar nodes from randomly distributed copper microsphere seeds (b–d).

Starting from a random, substrate-supported dispersion of nucleation sites for the electroless deposition of metallic fractals, simulation of the resultant network topology was carried out using a tesselation method based on Voronoi diagrams [120] in combination with the DLA model of electroless deposition as seen in Figure 4-1(b-d). By partitioning a plane of n points into convex polygons (called Voronoi cells) such that each polygon contains exactly one nucleation site and every point in a given polygon is closer to its generating point than to any other, the resulting simulations validated the design concept for generating fractal networks.

Building upon these simulation results, physical implementation of the concept began with fabrication of a device platfrom for subsequent electrical input/output (I/O) measurements using standard microfabrication techniques as summarized in Figure 4-2(a) . A macroscale electrode pattern was first fabricated on the surface of a Si wafer (525 μm thickness; p-type; 100 mm diameter) using conventional photolithography. Metal electrode pads were then patterned on the front side of the wafer via a lift off process of a Cr/Pt (15/150 nm) bilayer deposited using e-beam evaporation. Subsequently, SU-8 reaction wells for holding liquids were defined using SU-8 [121] by a sequence of spin coating, soft baking, UV exposure, post-exposure bake, development, rinsing, and hard baking [122].

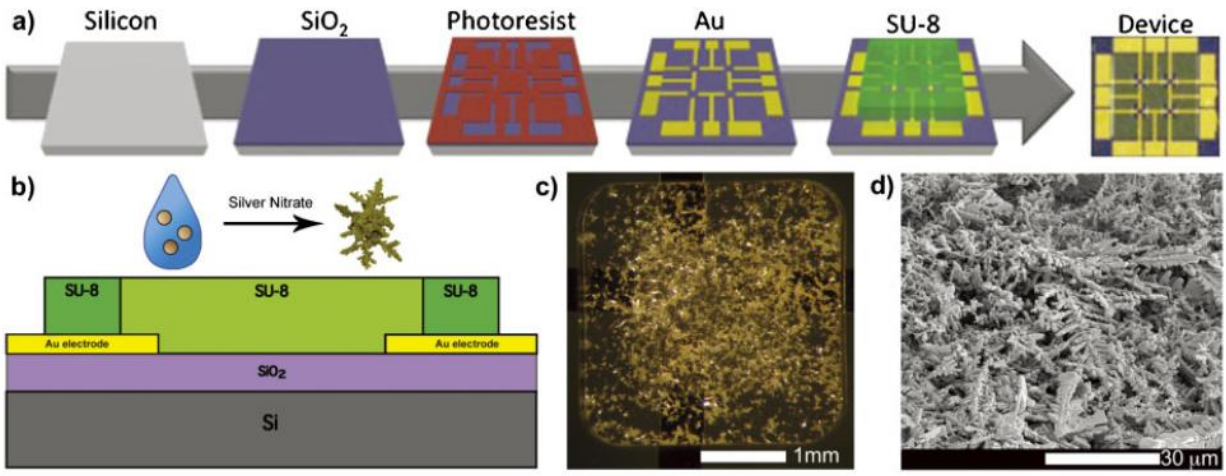

Figure 4-2. Sequential processing of the device platform employed in the preparation and characterization of fractal ASNs entailed photolithographic patterning of Au electrodes and SU-8 polymer provided four independent reaction wells per device (a). Silver fractal nodes were grown by spontaneous electroless deposition from drop-cast copper microspheres within the macroscopic electrical I/O platform (b). Characterization by optical (c) and scanning electron (d) microscopy revealed individual fractal nodes to be sparsely interconnected within a random micro- and nanoscale architecture.

Electroless growth of densely interconnected, metallic fractal nodes was carried out using of copper microspheres (99.995% purity, average diameter of ~10 µm) suspended in isopropanol (1 mg/ml) as reaction nucleation sites for the spontaneous galvanic displacement reaction with silver [114]. The size of the initial copper nucleation site was selected to preferentially result in fractal growth [123]. A small volume of this suspension was deposited into the reaction well of a pristine device and allowed to dry in ambient conditions overnight as seen in Figure 4-2(b). Dilute aqueous silver nitrate (50 mM) was then added and allowed to react to completion:

$$\begin{array}{ll} (1)\quad \mathrm{Ag^+(aq) + e^- \leftrightarrow Ag(s)} & \varepsilon_0 = 0.7996\,\mathrm{V} \\ (2)\quad \mathrm{Cu^{2+}(aq) + 2e^- \leftrightarrow Cu(s)} & \varepsilon_0 = 0.3419\,\mathrm{V} \\ \hline \mathrm{2Ag^+(aq) + Cu(s) \leftrightarrow 2Ag(s) + Cu^{2+}(aq)} & \varepsilon_0 = \varepsilon_0[2(1) - (2)] = 1.2573\,\mathrm{V} \end{array}$$

The resultant fractal networks were characterized by optical and scanning electron microscopy, revealing a macroscopic topology similar to that shown in Figure 4-1(a) as well as a self-similar

microscopic architecture indicative of fractal growth with the fractal dimensionality determined to be ~1.7.

4.3 Integrating nonlinear functionality

The emergence of dynamical structures in complex networks is the consequence of interactions amongst the constituent nonlinear elements. Given the highly interconnected topology of the metallic fractal networks, integration of nonlinear components required the production of functional interfaces distributed throughout the network architecture. The nonlinear operational requirements were met by the electronic properties of the class of solid-state devices generally known as resistive switches [37, 124]. In their simplified form, resistive switches behave as two-terminal devices controlled using solid-state redox coupled ion-migration reaction to form/annihilate filamentary structures across a metal–insulator–metal (MIM) interface shown in Figure 4-3. Typically fabricated as cross-bar arrays through standard lithographic techniques, resistive switches exhibit hysteretic resistance switching, multistate switching in increments of the quantized resistance, and have been integrated with massively parallel CMOS technology [125].

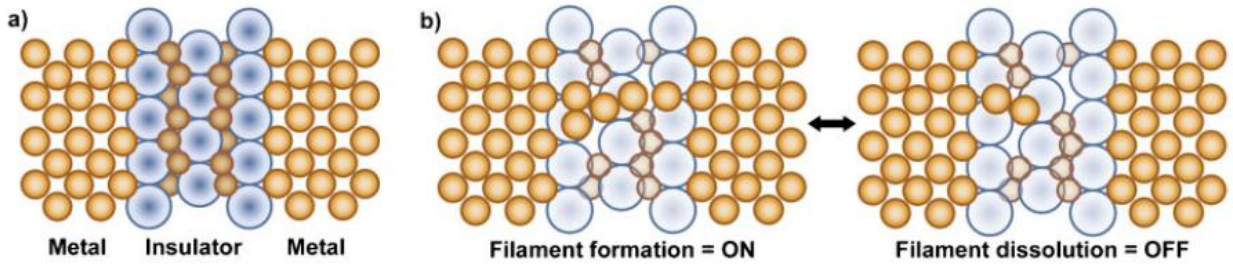

Figure 4-3. Structure of the symmetric atomic switch (a), comprised of an Ag|Ag_2S|Ag interface. Operational schematic (b) showing device activation to the ON state resulting from the formation of a conductive Ag filament across the insulator. A return to the OFF state, either by removal or reversal of the applied bias, occurs due to filament dissolution. Applied voltage across the interface stimulates the migration of and reduction/oxidation of Ag^+ cations during the switching process.

One member of this family, the atomic switch [39], has shown fascinating electrical properties analogous to sensory-, short-, and long-term memory (SM, STM, and LTM) at synthetic synaptic junctions [41-43]. Individual atomic switches exhibit time-dependent nonlinear conductivity behaviors due to several related mechanisms: (1) bias induced Ag^+ migration, (2) electrochemical redox reactions involving Ag^+/Ag^0 to produce metallic filaments, and (3) an associated non-equilibrium α/β-Ag_2S phase transition, which all compete with thermodynamically driven stochastic renormalization to the equilibrium OFF state[126]. Though atomic switches can be configured to operate in an essentially nonvolatile manner similar to memristors [33, 38] — two-terminal circuit elements whose resistance depends on the history of charge passed through them — their volatility indicates that they can be considered to be "memristive systems".

Spontaneous, system-wide functionalization of the fractal network entailed conversion of as-grown metallic interfaces into MIM) junctions (Ag|Ag_2S|Ag through gas phase sulfurization [53] within a Pyrex reaction tube from a crucible containing sulfur (99.5% purity, Sigma-Aldrich) heated to 120 °C under nitrogen flow by the following reaction:

$$\begin{array}{lll} (1) & \mathrm{Ag_2S + 2e^- \leftrightarrow 2Ag + S^{2-}} & \varepsilon_0 = -0.691\,\mathrm{V} \\ (2) & \mathrm{S + 2e^- \leftrightarrow S^{-2}} & \varepsilon_0 = -0.47627\,\mathrm{V} \\ \hline & \mathrm{2Ag + S \leftrightarrow Ag_2S} & \varepsilon_0 = \varepsilon_0[(2) - (1)] = 0.214(7)\,\mathrm{V} \end{array}$$

Diffusion of sulfide through the wire junctions lead to the formation of high interconnect density (~$10^9/cm^2$) of nanoscale interfacial atomic switches as estimated from SEM analysis.

Confirmation of successful network functionalization was interrogated through standard methods for operation of resistive switches. In common with the current understanding of

switching mechanisms in standard devices based on various materials such as Ag_2S, TiO_2, Ta_2O_5 as well as prior reports of ASN operation [73, 77, 114-116], device activation required an initial forming step. Application of either a DC bias across the device electrodes (0–10 V), sequential bias sweeps (±10 V), or a combination thereof created a short-lived (minutes) high conductivity "ON" state as shown in Figure 4-4(a) as a sequential series of representative *I–V* curves. Devices were characterized in this fashion before and after functionalization in order to illuminate any underlying electrical characteristics resulting from the individual device components themselves. The observed nonlinear *I–V* curves exhibit the expected decrease in network resistance with consecutive bias sweeps [73], a behavior attributed to the operational phase transition between weak and soft memristive switching [79, 115]. In contrast, un-sulphurized control devices comprised of a purely metallic network have substantially lower resistance and exhibit linear, ohmic *I–V* characteristics at intermediate voltages (±3 V) followed by irreversible breakdown at high bias.

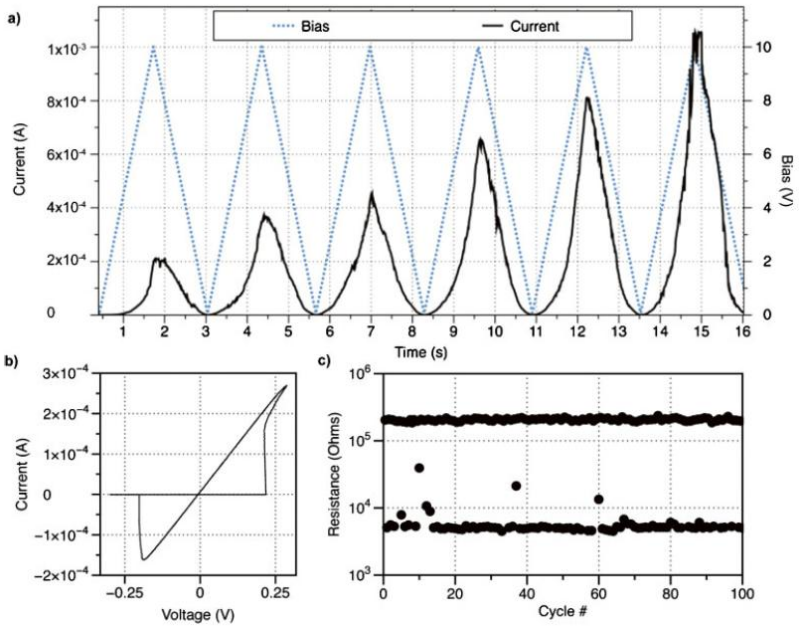

Figure 4-4. ASN activation by repeated application of unipolar bias voltage sweeps demonstrating the formation of a high conductivity "ON" state (a). Nonlinear hysteretic switching observed after network activation (b) was highly robust, operating reliable over extended cycling (c).

Following network activation, ASNs operated consistently as nonlinear switching devices, switching between two distinct resistance states as shown in Figure 4-4(b). Device-to-device variability in the operational parameters was observed and is attributed to variations in the initial fractal configuration due to the nature of the fabrication process. Nevertheless, the devices generated consistent dynamical responses and operated reliably with stable R_{ON}/R_{OFF} ratios [116].

4.4 Emergent Criticality

The resultant correlations, patterns, and dynamical properties generated as a consequence of nonlinear interactions between individual elements comprising a complex network can be considered emergent in that they belong to the system collectively rather than to any constituent

element [7]. In the context of critical dynamics, those elements are required to be governed by threshold dynamics capable of fast relaxation compared to an relatively slow external driving force, thereby allowing the system to settle into a range of correlated metastable states [113]. Observations of nonlinear network dynamics and emergent criticality have been recently reported in ASNs comprising highly interconnected nanowire networks prepared through a blend of top-down lithography and bottom-up self-organization [77, 116].

To confirm the functional connectivity of fractal ASNs, devices were investigated with the aim to find persistent fluctuations in network conductance under relatively "un-tuned" energetic stimulation [73]. Fluctuations in network conductance have been attributed to a competition between bias-driven ion migration in opposition to a stochastic, thermodynamically driven return to equilibrium stoichiometry of the silver suphide junctions. Both factors lead to fluctuations in local resistance within the network that cause cascading resistance changes throughout the system [115]. Application of a DC bias voltage across the ASN resulted in fluctuations in conductivity for up to 60 h as shown in Figure 4-5. This emergent property, in contrast to the known behavior of an isolated atomic switch under DC bias, represents a primary indication of distributed electroionic coupling throughout the interconnected network.

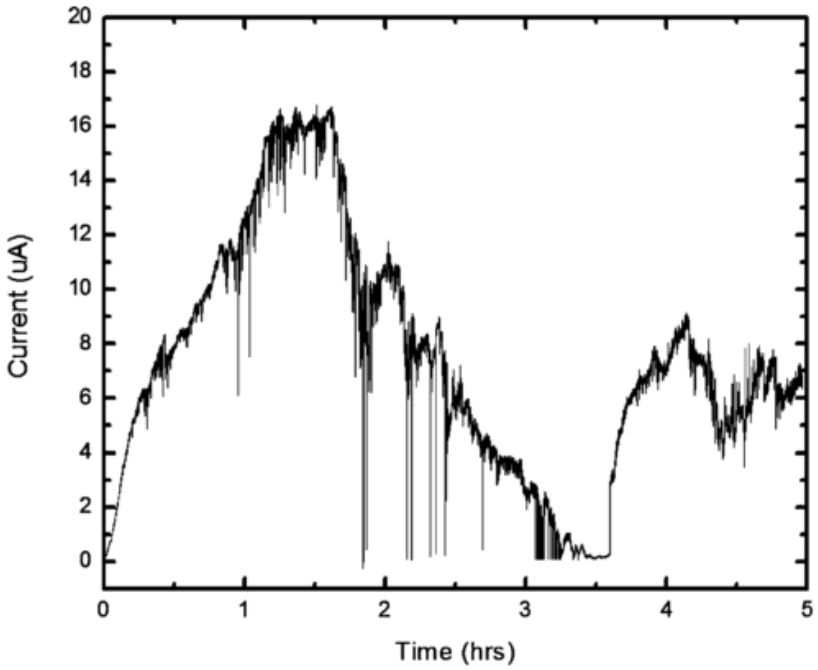

Figure 4-5. Persistent fluctuations in device conductivity under un-tuned, sub-threshold DC bias voltage following device activation indicate distributed functional connectivity.

Indicators of criticality include power-law (log–log) scaling of $1/f$ fluctuations and spatiotemporal correlations. Analysis of the power spectral density of network conductivity in the activated state revealed linear $1/f$ power law scaling over five orders of magnitude with $\alpha = 1.6$ indicating cooperativity during the integration of signals originating at different points in time which is ascribed to spatially correlated structures in local network activity. Temporal correlations were further explored by stimulation and device interrogation using sub-activation threshold, square-wave voltage pulses as shown in Figure 4-6(a) . This stimulation protocol was chosen for two primary reasons. First, to allow for the manifestation of threshold dynamics requires a separation of timescales (slow driving) between energetic stimulation and system relaxation. Second, voltage pulses are the common method of stimulation for single point atom switches that exhibit SM, STM, and LTM. A wide range of stimulation parameters including

interval, duration and magnitude, were examined to ensure sufficient separation between the timescales on which stimulation and relaxation dynamics occur.

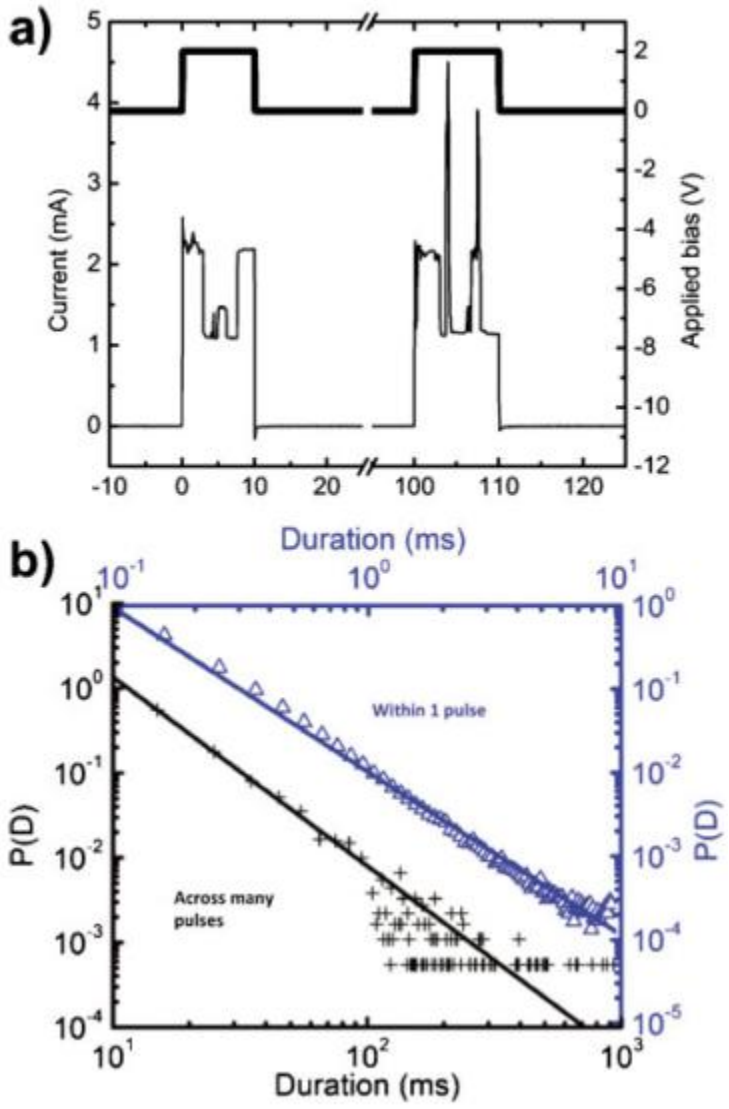

Figure 4-6. Temporally metastable conductance states were observed in the device response to intermittent voltage stimulation (a). Temporal correlation of metastable states observed during pulsed stimulation demonstrated power law scaling ($\alpha \approx 1.7$) for residence time both within a single 10 ms pulse and over 2.5 s during extended periods of pulsed stimulation (b).

Correlated internal dynamics enabled observation of temporal correlations in residence times across a series of metastable states and indicates system memory. In terms of the

interfaces, information of previous events is stored in terms of the ionic distribution of soluble cations and accompanying crystalline phase within the ionic conductor. Metastable state times were determined by searching the pulse response time series for regions with point-to-point current fluctuations less than the noise floor. For the longer term, pulse-to-pulse correlations, the time series was smoothed by a moving average over 1 ms (10 timesteps), which was the interval of analysis for determining residence times greater than 100 ms. Scale-invariance of these temporal correlations was found to extend from short timescales (ms) within individual pulses to extended timescales (s) including multiple cycles of stimulation and relaxation as seen in Figure 4-6(b). Analysis of temporal self-similarity revealed power law distributions ($\alpha \approx 1.7$) within the residence time probability observed in these metastable states. These temporally metastable states are postulated to represent basins in the attractor landscape of the critical phase space produced by the ASN [127]. In the brain, periodic oscillations in the magnitude of neural activity push the network back and forth across the critical-subcritical boundary, moving through and modifying an attractor landscape, a process which may form the basis of associative memory and action-generating mechanisms [128, 129].

4.5 Conclusions

The collective behavior of coupled atomic switches within a self-organized network exhibits emergent device characteristics not observed in single atomic switches. These properties are attributed to a collective interaction of switching junctions across a shared ionic conductor. Here the activity of individual switches serves to influence the local environment of nearby switches as a result of variations in the surrounding electric field and distribution of Ag+ in the ionic conductor. The fractal network provides an additional layer of interconnect complexity, enabling system-wide conductance switching behavior. If local interactions were the sole

dynamic feature, one would expect to observe a continuum of conductance states. In contrast, switching between discrete states indicates correlated activity, where the class of emergent dynamical behavior satisfies numerous crucial criteria of criticality.

A multitude of research has demonstrated the potential utility of criticality to describe and characterize complex systems and natural phenomena. However, only limited experiments have been reported in functional, non-biological system, a fact that inhibits probing their underlying dynamics. We demonstrate that combining fractal networks of self-assembled metallic wiring with the fascinating physiochemical properties of solid-state atomic switches, enables the operation of dissipative, scale-invariant systems with interactive degrees of freedom. ASNs exhibit rapidly emergent (<1 min) self-organization to persistent critical states over time periods of days which are comprised of multiple temporally correlated metastable states. These findings strongly suggest an important link between the requirements for predictive forms of real-time computation and ongoing advances in neuroscience through a readily addressable complex physical system with collective behaviors analogous to those currently observed in biological neural networks.

5. Neuromorphic atomic switch networks

Abstract

Efforts to emulate the formidable information processing capabilities of the brain through neuromorphic engineering have been bolstered by recent progress in the fabrication of nonlinear, nanoscale circuit elements that exhibit synapse-like operational characteristics. However, conventional fabrication techniques are unable to efficiently generate structures with the highly complex interconnectivity found in biological neuronal networks. Here we demonstrate the physical realization of a self-assembled neuromorphic device which implements basic concepts of systems neuroscience through a hardware-based platform comprised of over a billion interconnected atomic-switch inorganic synapses embedded in a complex network of silver nanowires. Observations of network activation and passive harmonic generation demonstrate a collective response to input stimulus in agreement with recent theoretical predictions. Further, emergent behaviors unique to the complex network of atomic switches and akin to brain function are observed, namely spatially distributed memory, recurrent dynamics and the activation of feedforward subnetworks. These devices display the functional characteristics required for implementing unconventional, biologically and neurally inspired computational methodologies in a synthetic experimental system.

5.1 Introduction

The human brain is the most powerful information processor known to man. Although the activity of individual neurons occurs orders of magnitude slower (ms) than the clock speeds of modern microprocessors (ns), the human brain can greatly outperform CMOS computers in a

variety of tasks such as image recognition, especially in extracting semantic content from limited or distorted information, when images are presented at drastically reduced resolutions [130-133]. These capabilities are thought to be the result of both serial and parallel interactions across a hierarchy of brain regions in a complex, recurrent network, where connections between neurons often lead to feedback loops [134-136]. Recent research in systems neuroscience has developed models to explain this combination of rapid and complex processing which view the brain as a large network containing many recurrent loops with both excitatory and inhibitory connections, within which feedforward sub-networks are embedded for fast signal propagation [134, 137, 138].

In the brain, these excitatory/inhibitory connections between neurons, known as synapses, are nonlinear electroionic junctions whose conductivity changes in response to electrical and chemical signals. The relative timing of signals arriving from either side of the synaptic terminals, as well as larger-scale spatiotemporal patterns of network activity during these events, strongly influence the resultant change in synaptic strength, or plasticity [21, 139], a property postulated as the mechanistic basis for memory and learning [140]. Recently, nanoscale electroionic circuit elements known as atomic switches [39] have been shown to exhibit input-dependent memory behaviors similar to short-term plasticity and long-term potentiation in neuronal synapses, where the time constant for conductance decay to the high resistance OFF state depends on the strength and timing of applied voltage pulses [41]. This tendency to equilibrate produces short- and long-term memory behaviors that enable atomic switches to function as "inorganic synapses" [43].

We present a detailed analysis regarding the consequences of coupling many atomic switches together in a highly interconnected, recurrent structure to create an operational

neuromorphic device that self-assembles into a functional state. The motivation for building complex network-based computing devices extends beyond an interest in understanding and emulating brain function. Alongside efforts to reduce the dimensions of circuit elements while increasing their integration, the wiring of interconnects has become the limiting factor in both design and performance of electronic devices [141]. Wire delays are significantly slower than transistor switching speeds, producing a situation where more logic gates can be fabricated on a chip than are able to communicate in one processor cycle [90]. This communication bottleneck can be addressed theoretically through the use of different network topologies, varying the number and type of interconnections. Complex nanowire networks are relatively simple to fabricate using self-assembly and would therefore be ideal wiring architectures, provided that they are useful.

Previously we reported an operational regime near the "edge of chaos" in similar network devices, as characterized by power law scaling of temporal metastability, avalanche dynamics and criticality [77] reminiscent of electrical activity in biological neural systems [19, 23]. In such a state, the system is highly correlated and theoretically achieves maximum efficiency of information transfer while retaining a fading memory of prior states. These results indicate a potential capacity for efficient information processing, thereby surmounting problems associated with wire delays and interconnect structures. The distributed nature of the atomic switch array's dynamics makes it a candidate platform for efficient kernel design in the emerging field of "Reservoir Computation" (RC) [142]. The fact that RC does not require subtle control of internal network dynamics and is therefore simpler to execute, makes it an appealing route to begin using neuromorphic devices to perform computational tasks. Complex network architectures generated through self-assembly of functional nanoscale elements, like those described here, offer the

benefits of scalability and ease of fabrication combined with control of distributed nonlinear dynamics that may represent the architectural basis of a new computational paradigm.

5.2 Results

Atomic switch network devices were characterized using a range of potentiostatic inputs, including constant and ramped DC as well as sinusoidal AC signals. These complex atomic switch networks are shown to exhibit various nonlinear behaviors, depending on the magnitude and timing of both present and prior input signals. Behaviors include both weak (continuous I–V loop hysteresis) and strong (discrete threshold switching) memristance as well as nonlinear frequency response (higher harmonic generation) and persistent fluctuations in conductivity under constant bias (recurrent connectivity); results which were found to agree with a recent theoretical study of current flow in memristor networks [79]. Operation of the device using pulsed voltage stimulation produced network-specific emergent behaviors, as spatially localized conductive channels akin to feedforward subnetworks were formed within the embedding recurrent network. While there are significant differences between these atomic switch networks and biological neural networks (NNs), we demonstrate the physical implementation of high-level NN features in an inorganic structure, including bottom-up self-assembly that is reminiscent of neuronal growth in the brain [143], nonlinear input-dependent conductance response which strongly resembles the function of biological synapses [139, 140], and emergent properties considered fundamental to brain function - recurrent dynamics which gives rise to large persistent, correlated network responses and the activation of feedforward subnetworks [137, 138, 144-147].

5.3 Atomic switches, complex networks, and neuromorphic hardware

Previous reports on the synapse-like properties of single atomic switches have demonstrated features similar to short-term plasticity and long-term potentiation, where applied bias voltage produced a junction conductance dependent on the history of stimulation (pulse frequency, length) [41]. Individual atomic switches exhibit time-dependent nonlinear conductance due to several related mechanisms: (1) bias induced Ag^+ migration, (2) electrochemical redox reactions involving Ag^+/Ag^0 to produce metallic filaments, and (3) an associated non-equilibrium α/β-Ag_2S phase transition [40], which all compete with thermodynamically driven stochastic renormalization to the equilibrium OFF state. Though atomic switches can be configured to operate in an essentially nonvolatile manner similar to memristors—two-terminal circuit elements whose resistance depends on the history of charge passed through them [36]—their volatility indicates that they are more properly classified as "memristive systems" [33, 34].

These mechanisms collectively produce the memristive switching and synaptic memory functions exhibited by a single atomic switch. Specifically, 'weak' memristance resulting from redistribution of Ag^+ dopant cations across the insulator leads to 'strong' memristance characterized by abrupt switching through metallic filaments formed once the Ag^+ cations reach the cathode and are reduced to metallic silver [39]. TEM studies have shown that the metallic silver filaments formed during switching are surrounded by a sheath of β-Ag_2S, a conductive phase of silver sulfide normally unstable below 170°C [40], possessing a body-centered cubic structure with sulfide anions forming channels in which silver cations are delocalized, highly mobile and dynamically correlated [61, 62]. This non-equilibrium phase transition is attributed to a relaxation of strain induced by lattice mismatch between Ag^0 and α-Ag_2S, the electrically insulating room temperature phase [148]. In the absence of applied bias, thermodynamic

pressures return the Ag_2S to its room-T α-phase, which drives the dissolution of the Ag^ofilaments and turns the atomic switch OFF at a rate dependent on the history of applied bias, producing the observed memory effects.

A great deal of effort has been put towards building biologically inspired computational hardware [24-27, 57, 149-151], though matching the complexity of the brain in a usable electronic device presents an exceedingly difficult engineering challenge. Fabrication requirements force design concessions, such as approximating the complex, recurrent connectivity between neurons by a simpler network geometry. The amenability of crossbar structures to conventional fabrication techniques has led to their use in neuromorphic hardware, with pre- and post-synaptic CMOS neurons connected by memristive elements at the crosspoints [46]. This is an ideal hardware implementation of a 3-layer neural network model [152], where input and output neurons are connected by a synaptic "hidden layer" of variable strength, and is also a promising platform for building dense, fast solid-state memory devices [35]. However, the structural simplicity of the crossbar architecture is both a strength, enabling independent control of each synaptic element, and a weakness, since the well-defined grid lacks complex structures with the recurrent connections believed to be essential to brain function [134, 146]. While it is possible to program these features into a software model implemented on neuromorphic hardware, the physical existence of these complex structures may be essential to successfully generate the requisite spatiotemporal interactions between multiple signals simultaneously traveling through the network [139, 153].

5.4 Device fabrication and characterization

Based on the view that recurrent connectivity is essential to brain-like function, we have built, characterized and operated devices using massively interconnected (10^9 junctions/cm^2according to analysis of SEM images), silver nanowire networks functionalized with interfacial $Ag|Ag_2S|Ag$ atomic switches. These nanowire networks were prepared through self-assembly without pre-patterning of the network topology using the electroless deposition of Ag from Cu inside the SU-8 reaction well of an I/O device platform [77, 121]. Specifically, spontaneous oxidization of metallic copper through reaction with dilute aqueous solutions of $AgNO_3$produces a metallic silver structures with variable morphologies depending on the concentration of Ag^+ and distribution of Cu [52, 74, 75]. Dendritic silver nanowires with minimum feature sizes <100 nm seen in Figure 5-1b were produced by using lithographically patterned Cu posts shown in the inset of Figure 5-1a. Control over the size and distribution of Cu seeds increased device yield by ensuring the formation of conductive pathways between the Pt device I/O electrodes as seen in Figure 5-1b. $Ag|Ag_2S|Ag$ interfaces were formed spontaneously within the network during gas phase sulfurization [53]. Following optimization of fabrication protocols, a total of 96 networks were used for the device characterization described below.

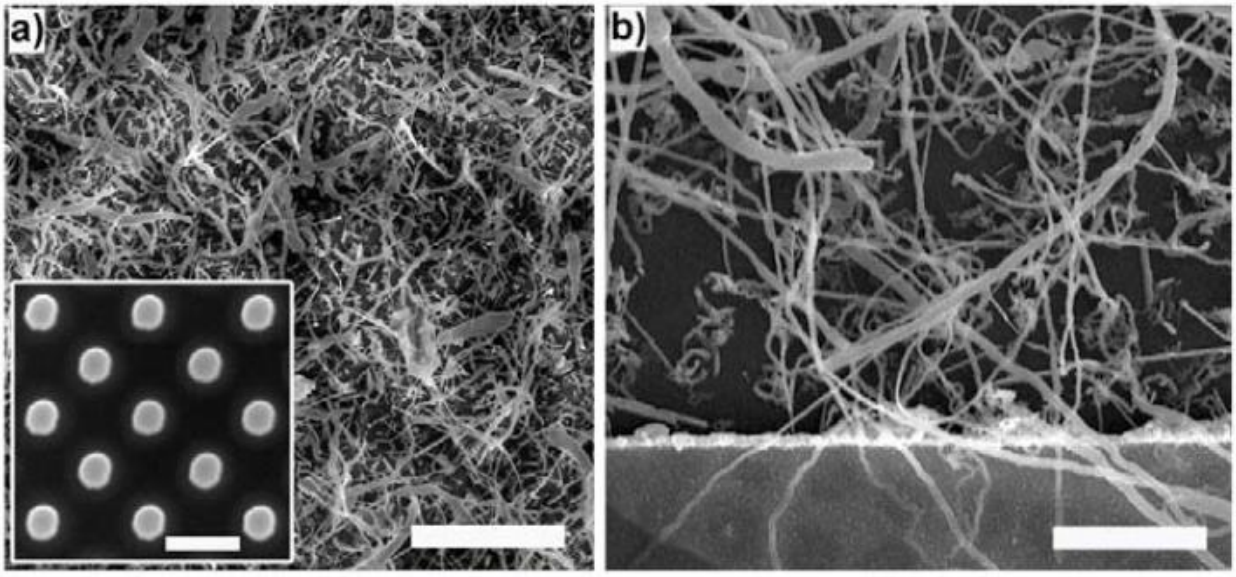

Figure 5-1. Device fabrication. (a) SEM image of complex Ag networks (scale bar = 10 μm) produced by reaction of aqueous $AgNO_3$ (50 mM) with (inset) lithographically patterned Cu seed posts (scale bar = 1 μm). (b) High resolution image of the functionalized Ag network at the device electrode interface (Pt) showing wire widths ranging from 100 nm to 3 μm (average <1 μm) and lengths extending from a few microns to almost a millimeter (scale bar = 700 nm).

Theoretical analysis of current flow in memristor networks during bias voltage sweeps indicated the possibility of a phase transition in device behavior from 'weak' to 'strong' memristive regimes [79]. Initial voltage sweeps of these network devices (Figure 5-2a) typically demonstrated smooth, pinched hysteresis loops characteristic of weakly memristive systems followed by an abrupt, nearly discontinuous jump to a distinct, high conductance ON state occurs at an activation bias voltage (V_a). This behavior represents activation of the network and is shown as an illustrative example of a network device undergoing a behavioral phase transition similar to the bias-driven forming step required to activate single resistive switches. Following network activation, devices subjected to repeated bias sweeping generally exhibit robust, strong memristive behavior, typified by hard switching (inset). Robust switching over 10,000 cycles was demonstrated at an operational threshold voltage (V_t) of reduced magnitude as compared to the formation bias voltage, a general phenomenon in resistive switches [124]. While the specific

magnitude of V_a and V_t differ significantly between devices due to inherent variability in the solution-phase methods used to fabricate them, the qualitative transition from weak to strong memristive behavior was observed regularly, consistent with theoretical predictions [79].

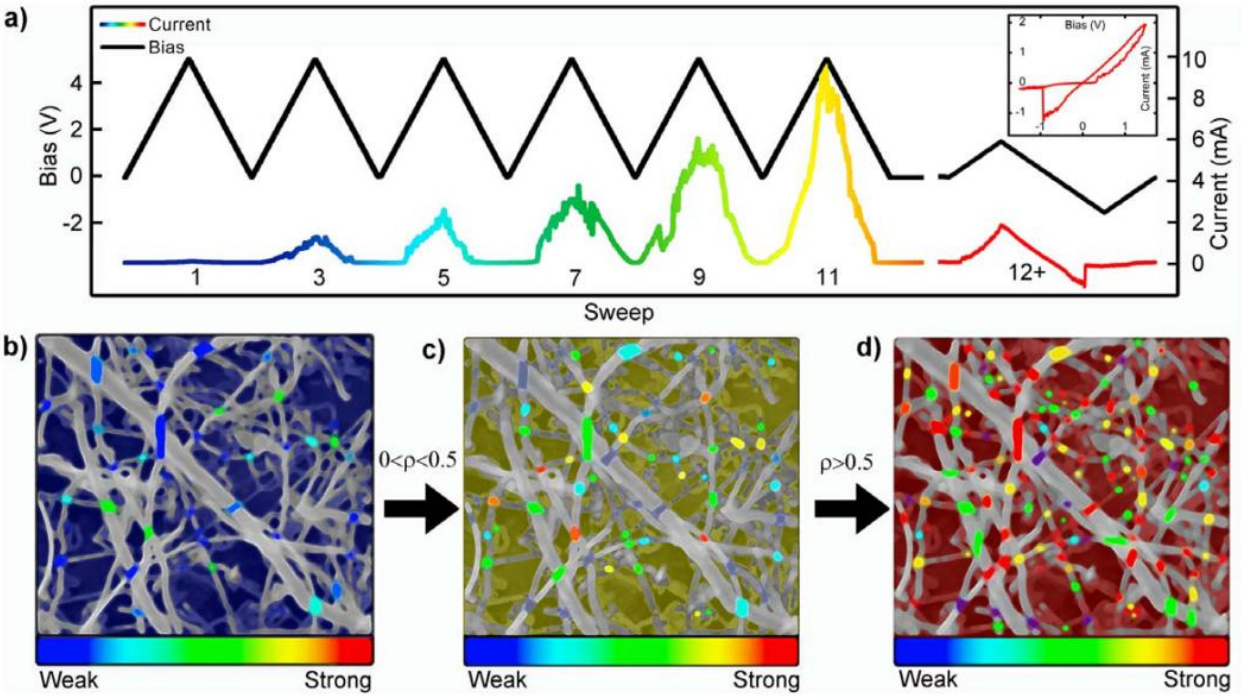

Figure 5-2. Network Activation - memristive behavior. (a) Representative example of initial bias sweeps (0–5 V sweep at 1 V/s) applied to a pristine device which steadily activate higher percentages of atomic switches, resulting in increased current. After 11 sweeps, the device resistance decreases from ~10 MΩ to ~500 Ω. Subsequent ±1.5 V bipolar sweeps result in repeatable pinched hysteresis behavior (inset: R_{OFF} = 25 kΩ, R_{ON} = 800 Ω), and bistable switching. (b–d) Schematic representation of the mechanism producing the I–V characteristics shown in (a). The network initially consists of weakly memristive junctions and ohmic contacts (b). Continued application of unipolar bias voltage (c) drives the dissolution of silver into silver sulfide, increasing the number of memristive elements, while cation migration across extant memristive junctions leads to filament formation and the onset of hard switching behavior. (d) After the proportion of strong memristors exceeds the percolation threshold (ρ>0.5), the network functions reliably in the hard switching regime.

Similar to the electroforming step usually required to activate single atomic switches and memristors [124], the observed transition from weak to strong memristive behavior is assigned to two related mechanisms. In poorly conducting regions comprised mainly of Ag_2S, anodic silver dissolves into and travels across the electrically insulating sulfide as Ag^+, decreasing resistance

and producing a weakly memristive effect. In regions of higher Ag^+ dopant concentrations, mobile cations reach the cathode and are reduced to Ag^0, creating metallic filaments across the insulator that cause an abrupt change to an ON state with a sharp increase in conductance at V_t associated with the electrochemical process of filament formation. At the network level, the bias-induced creation of additional memristive junctions and filament formation across existing ones combine to produce the theoretically predicted transition of network I–V behavior to a strongly memristive phase (schematically illustrated in Figure 5-2 b–d) as the proportion of switching elements in the network exceeds the percolation threshold (50%) [79]. Having undergone this transition, the continuously swept network operates as a hard switching memristor shown in Figure 5-2a (inset). All further data presented was acquired from devices following activation.

5.5 Network-specific properties

While weak and strong memristive behavior can be exhibited by single resistive switches, the most interesting features of this complex atomic switch device are its network-specific properties. In order to confirm that the entire network was involved in processing the input signals, devices were imaged using an IR camera with 20 mK sensitivity to track Joule heating from current flow during slow bias sweeps. The IR images revealed power dissipation occurring across the network, indicating that the phase change in network I–V behavior was not attributable to the formation of a single maximum conductivity pathway of switches arranged in series between the active electrodes [77]. The distribution of activity indicates that the observed I–V characteristics are due to the sum of parallel current flow, meaning that network structure and connectivity are actively influencing device function.

As recent theoretical models predict passive generation of second harmonics in both singular memristors and in random networks, the distribution of switch function throughout the network was examined through analysis of the device's frequency response [79, 154]. Simulation of current flow in memristor networks indicate that 2nd harmonic generation will occur under an applied sinusoidal voltage in networks whose percentage of hard switching junctions exceeds the percolation threshold [79]. Further, the relative magnitude of higher harmonics is predicted to increase with the relative number of hard switching junctions. Following activation, device response to a 10 Hz sinusoidal voltage signal varying in strength from 250 mV to 4 V shows a large increase in higher frequency components after functionalization (Figure 5-3b). The proportion of higher harmonics generated increases with signal amplitude (Figure 5-3c), with the largest increase occurring between 250 and 500 mV. A larger degree of higher harmonic generation is consistent with an increased number of memristive junctions operating in the hard switching regime above V_t (~0.5 V). Both the distributed power dissipation [77] and harmonic generation are characteristic of activity distributed throughout the network.

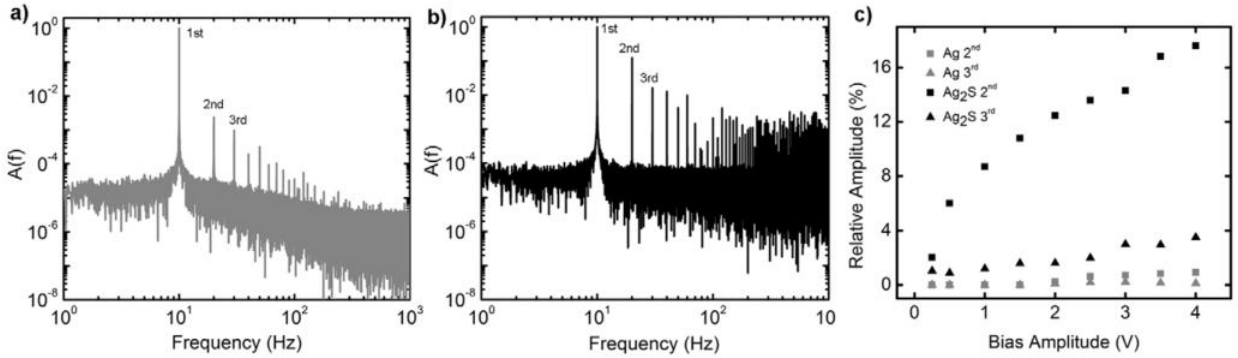

Figure 5-3. Frequency Response – distributed conductance. (a) Amplitude spectrum from a Fourier transform of a control device's response to a 2 V, 10 Hz sinusoidal input signal compared to (b) that of a functionalized device which shows enhanced overtones of the input signal with respect to (a). (c) Plot of 2nd and 3rdharmonic generation in current response as a function of bias voltage in both functional (black) and control (gray) networks. Harmonic magnitudes are represented as percentage of the fundamental for a 10 Hz sinusoidal input signal.

Having characterized atomic switch operation in an interconnected complex network, we examined the device for emergent behaviors specific to its brain-like recurrent structure. Structurally, the atomic switch network is recurrent in the sense that there exist pathways such that electrical signals produced at one junction may lead to (delayed) feedback at the same junction. Here we present experimental evidence of spatially distributed and correlated network dynamics, which are attributed to such recurrent connectivity. These recurrent dynamics are presented as an emergent property of the atomic switch network.

Applying a constant 1 V DC bias (Figure 5-4a) produced persistent, bidirectional fluctuations—both increases and decreases—in network conductivity of large magnitudes (~20–150%) over a range of time scales (seconds-hours). In the absence of recurrent structures within the network, the filamentary mechanism of an atomic switch implies that conductivity would increase monotonically under constant DC bias. The applied voltage leads to the thickening of filaments until the potential drop across the junctions is insufficient to reduce more silver cations [39]. However, large bidirectional fluctuations (ΔI greater than 100% on the scale of hours) in the current response persisted for several days under constant applied voltage, demonstrating that the complex network connectivity inherently resists localized positive feedback that would lead to the serial formation of a single, dominant high conductivity pathway between electrodes. Rather, recurrent loops in the network create complex couplings between switches, resulting in network dynamics that do not converge to a steady state even under constant bias. A single switch turning ON does not simply lead to an increased potential drop across the next junction in a serial chain, but redistributes voltage across many recurrent connections that can ultimately produce a net decrease in network conductivity. This behavior represents a network-scale analog of defect-defect interactions that have been observed to

produce current fluctuations in metal nanobridges [155]. The nanoscale switch filaments couple these interactions with electrochemical redox processes, leading to significant changes in the conductivity state of the entire network.

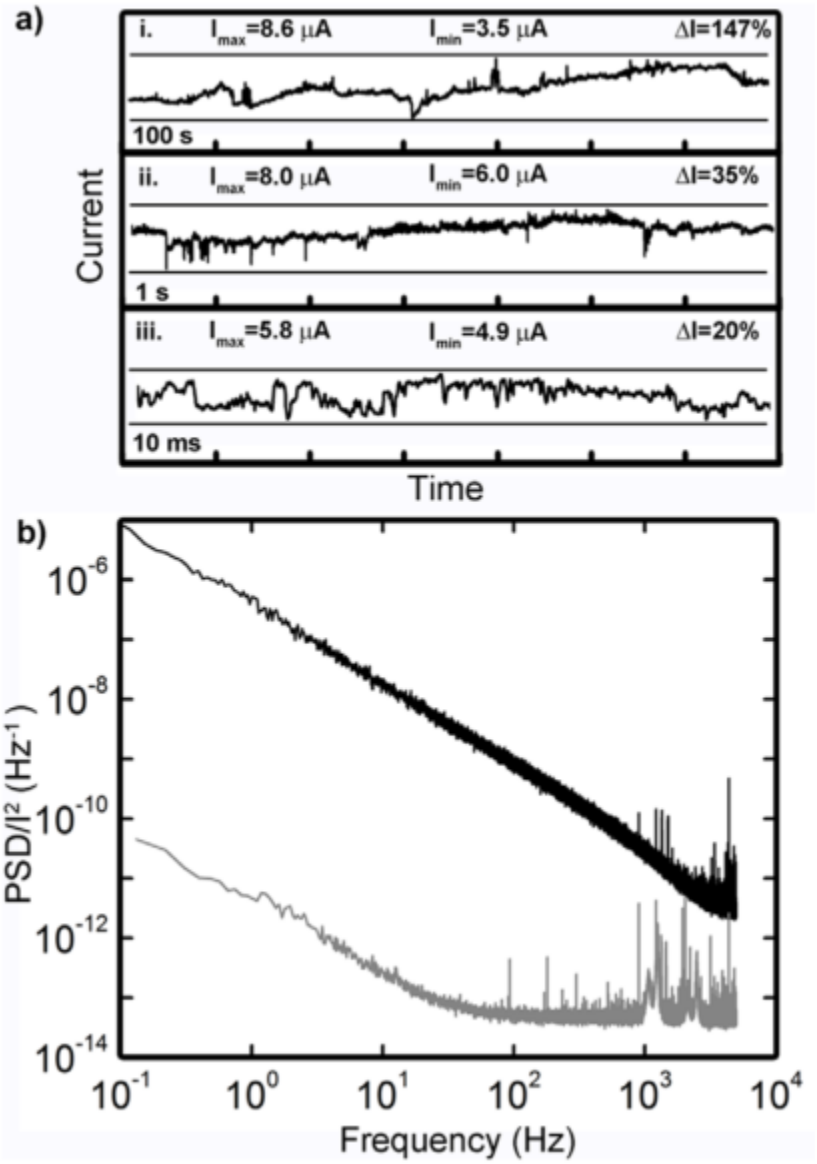

Figure 5-4. DC Response – recurrent dynamics. (a) Time traces of current response to 1 V DC bias show large current increases and decreases at all time scales around a mean of 5.81 μA (172 kΩ); shorter time traces (ii–iii) are subsets of (i). Representative device parameters: R_{OFF}>10 MΩ, R_{ON}<20 kΩ, V_T= 3 V during activation (b) Fourier transforms of DC bias response for Ag control (grey) and functionalized Ag-Ag_2S (black) networks. The power spectrum of the functionalized network displays $1/f^{\beta}$ power law scaling (β = 1.34).

These fluctuations are of a magnitude significantly greater than what can be considered noise. An internal control experiment compared Fourier transformed current responses (Figure 5-4b) of the devices to constant voltage before and after functionalization. The formation of atomic switch junctions expands the degree of correlation in current fluctuations, producing 1/f-like behavior across the entire sampled range, far exceeding that of control devices (unsulfurized silver network, grey line in Figure 5-4b), which flattens to white noise and some high energy, high frequency fluctuations attributed to arcing between neighboring wires. Functionalization with atomic switch elements increases the influence of past events on the present state of the network, in accordance with their memristive characteristics [41, 43, 156]. This results in an expanded degree of correlation in the measured frequency response. Similar 1/f spectra have been observed along with current fluctuations in other resistive switching systems, exhibiting relative resistance changes $\Delta R/R$ ranging from <0.002 for metallic filaments to an experimental and theoretical maximum of 0.5 in the semiconducting high resistance OFF state [157]. The network device of Figure 5-4 is operating in an intermediate state with an average resistance of 172 kΩ (compared to $R_{OFF}>10$ MΩ) and fluctuations of $\Delta R/R\sim1$. In order to produce relative resistance changes of such high magnitude, switching events within the network must be correlated. While stochastic processes may be involved in the correlation of these fluctuations [156, 158] their magnitude and persistence is an emergent feature of recurrent connectivity in the device architecture that has not been observed in simpler atomic switch geometries.

Inside the generally recurrent structure of the brain's neural network, there is evidence for the existence of feedforward subnetworks utilized for the fast propagation of certain signals [147]. In this device, persistent fluctuations in current under constant DC bias are produced by the recurrent network architecture, creating operational dynamics that resist the

feedfoward activation of serial chains of switches. However, by altering the form of the input signal, we were able to independently operate conductance channels between different pairs of electrodes within the same device. The application of a single, large voltage pulse (±3 V, 1 s) selectively switched connections between electrode pairs ON and OFF (Figure 5-5a) with a R_{ON}/R_{OFF} ratio greater than 30. In the example shown, the conductive paths between the two channels overlap spatially, yet are switched independently, indicating that local sub-regions of the network can transition to distinct operational modes despite being embedded within a highly interconnected, largely metallic structure. This is analogous to the presence of feedforward subnetworks within the recurrent architecture of the cortex. Single pulses of sufficient magnitude overwhelm the recurrent dynamics and induce feedforward activation of local sub-regions along a path connecting the involved pair of electrodes without significantly altering the conductivity of other spatially intertwined channels within the same nanowire network.

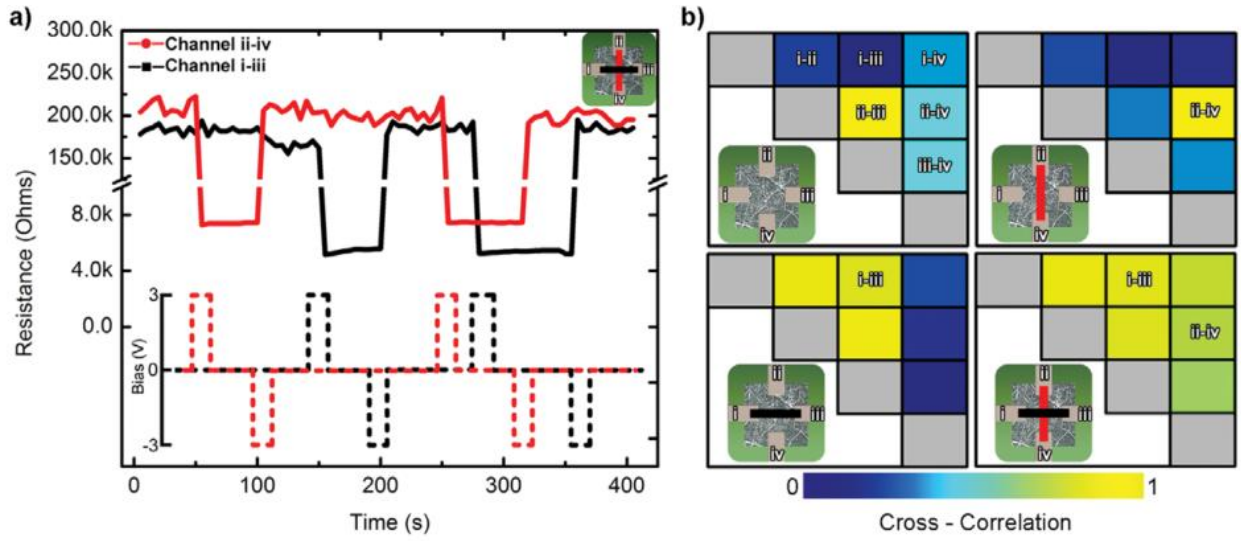

Figure 5-5. Distributed Memory Storage from Network-scale Switching. (a) The device operates as a 2-bit non-volatile memory device. The resistance states across two channels (i–iii and ii–iv) are monitored. ON/OFF switching of each channel is induced using super-threshold pulses (3 V, 1 s in duration); the threshold voltages for each channel are ,1.5 V. The resistances are measured every 5 s with a sub-threshold 200 mV, 100 ms pulses. (b) Although the device operates with a four state output (both channels ON, 1 ON/1 OFF, etc), the network's internal configurations show diverse correlated patterns, from no correlation (blue) to total correlation (yellow). The figure

shows correlation coefficients of channel resistances for all 6 pairwise electrode combinations. The correlation coefficients are calculated during each of the 4 network switching configurations; the black and red bars (insets) show the channels that are ON in the switching state.

The degree to which pulse-mode channel creation influences overall network connectivity can be visualized in electrode resistance cross-correlation matrices (Figure 5-5b). In this case, net electrode resistance is calculated from the pair-wise resistances to be a representative measure of the overall connectivity of a given electrode to the network. The correlation strength (denoted by color) represents the degree to which a pair of net electrode resistances fluctuate in unison, interpreted as a measure of the number of shared network sub-regions connected to both electrodes. Correlation strength increases strongly between electrodes connected by an ON channel, and decreases again when the channel is switched OFF, with a varying degree of influence on electrodes not directly involved in the switching. This implies that spatially central regions of the network can be selectively associated with particular pairs of electrodes without globally increasing the network connectivity. However, when conductive channels exist between all four electrodes, the overall magnitude of correlation in the network is correspondingly large, as fluctuations are spread evenly throughout the increasingly metallic network. This simple example of the interaction between local and global operational characteristics is a promising indicator of the possibility for the creation of a brain-like hierarchy of distinct functional regions within a single network where the functional connectivity of the network itself is both dynamic and self-organized [159].

5.6 Discussion

Using a simple, two-step fabrication procedure combining top-down and bottom-up fabrication techniques, we have created functional neuromorphic devices based on a self-assembled, complex network architecture. We describe these atomic switch networks as

neuromorphic not only in that the massively interconnected, dendritic features observed in biological neural networks inspired the device architecture, but also due to several important network scale properties reported here. The devices demonstrate weak and strong memristive behaviors, as well as higher harmonic generation, confirming theoretical predictions on current flow through memristor networks. Previously unreported emergent behaviors specific to the complex architecture were observed as persistent bidirectional fluctuations of the current in response to constant applied voltage and the pulse-based feedforward switching ON and OFF of localized conductance channels within the highly interconnected network. Despite lacking the brain's rich assortment of neurotransmitter systems, with distinct excitatory and inhibitory neurons, the complex network of atomic switches produces multiple behaviors from a single basic unit through a capacity for localizing function in subnetworks inside a structure correlated by the nonlinear memory response of individual atomic switches. This diversity of function indicates the device's potential as a universal approximator of dynamical systems [160], with possible applications in physically implementing unconventional computational strategies [142] and as an inorganic experimental platform for the investigation of systems neuroscientific theories of biological brain function.

5.7 Materials and methods

Electrodes were patterned on the surface of a Si wafer (525 μm thickness; p-type; 100 mm diameter; 500 nm thermal oxide) by photolithography. A Cr/Pt (15/150 nm) bilayer was deposited using e-beam evaporation. Subsequently, microfluidic reaction wells were patterned from a thick layer of SU-8 (approx. 500 μm) deposited by spin coating. The resist was UV exposed with a dose of 1200 mJ/cm^2 followed by a post-exposure bake beginning at 65°C and

ramping up to 95°C before cooling to room temperature at 1°C/min. The SU-8 was developed by immersion in PGMEA (Propylene Glycol Methyl Ether Acetate). Fully developed wafers were rinsed with isopropanol and hard baked at 130°C on a hotplate in N_2 atmosphere to increase SU-8 resistance to high temperatures.

Electroless deposition of Ag from Cu was performed by pipetting aqueous $AgNO_3$ (Fischer, 99.98%) at concentrations ranging from 0.1–100 mM into microfluidic cells containing Cu seed posts, leading to a spontaneous reaction between Ag^+ and Cu. Optimal conditions were achieved with Cu posts ranging from 0.25–4 μm in diameter at pitches of 0.5–4 μm reacted with 50 mM $AgNO_3$, sulfurized at 130°C for 10 minutes under N_2 flow at atmospheric pressure. The silver networks self-assembled during this processes, and were then functionalized by reaction with sulfur (Sigma-Aldrich, 99.5%) in a Pyrex tube. The sulfur was melted in an evaporation boat at 130°C and delivered to the substrate by N_2 flow.

Electrical characterization of the devices was conducted using four Pt electrodes positioned around the edges of the Ag network. Current-voltage spectroscopy was conducted using a bipotentiostat (Pine Instruments model AFCBP1) in conjunction with a DAQ module (National Instruments USB 6259) at a sample rate of 10 kHz. Measurements were performed in a two-electrode configuration. Multi-channel resistance measurements were obtained using a multiplexed (National Instruments PXI 1073) SMU (National Instruments PXI 4130). The entire I/O system was housed in a Faraday cage and mounted on a vibration isolation table (TMC). Devices were characterized after each stage of the fabrication cycle. Subsequent data analyses were carried out using MATLAB 2010b (MathWorks) and Origin 8.1 (OriginLab Corporation).

The full dataset used in Figure 5-5b contained resistance data from all 6 combinations of the 4 electrodes in a device (for clarity, only 2 combinations are shown in Figure 5-5a). The network resistance of each electrode was calculated as the parallel resistances to the other 3 electrodes. The dataset was parsed into the appropriate subsets (A on and B off, etc.) and the MATLAB function corrcoef() was used to calculate the correlation coefficients for the different configurations.

6. Emergent criticality in complex Turing b-type atomic switch networks

Abstract.

Recent advances in the neuromorphic operation of atomic switches as individual synapse-like devices demonstrate the ability to process information with both short-term and long-term memorization in a single two terminal junction. Here it is shown that atomic switches can be self-assembled within a highly interconnected network of silver nanowires similar in structure to Turing's "B-Type unorganized machine", originally proposed as a randomly connected network of NAND logic gates. In these experimental embodiments, complex networks of coupled atomic switches exhibit emergent criticality similar in nature to previously reported electrical activity of biological brains and neuron assemblies. Rapid fluctuations in electrical conductance display metastability and power law scaling of temporal correlation lengths that are attributed to dynamic reorganization of the interconnected electro-ionic network resulting from induced non-equilibrium thermodynamic instabilities. These collective properties indicate a potential utility for real-time, multi-input processing of distributed sensory data through reservoir computation. We propose these highly coupled, nonlinear electronic networks as an implementable hardware-based platform toward the creation of physically intelligent machines.

6.1 Introduction

Modern state-of-the-art computers are the product of over half a century spent refining implementations of Turing's automatic machine (TAM) [29] using Von Neumann's computational architecture [30]. The TAM is the principal theoretical framework for

computation using sequential logical operations on single- purpose hardware consisting of an infinite tape of symbols, a read/write head, and a control mechanism that acts based on a transition table or instruction sheet. Von Neumann's introduction of the concept of memory into the computer architecture provided a blueprint for the physical realization of multifunctional TAM machines that utilize multiple stored programs via two main functional units – processors and memory. This flexible control mechanism made the TAM truly universal in its capacity to complete any algorithmically defined task.

The von Neumann architecture has the principle advantage of clarity from the engineering perspective. Reduction in the physical size and increased areal density of electronic components directly scales up performance in terms of increased bytes of storage and processor cycles per second. The extension of this trend toward biologically inspired or artificially intelligent computation has resulted in attempts to simulate every neuron in the mammalian cortex and to outperform human experts in games of strategy [161, 162]. These achievements, while impressive, are not readily scalable due to the basic constraints of the CMOS architecture, its associated methods of fabrication, and the limits of its operational mechanism [163]. Further, the requisite passage of program instructions and data between processor and memory has evolved as a speed-limiting step known as the “von Neumann bottleneck” (vNB) [164] (Figure 6-1a), which results in idle processor cycles and power dissipation as information is simply being transferred, not processed. In combination, these factors generate a computational architecture that consumes orders of magnitude more space and energy than intelligent biological systems.

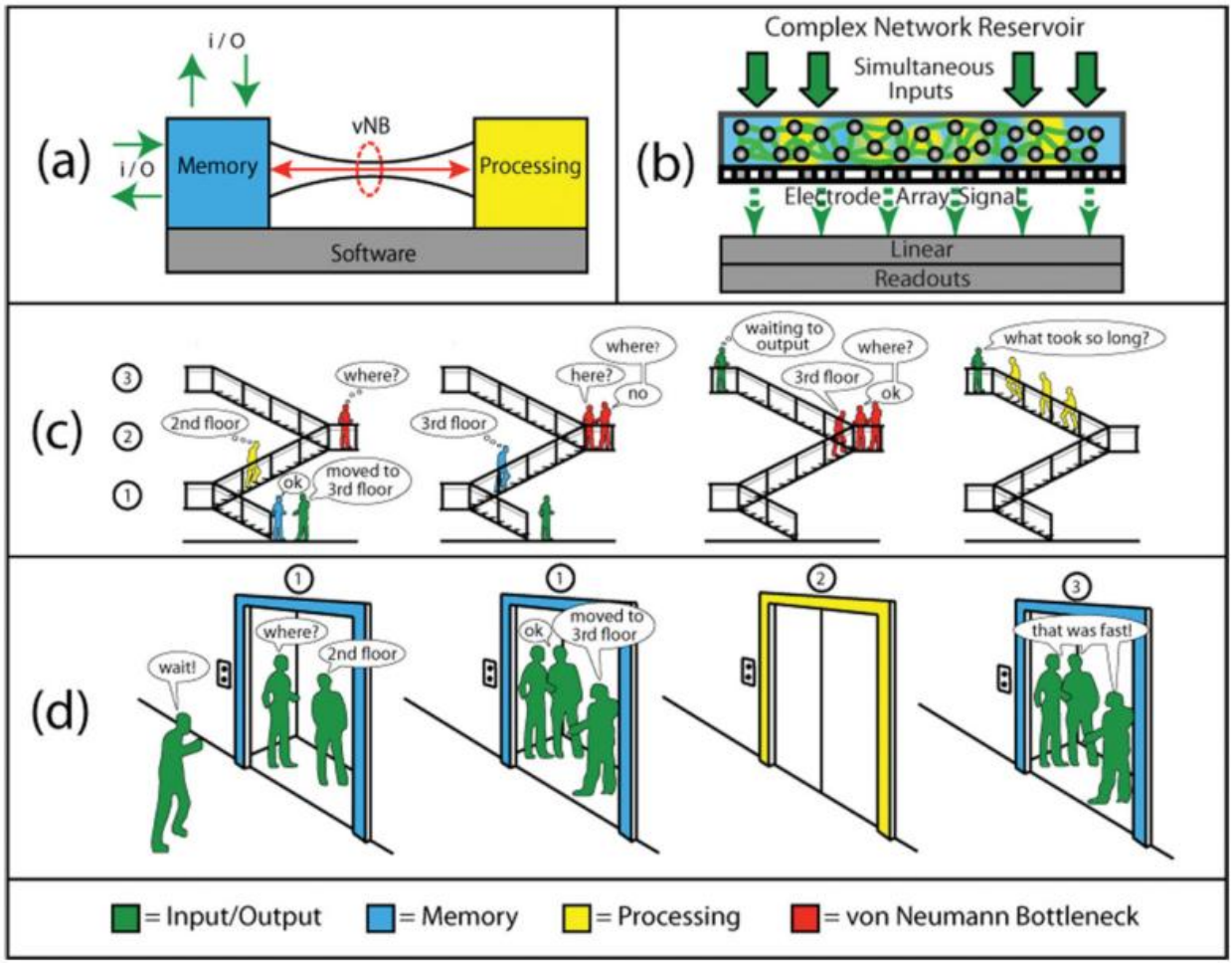

Figure 6-1. Comparison of computation using Turing automatic machines (TAM) and Turing B-Type unorganized machines (TBTu)/Complex Network Reservoirs (CNR). (a): Conventional TAM computation suffers from the intrinsic von Neumann bottleneck (vNB), as instructions and data must be shuttled back and forth between memory and processor cores. (b): TBTu/CNR computation transforms simultaneous input streams into a higher dimensional forms/patters that are converted to intelligible outputs by a linear classifier, which can be readily trained to detect various categories of CNR behavior. (c) As calculations proceed sequentially in TAM (yellow figures), new input is delivered to memory (blue and green figures, respectively). Earlier processes are unable to produce desired output due to outdated instructions and must idle in the vNB (red figures). Upon the arrival of new instructions from memory, calculations can resume and proceed towards the output (green figure on third floor). (d) In TBTu/CNR computation, inputs combine simultaneously to fill the waiting elevator. This process is more time consuming (it is a slow elevator!), but upon arriving at the third floor (output), they have undergone a complex transformation, having spent time interacting to create a new state of the system.

While current state of the art approaches to computation represent tremendous progress in performance and efficiency versus their historical counterparts, computer scientists have drawn inspiration from biology in an effort to develop computational strategies that are able to match the capabilities of biological neural networks (BNN). Remarkably, such concepts were proposed

over sixty years ago as Turing's “B-Type unorganized machine (TBTu)” [165], and have been subsequently popularized by Rosenblatt's perceptron, recurrent neural networks, and reservoir computing [112, 142, 152, 166-170]. These bio-inspired designs are generally associated with the notion of “connectionism”. Connectionist theories are based on complex networks composed of simple units, which, as a whole, produce emergent behavior not found or associated with any particular unit [13]. What constitutes a “complex system” is difficult to define precisely. However, extensive studies of complex, real-world networks have revealed the importance of both structural topology and internal dynamics. Various models of connectivity and interaction have been shown to accurately describe phenomena ranging from relationships between corporate directors to the backbone of the Internet [108].

To date, artificial realization of connectionist architectures has been limited by the capacity to fabricate robust interconnects between electronic components in a cost-efficient manner, especially in designs utilizing unconventional topologies. Recent advances in nanoscale science and technology have enabled the direct self-assembly and integration of functional circuit elements within the wiring scheme of nanoscale devices with the unique architectures [27, 73, 149, 164, 171]. Here, we utilize these concepts to construct a densely interconnected network of synapse-like memristive atomic switches using bottom up self-assembly. We find that this system demonstrates some of the emergent behaviors commonly observed in biological neural networks [23, 129, 172-174]. These complex atomic switch networks provide as a promising new direction for the development of functional TBTu-inspired neuromorphic computing devices, with specific implications toward physically implementable reservoir computation.

6.2 Computational models

Building upon decades of inspired research based in the TAM/von Neumann computational paradigm, modern processors routinely include multiple cores and large memory caches to maximize efficiency by parallelizing computations and reducing memory access times. In addition to physical limitations on component size and the vNB, leakage currents through gate dielectrics, programming challenges in parallel processing, and intolerance to faulty elements have begun to impact performance. These obstacles provide strong motivation to develop and implement alternative computational strategies. To this end, numerous theories and proposals have been put forth toward biologically inspired, neuromorphic computing devices [25].

Biological neural networks utilize self-configuring, hardware-based architectures capable of dynamic topological alteration and function without the need for pre- programming or an underlying software algorithm. These intrinsically nonlinear, complex systems demonstrate extraordinarily efficient transmission of information and emergent behaviors commonly associated with intelligence such as associative memory, learning, and predictive capacity in non-deterministic environments. One related theoretical construct, the TBTu, was conceived of as a randomly interconnected network of nothing more than modifiable NAND logic gates. Since NAND gates may be combined to perform any other logic function, Turing hypothesized that a sufficiently large network could serve as a usable computer, capable of any TAM operation [29]. Moreover, he showed that its connections and operations could be trained over time to alter its behavior, in a similar fashion to that of a biological brain.

This concept has been applied in the fields of systems neuroscience and artificial intelligence to form the basis of contemporary research into artificial neural networks (ANN). These ANNs are typically implemented as software running on conventional TAM systems, mimicking information processing in natural systems. The earliest ANNs, commonly known as

the “perceptron”, utilized a feed-forward design in which artificial neurons are connected by modifiable synaptic weights and can ‘learn' to map input-output relationships according to any (mathematical) function [152]. The development of recurrent neural networks (RNN) enabled the inclusion of adaptive capacities through feedback strategies [112]. The existence of cyclical connections makes the RNN a dynamical system, capable of sustaining internal activity in the absence of additional signals, not merely mapping input to output. However, basic RNN training strategies still involve the direct modification of internal synaptic weights implemented abstractly using algorithms inspired by biological neural networks. In addition, ANNs are generally designed and optimized to perform specific computational tasks, occasionally utilizing purpose-built hardware for increased functionality [175]. This enhanced performance comes at the expense of flexibility, adaptability, and the capacity to synthesize multiple time- varying input signals or to operate in a non-deterministic fashion–all hallmarks of biological neural systems.

Reservoir computation (RC) is a promising extension of RNNs towards more accurately modeling biological neural networks that has been successfully implemented in various engineering applications [142, 166-168]. Instead of tracking and modifying individual synaptic weights, the complex network of artificial neurons is treated as a kind of “black box” which is dynamically modified by the input and retains some (fading) memory of previous input signals. The complex network reservoir (CNR) acts to map these lower-dimensional input signals into a higher-dimensional space, represented by patterns in the state of the system and contains temporal information through integration of the input history. Poised between simply periodic and wildly unpredictable oscillations, the CNR operates at the edge of chaos [176].

This approach overcomes the challenge of training individual synaptic weights inside RNNs by not explicitly modifying them at all. Instead, a separate readout/output function is trained to examine the response of the reservoir, interpreting the spatiotemporal patterns formed by the collective effect of the input signals and transforming this higher-dimensional information into the desired output. Through appropriate training, RC methods are capable of simulating any Turing-type computational machine. Since the reservoir functions autonomously, multiple linear readout functions can be used simultaneously, thereby allowing the system to carry out multiple computational tasks on the same input stream in real time [167, 168].

While simulation and modeling efforts implemented on traditional computational architectures remain the general, near-term focus of reservoir approaches, calls for the development of hardware-based CNR systems continue to form the basis for inquiry into a new paradigm of computational methods. Achieving these goals requires the development of physical systems whose properties mimic those of artificial, simulated reservoirs as well as a means to harness the power of information-rich output patterns they generate. We propose that the former can be achieved by applying the concept of Turing's connectionist networks to the fabrication of complex device architectures consisting of highly interconnected, nonlinear electronic elements. A near-infinite set of internal system states capable of receiving/storing information from parallel input streams is necessary to combine complex, dynamic signals into a single, higher-dimensional output. This property is characteristic of systems operating in a critical state, a hallmark of complex networks of nonlinear elements, where the divergence of the system correlation length in both space and time provides all these requisite characteristics [5, 13].

6.3 Complex device architectures

The structure and activity of the biological brain is intrinsically complex, comprised of billions of neurons interacting recurrently through trillions of synaptic interfaces by utilizing a range of signaling chemicals to produce excitatory and inhibitory changes in electro-ionic conductivity. This dynamic, evolving system produces emergent phenomena with which we are intimately familiar such as consciousness, intelligence, learning, and prediction. The realization of hardware-based neuromorphic networks requires the ability to fabricate highly interconnected, complex wiring architectures with integrated circuit elements whose nonlinear properties emulate those of biological neurons and synapses.

Fabrication of micro- and nanoscale devices with complex architectures, especially those with some degree of random structural topology, is difficult using solely lithographic methods due to challenges in forming robust intra- and interdevice connections in a cost-efficient manner. However, combining directed and self-assembly of nanoscale building blocks into functional device components offers a promising route to creating intricate patterns of nanoscale components. To create operable devices based on nanoscale architectures, two basic issues must be addressed: which materials to use and how to pattern them into networks that have some degree of randomness without negatively affecting their functional characteristics.

Simple metals continue to be the material of choice for wires and interconnects in the fabrication of electronic devices. The power-law relationship known as Rent's Rule formalized the trend between the number of connections in integrated circuit designs and the number of internal components, such as logic gates, and how these are strongly related to both logical capacity and complexity of the interconnect architecture. This relationship infers that the limits on synthetic complex architectures lies in the cost of fabrication, with specific focus on interconnect and wiring strategies [48, 49]. Research has shown that biological neural systems

also obey this relationship [50]. Whereas biological networks realize a balance of cost and complexity through structural self-similarity and hierarchical modularity, ANN implementations based on TAM/von Neumann architectures remain at the mercy of this "cost of wiring". While motivating the creation of bio-inspired devices, Rent's Rule further underscores the fact that new methods, differing not only in scale but also in kind, must be developed to meet these challenges. Solution phase electrochemistry offers an intriguing approach to the unconventional fabrication of complex metallic structures. In particular, the electroless deposition of various metals through the spontaneous reduction of soluble metal cations is a mature technology that has been employed extensively in macroscopic plating applications and the manufacture of printed circuit boards (PCBs). In contrast to plating applications, dendritic (fractal) growth processes have been studied extensively for various reasons [51, 52, 97]. Unwanted, spontaneous growth of dendritic metal protrusions through insulating layers has posed an engineering challenge as the resulting electrical shorts lead to device failures. In a more positive light, interest in these intricate structures generated insightful mechanistic models, such as diffusion-limited aggregation (DLA), that were tested and confirmed through comparison of simulated structures to physically produced metallic silver fractals by reducing controlled concentrations of Ag^{+} using seed metals such as copper and zinc.

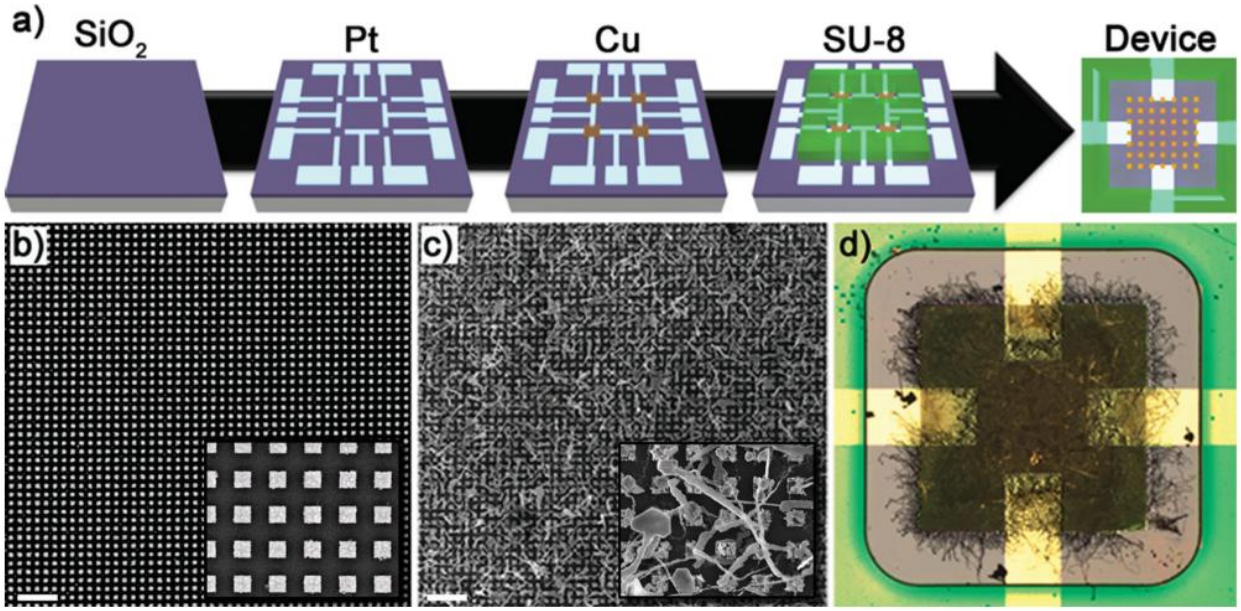

Figure 6-2. Fabrication scheme for complex, electronic networks. (a) Schematic of the substrate/device microfabrication through various lithographic techniques. (b) Cu seed posts (1 μm^2, 1 μm pitch, 300 nm height) deposited onto the substrate by electron beam lithography react with $AgNO_3$ within a reaction well formed from SU-8 epoxy photoresist, (c) resulting in electroless deposition of complex Ag nanowire networks. (d) The network extends throughout the device well and is electrically probed via macroscopic Pt electrodes.

Here, the electroless deposition process has been extended to produce devices with complex architectures possessing both regular and random features by combining top-down directed patterning of seed materials at the microscale with bottom-up self-assembly of functional nanomaterials. Lithographic patterns of metallic copper were reacted with dilute solutions of silver cations to create complex networks of metallic silver nanostructures (Figure 6-2). Optimization of this process enabled the controlled production of structures ranging from extended nanowires to dense fractals, similar to biological neural assemblies such as axons and dendrites [123]. Spontaneous generation of nanogaps between these as-prepared metallic nanostructures has been attributed to ionic depletion in the interfacial regions, due to the DLA growth mechanism. In addition, the formation of nanowire crossbar-like junctions resulted from the three-dimensional nature of the solution deposition process. By combining this wiring

approach with compatible materials that demonstrate synaptic properties, we have generated a complex network of randomly distributed, highly interconnected inorganic synapses.

6.4 Synthetic Synapses

Performing distributed, real-time computation of complex information requires suitable electronic device elements capable of mimicking salient aspects of biological synapse function at the relevant physical scales. Recent research has developed a vast catalogue of nonlinear, solid-state electronic elements for use in integrated circuits and solid-state memory. A class of these, known as hysteretic resistive (memristive) switches, has received substantial attention as a synapse-like element for use in next generation neuromorphic computers. Resistive switches (RS) are two-terminal circuit elements that are distinguished from simple resistors by nonlinearities in the relationship between current and voltage across their terminals [124]. These nonlinearities, generically referred to as memristance, can take various functional forms, from a smooth dependence on the time integral of current passed through the device, to discontinuous jumps at some threshold value, or combinations thereof [33]. The resultant nonlinear dynamics can produce behaviors typically associated with biological neural networks, including long-term potentiation, long-term depression, spike timing dependent plasticity, and associativity [41, 43, 177, 178]. The basic RS is a nanoscale device composed of a metal-insulator-metal (MIM) junction that can be fabricated using a variety of materials.

An exciting subset of electro-ionic RS known as atomic switches exhibit common RS characteristics including pinched *I–V* hysteresis and large ON/OFF switching ratios as well as more exotic behaviors such as multistate switching in quantized increments of conductance [39]. The distinguishing feature of the atomic switch as compared to other memristive systems is its operational mechanism: atomic switches utilize metal filament formation/annihilation and a

concurrent bias-catalyzed phase transition within a solid-state electrolyte metal-insulator-metal (MIM) interface. One prevalent atomic switch configuration employs MIM interfaces of silver and silver sulfide (Ag_2S). This chalcogenide undergoes a temperature-dependent and bias-catalyzed transition from the monoclinic, semiconducting α-Ag_2S phase (acanthite, $2.5 \times 10^{-3} \Omega^{-1} cm^{-1}$) to a body-centered cubic, metallic β-Ag_2S phase (argentite, $1.6 \times 10^{3}\ \Omega^{-1} cm^{-1}$) [40]. The argentite phase has a remarkably high diffusion coefficient for silver, approximately equal to that of gaseous silver atoms at an equivalent temperature and density. Under applied external bias, this formulation operates via redox coupled ion migration of silver ions within the metallic argentite phase. While some RS are strictly non-volatile, the Ag-Ag_2S atomic switch exhibits nonlinear, time-dependent conductance that has lead to the observation of a number of fascinating synapse-like properties including short- (volatile) and long- (non-volatile) term memory [41, 43]. Robust operation of these devices at rates up to 1 MHz over 10^5 cycles further enhances their potential applicability as a synthetic synaptic element.

To date, atomic switches have been primarily fabricated through advanced lithographic methods in regular, crossbar-type architectures that are promising candidates for nanoscale memory applications when operated in isolated, single device configurations. However, their operational characteristics are less well understood when connected in series, parallel, or directly coupled through their ionically conductive active layer, as would be required to implement computation in the TBTu/CNR paradigm. Inspired by the exciting synaptic properties of the Ag|Ag_2S|Ag atomic switch configuration and its and material compatibility with our scheme for fabricating complex nanowire networks, we have characterized the properties of interconnected atomic switches as a means to examine their potential applicability as physical implementations of TBTu/CNR-based computation.

6.5 Critical atomic switch networks

Complex networks of coupled nonlinear elements commonly manifest non-trivial evolution through dynamic system reconfigurations [40, 179] which enable enhanced maintenance of spatiotemporal correlations and maximally efficient signal propagation [108]. These features are associated with systems in critical states, and are crucial to the proposed implementation of hardware-based TBTu/CNR-inspired machines. We have fabricated and examined the operational characteristics of an electroionic device composed of a highly interconnected network of interfacial atomic switches wired through electroless self-assembly. Formation of the complex atomic switch network entailed conversion of as-prepared metallic nanogap and crossbar-like interfaces into metal-insulator-metal (MIM) junctions ($Ag|Ag_2S|Ag$) through gas phase sulfurization [53]. Due to the nature of the electroless deposition process and resulting random network topology, a thorough survey of sulfurization conditions was carried out to optimize the fabrication protocol.

Progressing from isolated, individual synthetic synapses to an assemblage of electro-ionically coupled units introduces an extensive set of collective interactions capable of producing emergent behaviors. Spatially distributed atomic switch junctions interact through local variations in ionic concentration and electrochemical potential that depend on the combined electrical resistance of the entire network and the memory-dependent state of all other electro-ionically interconnected switches. Dynamical complexity is expected given that atomic switch synapses are volatile memrsitive systems that exhibit a conductance decay time constant dependent on their operational history [34, 43].

To examine these properties, atomic switch networks were investigated by *I*–*V* spectroscopy. In common with isolated crossbar-type devices, as-fabricated atomic switch

networks required an initial forming step during which a sustained, high (~6 V) bias would bring about a large but temporary drop in resistance. While parameters of the forming step varied from device to device, this requisite step indicates the successful preparation of MIM interfaces within the network. After forming, slow voltage sweeps (1 $V \cdot s^{-1}$) resulted in pinched hysteresis curves (Figure 6-3a) with an ON/OFF ratio of 10^3, further validating the formation of a functional atomic switch network with behavior analogous to that of a two-terminal RS device. Repeatable switching was observed over 10^4 cycles, and was successfully operated up to a 1 kHz switching rate. Conditions of no applied bias resulted in a return to the OFF state, as expected from the operational mechanism of this particular $Ag|Ag_2S|Ag$ configuration. Un-sulfurized control devices comprised of a purely metallic network demonstrated ohmic *I–V* characteristics at intermediate voltages (±3 V) followed by irreversible breakdown at high bias.

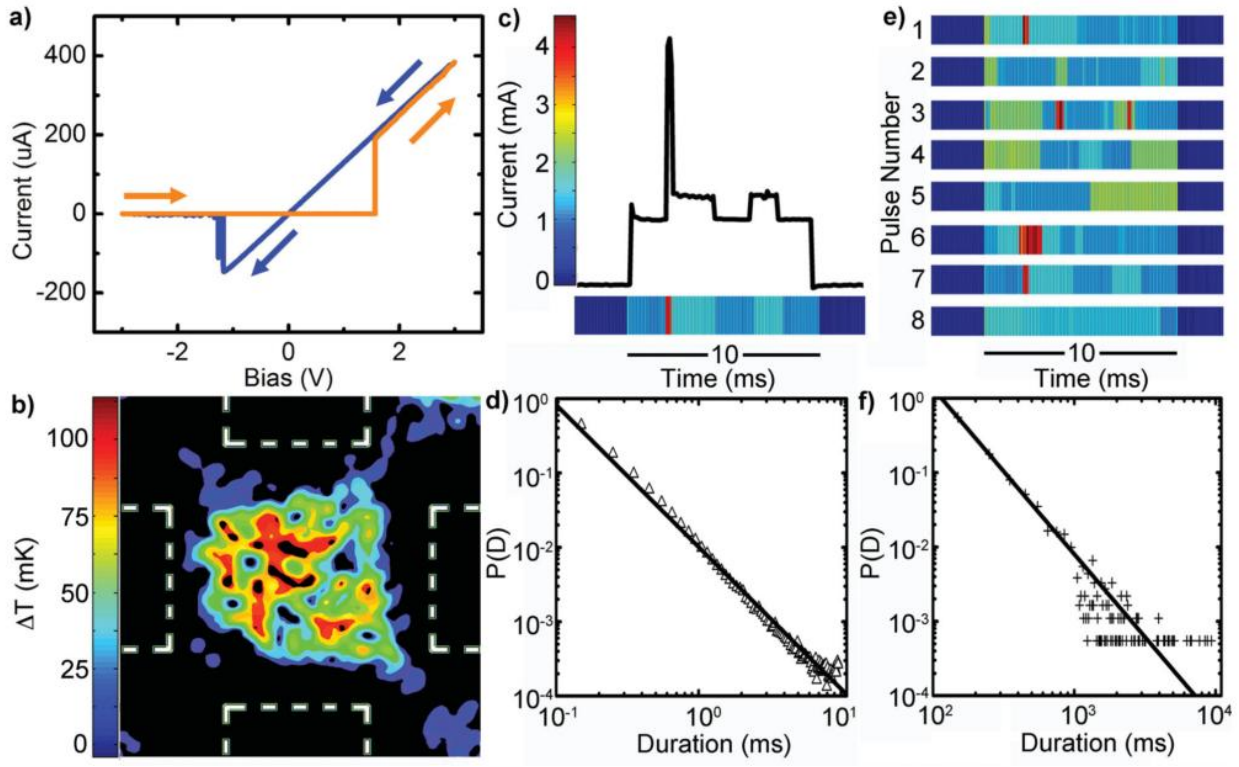

Figure 6-3. Electrical characteristics of complex nanoelectro-ionic networks. (a) Experimental *I–V* curve demonstrating pinched hysteresis; R_{ON} = 8 KΩ, R_{OFF}> 10 MΩ. (b) Ultrasensitive IR image of a distributed device conductance under external bias at 300 K; electrodes are outlined in white. (c,e) Representative experimental

network current response to a 2 V pulse showing switching between discrete, metastable conductance states. (d,f) Temporal correlation of metastable states observed during pulsed stimulation demonstrated power law scaling for probability, P(D), of metastable state duration. Power law scaling existed for residence time both (d) within a single 10 ms pulse and (f) over 2.5 s during extended periods of pulsed stimulation.

To rule out the possibility that network activity was simply the result of conductance localization along a dominant pathway, creating in essence a single large, serial atomic switch, the device was characterized using ultrasensitive IR imaging at room temperature (Figure 6-3b). These results revealed thermal emission from Joule heating throughout the network, indicating distributed and dynamic power dissipation during operation. Further, the application of spatially-defined voltage stimulation enabled controlled activation/deactivation of local regions within the network while enhanced overtones in the device frequency response were also observed [73] as predicted by recently reported modeling of current flows in random memristor networks stimulated with a sinusoidal voltage [79]. These results collectively indicate the successful formation of an interconnected network of nonlinear elements, in this case atomic switches.

Emergent behavior was observed during pulsed voltage stimulation, in analogy to methods employed in neuroscience to probe cortical cultures. Under typical conditions (2 V, 10 ms pulses, 10% duty cycle), the current response fluctuated through a wide range of metastable conductance states associated with discrete network configurations (Figure 6-3 c–f), as classified by residence times in a given state ranging from milliseconds (within a single stimulation pulse) to several seconds (across hundreds of pulses). Specifically, all conductance states whose persistence time exceeded that of the measurement bandwidth (10 kHz) were designated as temporally metastable. Observation of both increased and decreased conductivity during stimulation can be attributed to internal network dynamics, as conductance of isolated atomic switches only increases in response to sequences of identical stimulation pulses [39, 41, 43].

Previously unreported current fluctuations of this kind are ascribed to dynamic redistribution of network connectivity caused by actions of both individual switches as well as electro-ionic coupling throughout the shared active layer. Specifically, formation of a conducting filament results in localized depletion of silver cations within the solid electrolyte and thereby inhibits the formation of filaments at nearby MIM interfaces. Due to the high diffusion constant of Ag^+ in the β-Ag_2S, this non-stoichiometric region may extend relatively large distances and induce weak electro-ionic coupling even between distant switches. Furthermore, concurrent formation and annihilation of conductive filaments will redistribute current flow, thereby modifying local electrical potentials across the network. These local variations sum to produce the observed fluctuations in global network conductance. While direct mechanistic confirmation of the observed conductance fluctuations would be useful, the inferred mechanism proposed here provides a rationale for future optimization of the network architecture.

Critical dynamics are of ultimate importance for applications of TBTu/CNR-based computation. Indicators of criticality typically include power-law scaling of $1/f$ fluctuations and temporal metastability. Analysis of the power spectral density of network conductivity in the activated state revealed $1/f$ power law scaling over five orders of magnitude [73]. Electro-ionic coupling within the atomic switch network generated metastable conductance states, which were analyzed for temporal correlations. Comparing the probability of state duration with its likelihood indicated a power law distribution (Figure 6-3 c–f), indicating a diverging temporal correlation length. Observations of both spatially distributed electro-ionic activity within the network and the long-term persistence of metastable state residence times alongside short-term, rapid fluctuations between many available conductance states are strong indicators of critical system dynamics during intermittent pulse operation. These metastable conductance states

represent unique configurations of the network and infer behavior similar to those of spatiotemporal states associated with neural dynamics and those required by reservoir computation models.

6.6 Outlook and perspectives

The value of exploring new paradigms in computation cannot be overstated, as the challenges of moving "beyond CMOS" undoubtedly provide inspiration and motivation for the next generation of scientists and engineers. Likewise, elucidating the fundamental nature of intelligence remains a question for the ages in fields spanning all of human endeavor. Drawing on a historical perspective of seminal developments in computer science, complex systems theory and neuroscience, we have set out to propose a hardware-based approach to neuromorphic computation that aims to harness the power of highly coupled, nonlinear systems. We feel that the perspectives and results described herein represent a potentially important link between the requirements for real-time, multi-sensory computation and ongoing advances in neuroscience through a readily addressable physical system with collective behaviors analogous to those currently observed in biological neural networks.

Research into applications of artificial neural networks toward biologically inspired computation has been greatly facilitated by modern developments in neuroscience. Recent findings have shown biological neural networks to operate in a persistent critical state, a feature commonly associated with the critical point of a second-order phase transition and power law scaling of internal system dynamics [19, 180]. Under such circumstances, the system correlation length diverges in both space and time, indicating that the influence of past events decays slowly and physically distinct points within the system are coupled regardless of the magnitude of separation. Spatiotemporal correlations of this type have been shown to maximize memory,

transmission of information, and adaptability within complex networks, such that each part of the system is communicating with every other part of the brain, for every time of its history. A class of critical systems emerge from coupled networks of nonlinear elements governed by threshold dynamics that relax quickly compared to a slower external driving force, an arrangement that allows these systems to settle into a range of correlated metastable states. This model is more than superficially reminiscent of our current understanding of neural dynamics, and has been employed in recent forms of advanced neural network research including, but not limited, to reservoir methods such as liquid state machines and echo state networks.

To our knowledge, the self-assembled atomic switch network described here represents a unique implementation of a purpose-built electronic device composed of coupled nonlinear elements that clearly demonstrates critical dynamics. We propose that such a system provides a robust, flexible, and scalable experimental platform for controlled examinations of criticality and its potential applicability in the fields of neuroscience and neuromorphic computation. Further, the inherent properties of single atomic switches and emergent behaviors observed in these complex atomic switch networks indicate a capacity for memory and learning via temporally correlated, metastable critical states [181]. Such an approach has potential utility for real-time, reservoir computation of multi-domain data systems such as those used in autonomous locomotion, proximity sensing and global positioning as well as a wide variety of sensing applications. Technological trends toward the growth of multi-domain and distributed sensing systems represent the seminal challenge for new forms of emerging computation in the centenary of Turing's birth.

7. A theoretical and experimental study of neuromorphic atomic switch networks for reservoir computing

Abstract

Atomic switch networks (ASNs) have been shown to generate network level dynamics that resemble those observed in biological neural networks. To facilitate understanding and control of these behaviors, we developed a numerical model based on the synapse-like properties of individual atomic switches and the random nature of the network wiring. We validated the model against various experimental results highlighting the possibility to functionalize the network plasticity and the differences between an atomic switch in isolation and its behaviors in a network. The effects of changing connectivity density on the nonlinear dynamics were examined as characterized by higher harmonic generation in response to AC inputs. To demonstrate their utility for computation, we subjected the simulated network to training within the framework of reservoir computing and showed initial evidence of the ASN acting as a reservoir which may be optimized for specific tasks by adjusting the input gain. The work presented represents steps in a unified approach to experimentation and theory of complex systems to make ASNs a uniquely scalable platform for neuromorphic computing.

7.1 Introduction

Synapses play an essential role in cognitive function. Brain activity is characterized by spatio-temporal varying electrical signals travelling through a vast interconnected recurrent network of neurons, where the synapses mediate signaling. Until recently, research has tended to focus on an approach that promulgates that advances beyond complementary metal–oxide

semiconductors (*beyond-CMOS*) computation [182] may be achieved by fabricating electronic elements that recreate the fundamental behaviors of neurons and synapses [25, 183]. Accordingly, new generations of synthetic synapses have been demonstrated or modeled which display short- and long-term potentiation/depression (STP, LTP and LTD respectively), spike timing dependent plasticity, and other neuroscientific phenomena [150, 184]. These devices have been incorporated into hybrid-CMOS/molecular-CMOS [28, 184] circuitry with the aim of recreating synaptic spiking patterns typically realized with crossbar array geometries for optimized memory storage [44, 45, 47, 57, 185-189]. The architecture of the arrays is designed to address each functional element individually and sequentially in a programmed fashion, essentially precluding the elements from interacting within a network. However, actual complex systems exploit the non-trivial effects of interconnectivity [6, 108] that allow individual units to function in synchrony over multiple spatial and temporal scales resulting in self-organized patterns of activity [19, 23, 145, 174, 190]. Consequently, emergent phenomena are distributed throughout the entire system and cannot be associated with any particular node or local group [13, 20, 139]. In the brain, modification of these intricate networks is believed to form the basis of memory, motor pathways, and cognition [140, 191-193].

Through a combination of top-down and bottom-up fabrication techniques, highly interconnected wire networks containing synaptic functional units have been fabricated and studied [73, 77]. These atomic switch networks (ASNs), composed of more than 10^9individual inorganic synapses cm^{-2} [41, 43, 194], i.e. atomic switches [39], represent a unique class of physical devices capable of exhibiting synapse-like properties in neurally inspired architectures. Interfacing functionalized networks with multielectrode arrays offers the ability to harness intrinsic system dynamics through input and read out of real-time electrical signals at various

spatio-temporal scales toward practical implementation of neuromorphic computation [73, 77]. ASNs retain the adaptive plasticity and memory of their component atomic switches while exhibiting emergent properties such as criticality and spontaneous switching between discrete metastable resistance states.

Most attempts to mimic the brain's function use simulated neural networks. Recurrent neural networks consist of nodes, each with an adjustable connective weight, and allow signals to propagate forwards and backwards through the network [195]. Such structure allows information to be integrated at different time points, enabling online training. The main drawback of recurrent networks remains the difficulty of adjusting individual connective weights, which results in an inability to efficiently differentiate inputs or adapt to increasing noise levels in the environment [196]. The computational degrees of freedom are also too vast to permit convergence in a reasonable time.

Recently, reservoir computing (RC) was developed to overcome these issues, while retaining biologically relevant features such as feedforward and recurrent structures [142, 166, 168, 197-199]. RC is achieved through a two-step process. First, time varying input data are introduced to a fixed weight recurrent network or 'reservoir', in which the nonlinear action of nodes produces higher dimensional representations of the input data. This transformation permits the second step, where the new representations are read out through a feedforward network or 'linear readout'. Information that was not initially linearly separable can then be processed through simple linear regression techniques in the feedforward layer. Consequently, RC can perform complicated classifications in real time, and enables generalization of learned tasks. Currently, RC is the most effective technique available for certain tasks and has been realized in a variety of physical implementations as proof of concept [200-202].

ASNs were proposed as well suited to RC, because they contain a physically recurrent network of nonlinear elements which are amenable to serve as a reservoir while also exhibiting feedforward properties useful for the output layer [77]. ASNs also possess a readily scalable architecture, multiple spatio-temporal outputs, and synaptic nonlinear elements displaying critical dynamics. Consequently, ASNs are potential embodiments for enabling neuromorphic computational theories and represent physical neuromorphic devices that have a direct connection with neuroscience.

Understanding and harnessing the rich dynamics found in complex networks comprised of coupled nonlinear elements is challenging. In particular, practical engineering goals are based on stimulus–response relationships governed by internal system reorganization with minimal fine tuning at the microscopic level. Here we present a numerical model of ASNs which illustrates key aspects of the spatial and temporal dynamics of the system, and investigates their utility in the context of RC. Our simulation was built from the physical ASN devices: the design and implementation was based on the well-documented physics of single synaptic switches, and the connectivity was modeled on the known network architectures determined from SEM images. The goal of the simulation was to deepen our understanding of network function, optimize network design and explore the applicability of device architectures for neuromorphic computational tasks.

First, we validate the accuracy of the simulation by reproducing data from the devices such as controlled interconnect plasticity and emergent behavior, despite the simulation's much smaller network size. Second, we show that fluctuations in a simulated isolated single link are distinctly different from those of an identical link within the network. This highlights the role of the network where synaptic elements behave differently as a result of interconnectivity. The

simulation is also found to show emergent properties that are impossible to measure in a single device. Third, we show that higher harmonic generation reported experimentally [73] and theoretically predicted [79, 154] can be modeled and utilized for reservoir computing. We finally discuss the potential impact of ASNs as a unique physical embodiment that is capable of integrating neuromorphic architecture, dynamics, and computation.

7.2 Methods

The ASNs were grown using self-assembly of a rhizomic–dendritic network of highly interconnected silver (Ag) nanowires which were sulfurized to provide distributed nanojunctions comprised of inorganic synthetic synapses. The ASNs were interfaced to input–output electrodes fabricated using conventional micro-lithographic processing to create a functional device [73, 77] (Figure 7-1(a)). Electrodes were fabricated by electron beam evaporation following photolithography on the surface of a p-type Si wafer (boron doped, 0–100 $\Omega\ cm^{-1}$) insulated by a 500 nm thick thermal oxide layer. Deposition of 4–16 Cr/Pt (15/150 nm) electrodes with diameters of 10–50 μm at pitches between 50 and 500 μm was followed by spin-coating and patterning of an insulating layer of SU-8 deep UV resist, which served to expose only point contact regions of the electrodes. Micron diameter cylindrical copper seeds were then deposited at areal densities between 1×10^6 and 2.5×10^7 seed sites cm^{-2} for the electroless deposition (also referred to as galvanic displacement or cementation) of Ag from Cu on the SU-8 layer. Electroless deposition was performed under diffusion-limited conditions using 50 mM aqueous solutions of $AgNO_3$ [96]. This spontaneous electrochemical reaction produced the complex networks of metallic silver nanowires shown in Figure 7-1(b). Previous studies have shown that the geometry and spacing of pre-patterned Cu posts provides control over the global qualities of the network, generating structures ranging from extended nanowires to dendrites and

fractals [100, 123]. The pitch of the Cu posts was found to determine the relative density of the network (Figures 7-1(c), (d)) while seed size was used to control the presence of long-range connections. Typically, smaller Cu seeds (<3.5 μm) produce many long wires and larger seeds (>3.5 μm) produce spatially confined dendritic or fractal structures.

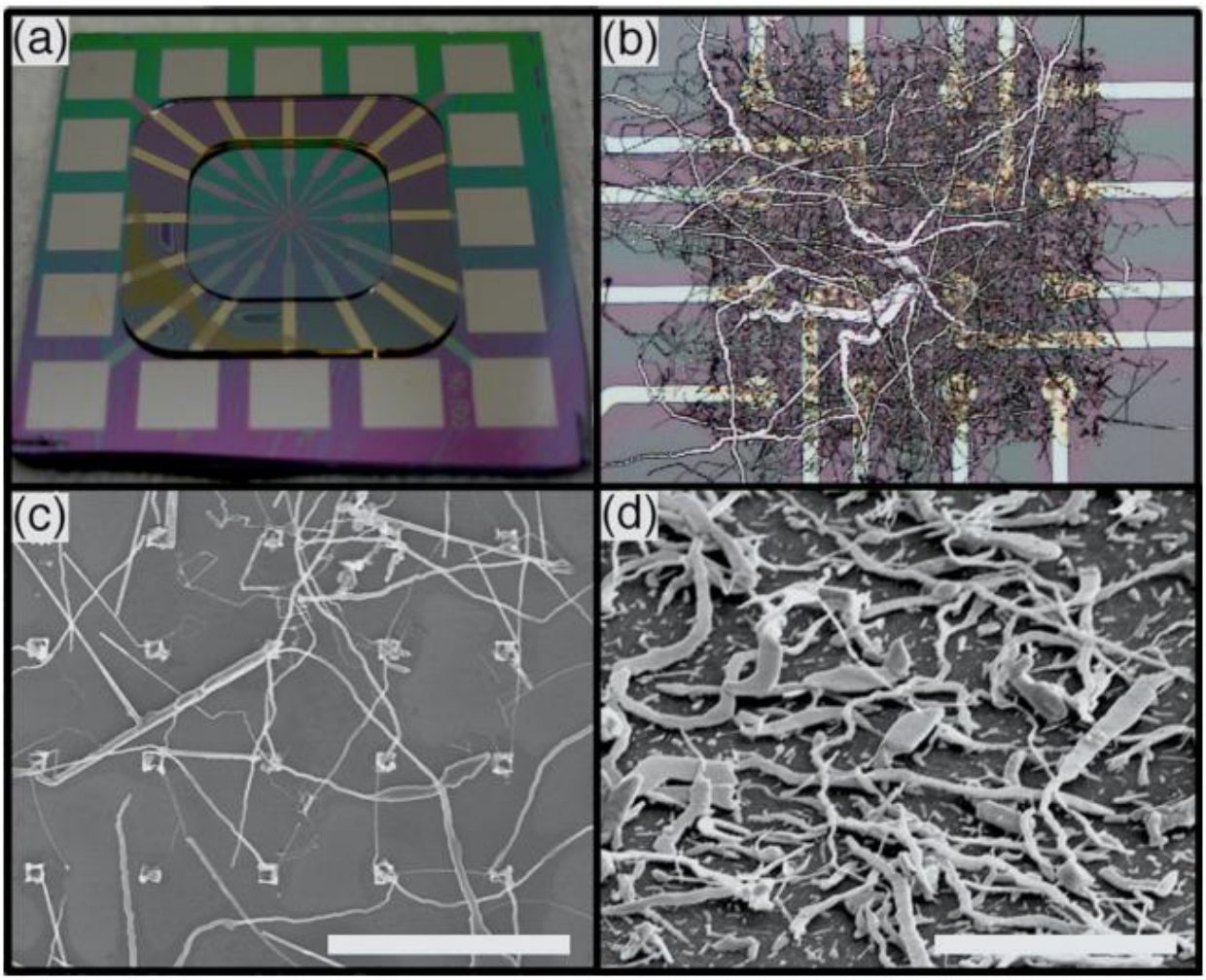

Figure 7-1. (a) Atomic switch network devices are fabricated on a SiO_2 substrate with 16 Pt electrodes and an insulating SU-8 layer. The devices are approximately 4 cm^2. (b) The resultant Ag wires vary in size (<100 nm to >1 mm) and create self-assembled networks with complex interconnections (10^9 cm^{-2}). The electrodes shown have 10 μm diameter and 50 μm pitch, and range up to 50 μm diameter with 500 μm pitch. (c), (d) The density of interconnections can be changed by altering the size/pitch of the Cu posts shown: (c) 1 μm/5 μm; (d) 1 μm/1 μm. Scale bars = 10 μm.

The self-assembled silver networks intrinsically contain crossbar-like junctions resulting from the three-dimensional nature of the solution deposition process. Upon exposure to sulfur gas [53] (10^{-1} Torr at 130 ° C for 3 min), the Ag nanowire junctions are functionalized to form thin Ag|Ag_2S|Ag metal–insulator–metal interfaces which, in the presence of post-processing activation with external bias potential, are transformed into 'atomic switches'. Electrical characterization of the devices was conducted through current–voltage (*I–V*) spectroscopy using a bipotentiostat (Pine Instruments model AFCBP1) in conjunction with either a data acquisition module (National Instruments USB 6259) or a multiplexed (National Instruments PXI 1073) source-measurement unit (National Instruments PXI 4130). The maximum bandwidth of the measurement systems was 1 MHz and 10 kHz enabling 2 Ms and 20 ks s^{-1} with 16-bit resolution. Subsequent data analyses were carried out using MATLAB 2010b (MathWorks) and Origin 8.1 (OriginLab Corporation).

Simulation efforts employed previously have reported physical properties of atomic switches composed of a Ag|Ag_2S|Ag interface, shown schematically in Figure 7-2, that exhibit both volatile and non-volatile memory properties as well as multi-state switching [39, 41, 43]. Atomic switches are known to operate through two mechanisms: (i) formation/dissolution of conductive filaments, and (ii) a phase transition between monoclinic acanthite (α) and body centered cubic argentite (β) Ag_2S. Application of a bias voltage across the junction induces the formation of nanoscale conducting channels across the Ag_2S interface through a bias-catalyzed phase transition, converting the surrounding α-Ag_2S matrix to a conductive and β-Ag_2S phase which exhibits high ionic mobility as illustrated by TEM-electron diffraction studies [40]. In the absence of continued applied bias, the conductive channels eventually return to their stoichiometric, thermodynamically favored equilibrium state, which reverts the atomic switch to

its initial high resistance. This transition gives rise to a weakly memristive behavior prior to the formation of Ag filaments across the interface.

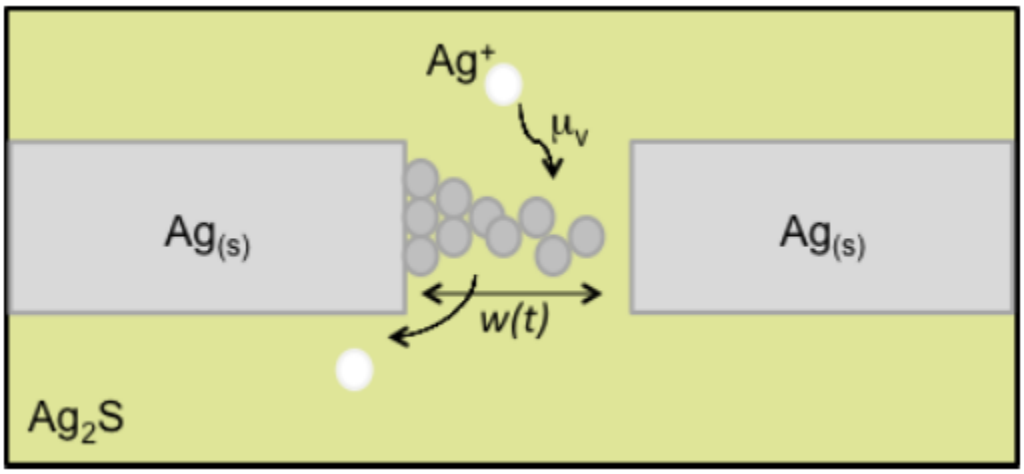

Figure 7-2. Atomic switches are comprised of a Ag|Ag_2S|Ag junction. Applied electrical bias causes Ag cation migration to the cathode where it is reduced, forming a stable metallic filament, resulting in resistance change. This migration is modeled by the filament length $w(t)$, Ag cation mobility μ_v, and additional stochastic terms.

Continued application of bias voltage results in a concurrent increase in current through the device, which then further drives migration of silver cations toward the cathode. At the cathode, mobile silver cations are subsequently reduced to Ag^0, forming a highly conductive Ag nanofilamentary wire. The completion of this filament results in a strong transition to an ON state with a dramatic increase in conductivity [40]. Removal of the applied bias results in filament dissolution as the device again returns its thermodynamic equilibrium state. The completion and dissolution of this filament characterizes strongly memristive behavior. Continuous application of a bias voltage serves to increase filament thickness as additional silver cations are reduced, causing thickening of the metallic filament. This dynamic process has been shown to alter the dissolution time constant, and can be externally controlled by changing the

input bias pattern (e.g. pulse frequency). Such changes in volatility can be interpreted as long-term or short-term potentiation (LTP and STP) [41, 43].

Using a similar construction, a recent report simulated a nearest neighbor grid of resistors and memristors [79]. Here, the memristive equations were augmented with new terms that reflect the known properties intrinsic to $Ag|Ag_2S|Ag$ atomic switches as well as network effects. The state variable of the memristive elements was chosen to be the length of the Ag filament, represented as $w(t) \in [0, w_0]$, where the junctions' gap sizes, w_0, were randomized with a mean of 5 nm according to known values [39, 41, 43]. The voltage across each atomic switch junction was given by

$$V(t) = \left[R_{\text{on}} \frac{w(t)}{w_0} + R_{\text{off}} \left(1 - \frac{w(t)}{w_0} \right) \right] I(t) \qquad (1)$$

where R_{on} and R_{off} represent the resistance values for the ON/OFF states of, and $I(t)$ the current across, the atomic switch junction. The rate of change in filament length was modeled according to

$$\frac{\mathrm{d}w(t)}{\mathrm{d}t} = \left[\mu_v \frac{R_{\text{on}}}{w_0} I(t) \right] \Omega - \tau (w(t) - w_0) + \eta(t) \qquad (2)$$

where μ_v signifies the ionic mobility [33, 36]. The window function, given by

$$\Omega = \left[\frac{w(t)(w_0 - w(t))}{w_0^2} \right] \qquad (3)$$

was included in (2) to incorporate the behavior of elements with state variables at the extreme limits due to ionic drift [36, 79]. The term $[\mu_v \frac{R_{\text{on}}}{w_0} I(t)] \Omega$ provided the dependence of the filament growth rate on the electronic flux, while $\tau(w(t) - w_0)$ operated as a dissolution term that

served to return the filament length to its original value w_0 due to the thermodynamic stability of the high resistance state. Although the dissolution rate constant (τ) has not been extensively investigated in the network setting, a numerical survey over three orders of magnitude (1–1000 s^{-1}) determined the value that best reproduced the prior experimental results for the size of the simulated network. Lastly, a stochastic term $\eta(t)$ accounted for fluctuations in the density of available silver ions and the stochastic nature of the filament formation/dissolution process in physical ASNs. This term, defined by

$$\eta(t) = \alpha(t)\Delta w(t) \qquad (4)$$

governed the growth rate of filament sizes, where $\Delta w(t)$ represented the change in filament length at time t reflecting the amount of electric flux through the switch junction. Here, the random variable $\alpha(t)$ introduced a noise factor to the term $\eta(t)$ that was distributed across the network following a random distribution centered at zero with a standard deviation σ_α. The probability distributions for bothw_0 and α were examined using simulated network sizes ranging from 3 × 3 to 10 × 10 arrays with varying degrees of connectivity density.

Finally, the connectivity in the simulation was modeled after the known interconnectivity of ASNs [77]. Physical networks are grown from copper seeds spatially distributed on the substrate, which serve as nucleation sites for the electroless deposition of silver metal under diffusion-limited conditions [123]. This directed self-assembly process generates networks with a large distribution of wire lengths, characterized by SEM in the range of 100 nm to over 1 mm. The networks contain elements of a nearest neighbor network, since the wires are likely to connect to those grown from nearby copper seeds (Figures 7-1(c)–(d)). They also exhibit

characteristics of a random network as long wires extend across the entire network, connecting distant nodes, and also connecting many nodes at once (Figure 7-1 (b)).

Connectivity in the simulation was created by starting with a square lattice of nodes, mimicking the copper posts in the hardware design. Links connecting nearest neighbors as well as distant nodes were then assigned randomly, with the total number of connections ranging from $N = 50$ to 400. The simulation results reported here represent the typical network response observed with connections reassigned for each run. Finally, the values of the physical parameters such as ionic mobility, R_{ON}/R_{OFF} ratio, and average gap size were chosen according to experimental literature values as schematically illustrated in Figure 7-2 [39, 41, 43], leaving only the network size and wiring density as free parameters. Table 7-1 summarizes the range of the values of the parameters explored to produce the results in this report.

w_0 (nm)	μ_v ($m^2\ s^{-1}\ V^{-1}$)	R_{on}/R_{off}	τ (s^{-1})	α	N
Ave: 5 σ_{w_0}: 0–40%	0.5×10^{-12}	Ave: 10^{-1}–10^{-3} $\sigma_{on/off}$: 0–40%	1–10^3	Ave: 0 σ_α: 0–30%of $\Delta w(t)$	50–400

Table 7-1. Parameters used in the simulation were tested over ranges that are physically relevant to the atomic switch network system: total gap width (w_0); ionic mobility (μ_v) of Ag^+ in Ag_2S; ratio of resistances (R_{on}/R_{off}) at $w = 0$ and $w = w_0$; filament dissolution rate constant (τ); modulation (α) level of noise in the $w(t)$ term with each time step; and total number of connections (N).

Network simulations were executed in MATLAB through a graphical user interface (GUI) that provides control over these parameters in addition to the locations and numbers of sources/drains, structure of input waveforms, and magnitude of input signals. The GUI also provides direct monitoring of simulated *I–V* statistics as well as the current, power dissipation and conductivity of each link within the simulated network.

7.3 Results and discussion

Various studies were carried out under conditions similar to the physical implementations in order to compare the numerical model's results with prior ASN device experiments [77]. Results from these simulations were examined in the context of network complexity on the basis of the underlying device physics and their associated emergent properties. The simulation was then used to explore the parameter space of ASNs, establishing a systematic approach to optimize network performance in the context of given training schemes and computational tasks.

Robust, hysteretic switching in ASN devices requires device activation by a symmetric triangle wave ramp applied across the network. As net flux through the network increases, connections become increasingly polarized and conductive, resulting in different behavioral regimes (insets of Figures 7-3(a)–(c)). A lack of completed metal filaments characterizes the initial state in Figure 7-3(a) (inset) as the 'soft switching' regime. Continued sweeping causes the formation of a continuously conductive path across the network, with intermediate connections operating in a higher conductance state. This transition is observed as a dramatic change in conductance, shown in the inset of Figure 7-3(b), where network response changes from 'soft' to 'hard switching' as the fraction of strongly memristive elements increases past the percolation threshold [77]. Continuous sweeping of the applied bias is known to encourage thickening and stabilization of as-formed nanofilaments [39, 41, 43], producing behavior that is robust to fluctuations in silver ion deposition/dissolution (Figure 7-3(c) inset). As a result, there is an increased likelihood for an element in the network to operate in the strongly memristive regime.

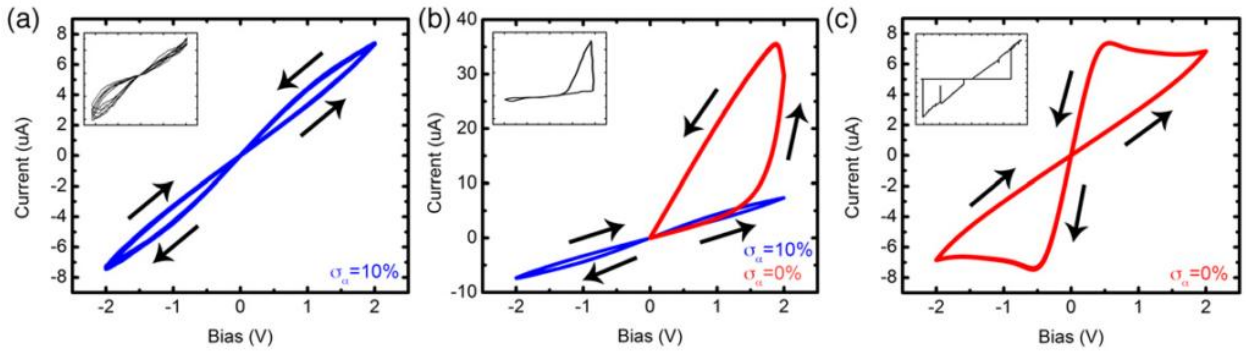

Figure 7-3. Simulation of device activation using a 10 × 10 network with $N = 126$, average $R_{on}/R_{off} = 10^{-2}$ and $\tau = 10\ s^{-1}$ under a triangle wave input bias of ±2 V at 10 Hz, demonstrating (a) an initial soft switching ($\sigma_\alpha = 10\%$) repeated indefinitely, until (b) a transition in behavior from soft (blue, $\sigma_\alpha = 10\%$) to hard (red, $\sigma_\alpha = 0\%$) switching. (c) Hard switching persists indefinitely with $\sigma_\alpha = 0\%$. This behavior was ubiquitous across all configurations with discrepancies in the bias amplitude/frequency. Experimental device activation curves are shown as insets for comparison.

To reproduce this activation process, the simulation included the effects of filament stability on network response by tuning the distribution of noise factor $\alpha(t)$ while holding input bias amplitude and frequency constant. A high noise level ($\sigma_\alpha > 7\%$) was found to inhibit stable transitions, or $w(t)$ from crossing the interfacial barrier in the window function, which enforced the soft switching state (Figure 7-3(a)). Lowering σ_α enables $w(t)$ to increase past the barrier without interruption, inducing the transition from soft to hard switching at the network level (Figures 7-3(b)–(c)). Consequently, the noise level serves as a control parameter for the number of strongly memristive elements and the soft/hard switching behavior, supporting the conjecture on the mechanism behind the different switching behaviors.

Selecting the appropriate strength of the stochastic term enabled the ASN simulation to agree qualitatively with the experimental memristive behavior. While simulation and experiment show a quantitative difference in the hard switching regime (Figure 7-3(c) and inset), specifically in the rate of change between the high and low resistance states, stronger agreement with respect to the R_{on}/R_{off}ratio and the rate of resistance state change (Figure 7-6(b")) was observed in a more

densely connected simulated network. To elucidate the underlying dynamics of the activation process, internal conductance maps of a sparse network reveal the conductive pathways responsible for maximum current flow when operating in the soft switching, transitional, and hard switching states. A single, dominant pathway emerged at the transitional state and was destroyed in the subsequent input bias sweeps that drove the network into the hard switching state. Further examination of functional connectivity over the entire activation process enabled identification of equivalent regions of network conductance for the transitional and hard switching states. In particular, the network followed different trajectories to achieve values of maximum conductance, whereby network conductance was increasingly distributed in nature for the hard switching case.

In the results described below, both w_0 and $\alpha(t)$ were sampled from Gaussian distributions. Parameters of the distribution of w_0 were selected to reproduce the experimental *I*–*V* curves by matching the bias voltage used in the simulation to our experiment.

Physically implemented ASNs are observed to exhibit non-equilibrium dynamics under applied DC bias [77]. These network fluctuations are attributed to two primary mechanisms: (i) external bias causes silver ion migration toward the cathode where the ions are reduced to form metallic filaments, in opposition to the stochastic, thermodynamically driven return to equilibrium, and (ii) fluctuations in local resistance within the highly recurrent network can trigger cascading resistance changes elsewhere in the system. The behavior can be likened to neuronal avalanches observed in multielectrode array studies of neuronal cultures [23, 77]. In a single isolated link (Figure 7-4(a)), the stochastic term $\eta(t)$ results in the generation of white noise in the current output. In contrast, when embedded within a recurrent network, single links display $1/f^{\gamma}$ power law scaling. This clear difference in characteristics shows the role of

connectivity in a network. Each link in the network receives voltage inputs from many locations in the system and integrates, which in turn modifies the link's instantaneous resistance. This behavior facilitates the emergence of spatially correlated structures in local network activity. The recurrent structure also enables the integration of signals originating at different points in time, giving rise to non-trivial correlations in the temporal domain as indicated by $1/f^{\gamma}$ power law scaling with $0 < \gamma < 2$ in the power spectral density (Figure 7-4). The current passing across the ASN in both simulation and physical measurements also displays $1/f^{\gamma}$ in the power spectrum (Figure 7-4(b)) [156]. Although challenging to characterize in physical devices, the simulation data provide insight to both spatial correlation and phase synchrony for experiment.

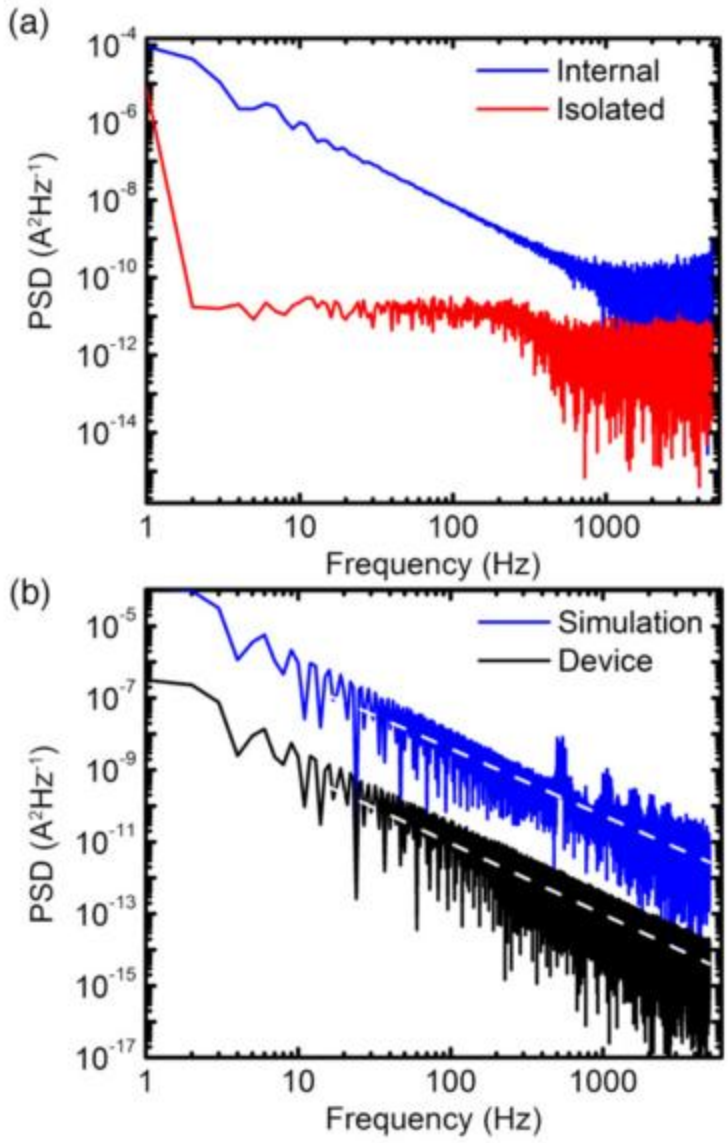

Figure 7-4. Comparisons of the power spectrum of a simulated 10 × 10 network $N = 332$, average $R_{on}/R_{off} = 10^{-2}$, $\tau = 10\ s^{-1}$,$\sigma_\alpha = 2.5\%$ (blue) with (a) a simulation of a single isolated atomic switch with identical parameters. The isolated atomic switch (red) shows a power spectrum dominated by white noise in contrast with a single element in the network (blue) show $1/f^\gamma$ power law scaling, and (b) that of a network device (black) that shows $1/f^\gamma$ power law scaling with $\gamma = 1.87$ (simulation) and 1.78 (device).

Network plasticity was investigated as a mechanism for the formation of feedforward pathways within ASNs, although they have an inherently recurrent architecture. Previous studies on physical ASNs have demonstrated their functionality as a two-bit memory storage device with spatially controlled, independent switching channels using pulsed electrical stimulation [77].

This experimental result, which used macroscopic electrodes in contact with a large area of the network to apply bias voltage stimulation, was also successfully simulated as illustrated in Figure 7-5. To comply with the experimental setup, a 10×10 network simulation was partitioned such that in each corner, a 4×4 block of nodes served the same purpose as a physical device electrode. A channel was defined by selection of one block as the source and another as the drain for application of an input bias voltage, with four blocks allowing for six possible channels. As shown in Figure 7-5, suprathreshold training pulses applied across two channels altered their respective conductances independently, even though the pathways were physically overlapping. By monitoring simulated connectivity maps of the other four conductance channels during this process, dynamical reconfigurations of the network connectivity were observed. Thus, non-volatile memory write/rewrite steps occur concurrently with non-trivial changes elsewhere in the network. Different write/rewrite pulse combinations can store information while simultaneously allowing the network to evolve through new configurations. Investigations of structures and stability of feedforward subassemblies may be conducted by carrying out random or targeted deletion of links belonging to a given channel in relation to the strength and duration of the external pulses that induced its formation. Scaling the network size increases the number of distinguishable network states, allowing for increased memory storage and diversity of nonlinear interactions.

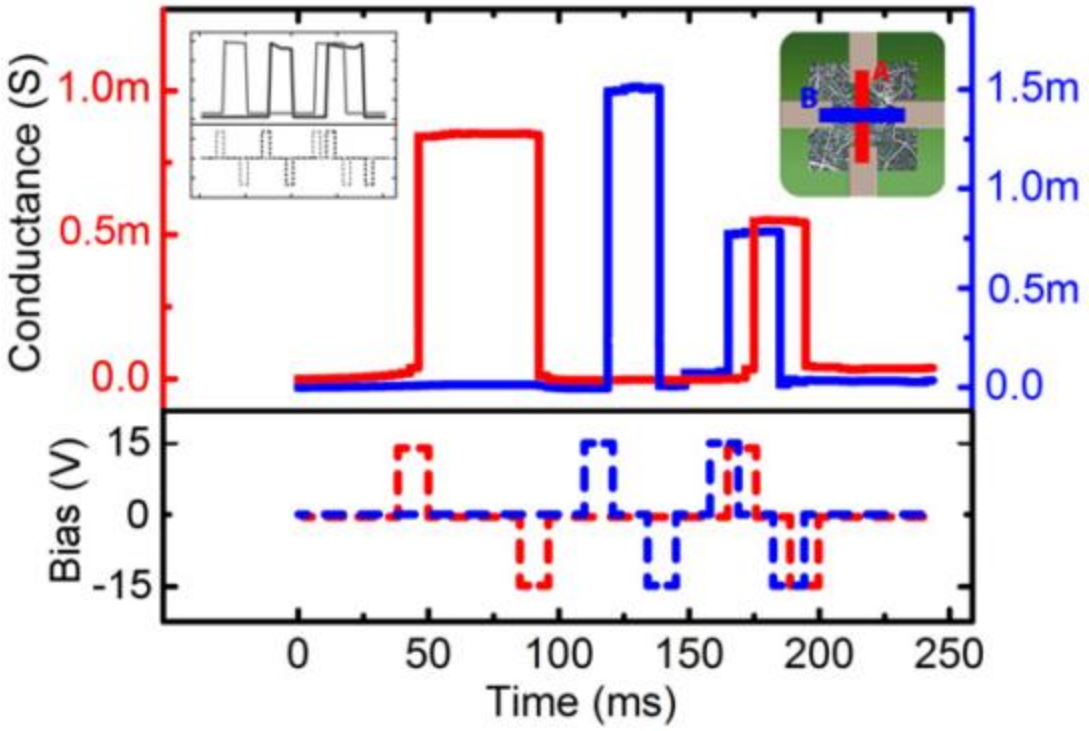

Figure 7-5. Spatially overlapping channels A and B can be modified independently by write/rewrite pulses, emulating the 2-bit switching functionality of actual device behavior (inset). This simulated 10 × 10 network (N = 219, average $R_{on}/R_{off} = 10^{-3}$,σ_{α} = 2.5%) was partitioned with four separate 4 × 4 blocks to serve as electrodes. Spatially defined ON/OFF switching was induced by applying write/rewrite voltage pulses (15 V, 10 ms duration) across the channels specified in the figure. Measurements of conductance across all six possible channels were conducted with 1 V read pulses of negligible period.

Resistive switches have recently attracted attention for higher harmonic generation (HHG), presented in both single switches and networks [79, 154]. Experimental atomic switch networks show HHG to be a function of applied input bias amplitude [77]. Here, numerical simulation was employed to explore HHG by stimulating a network with a sinusoidal input (10 Hz) while varying the input amplitude and network connection density (connectivity). For each simulated network of a given connectivity, the HHG analysis was performed on data collected over 10 cycles of the input signal. The network was then reset to the same initial state for the next level of input amplitude. A sharp rise in the ratio of higher harmonic amplitudes to

the fundamental at a threshold voltage was found in both experiment and simulation (Figure 7-6(a)).

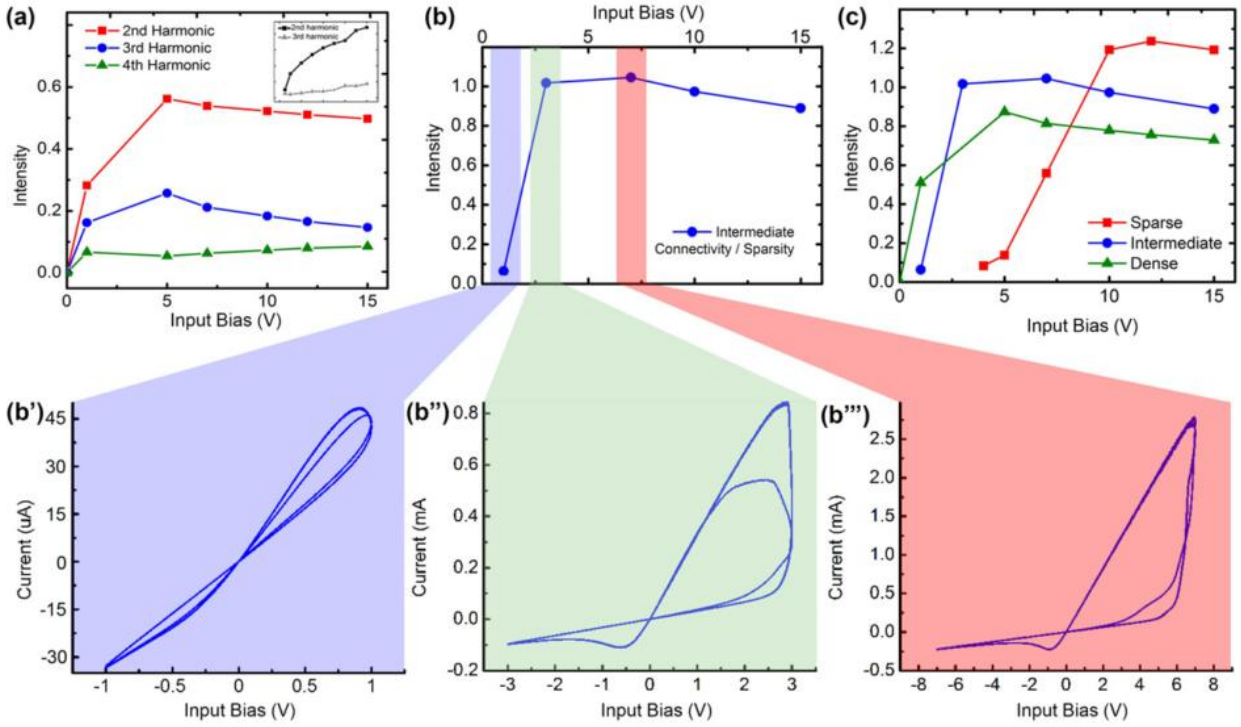

Figure 7-6. Higher harmonic generation can be influenced by network connectivity and input amplitude. Harmonic overtones of several simulated 10 × 10 networks with average $R_{on}/R_{off} = 10^{-2}$,$\sigma_{\alpha} = 2.5\%$, and $\tau = 10\ s^{-1}$. (a) The first three harmonic overtones of a network with $N = 332$ showed a threshold voltage for higher harmonic generation. Experimental device curves are shown as an inset for comparison. (b) Harmonic generation as a function of input bias amplitude for a network of intermediate connectivity ($N = 229$). (b',b'',b''') The network *I–V* characteristics tend toward hard switching behavior and increased higher harmonic generation as a function of input bias amplitude. (c) The sum of the first three harmonic overtones of several simulated networks with $N = (126, 229, 332)$ indicated a shift toward lower threshold voltages with increasing connectivity ascribed to an increasingly complex network.

The network *I–V* response curves at increasing levels of input bias amplitude (Figures 7-6(b')–(b''')) illustrate the onset of nonlinearity as characterized by HHG in Figures 7-6(a)–(c). As the voltage increased past the threshold magnitude, the switching behavior moved progressively toward the hard switching regime. The threshold voltage decreased with increased density of connections as shown in Figure 7-6(c). An increase in connectivity provides more recurrent substructures in the network and can be related to the nonlinearity in the integration of electrical

responses within the system. The decrease in the magnitude of the threshold voltage can be attributed to an enhanced nonlinearity in the network dynamics where, even at lower bias voltage levels, the system tends to reside outside of a linear regime. These changes in the behavior of HHG suggest a way toward quantitative characterization of functional connectivity within ASNs based on their dynamics. As illustrated in Figure 7-1 and described elsewhere [123], the fabrication conditions for ASNs allow substantial control over the size, morphology and density of interconnects. Simulations may therefore be used to optimize physical networks for specific applications.

7.4 Reservoir computing

Higher harmonic generation is potentially of great usefulness in a modern computational paradigm utilizing recurrent complex networks, called reservoir computing (RC). The amplitude and frequency characteristics of the produced higher harmonics may be used to quantitatively evaluate the efficiency of a reservoir in different dynamical regimes by accounting for the accessible degrees of freedom in higher dimensional representation space. Using voltage time traces as outputs, it is shown here that the ASN can effectively serve as a nonlinear reservoir capable of performing the waveform generation task (Figure 7-7) considered as a prerequisite to perform reservoir computing [196].

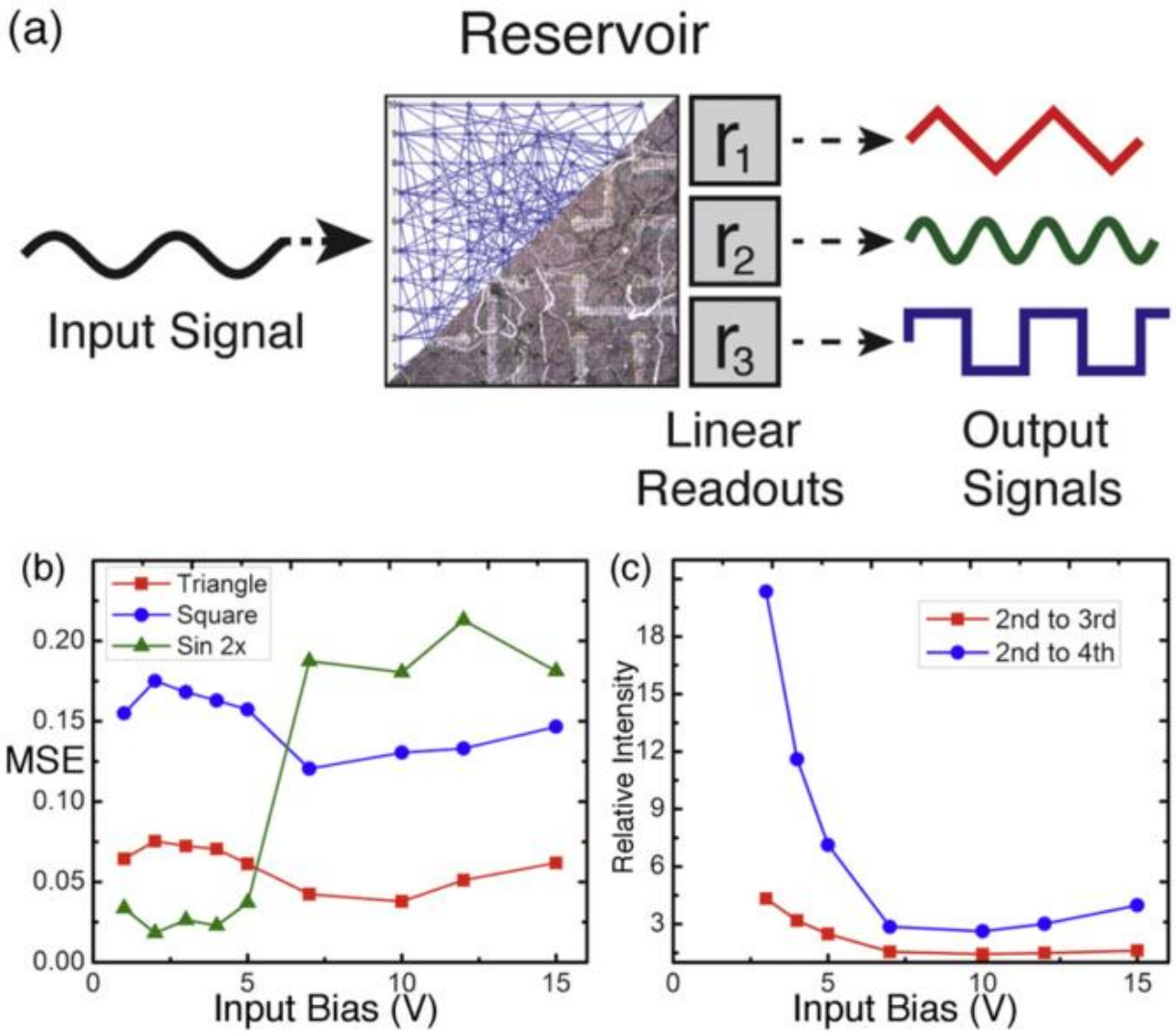

Figure 7-7. (a) Schematic of the network simulation used in the waveform generation RC task, with specific electrodes chosen as inputs/outputs (16 output electrodes). RC was implemented using a 10 × 10 network (N = 126,σ_α = 2.5%) with a 5 V, 10 Hz sinusoidal input signal and tasked to produce 10 Hz triangle/square and 20 Hz sinusoidal waveforms. (b) Mean-squared error (MSE) for each task with respect to driving amplitude showed minimal error in triangle/square waveform generation task at 10 V, corresponding to the onset of higher harmonic generation (see red curve of Figure 7-6(b)). Performance in the 20 Hz sinusoidal waveform generation task decreased when (c) the relative amplitude of the average second harmonic intensities of the readouts became increasingly diminutive. These results correspond to a strong dependence on the second harmonic for 20 Hz sine generation and the need for HHG in triangle/square generation as expected by Fourier analysis.

Maximizing the number of output signals is advantageous in the context of RC training. Each network node was therefore chosen to serve as an output electrode. By subjecting the network to a sinusoidal input at one corner electrode in the form of an input bias voltage,

multiple waveforms including triangle, square and frequency doubling sinusoidal waveforms were constructed through superposition of voltage outputs at each electrode in the simulation. The generated waveform r_q (q = 1, 2, 3) was then a weighted sum of the voltage outputs from the electrodes with the weights W_q^i calculated by linear regression,

$$r_q = \sum_{i=1}^{m} W_q^i V_i, \qquad q = 1, 2, 3 \tag{5}$$

where V_i are the output electrode voltages. Reservoir performance was assessed by the quality of waveform generation and compared across networks with different parameters by calculating the mean square error (MSE), which quantifies the differences between the target and the generated waveforms,

$$\mathrm{MSE} = \frac{\sum_{n=1}^{P} \left(y_{\mathrm{target}}(t_n) - \sum_{i=1}^{m} W^i V_i(t_n)\right)^2}{P} \tag{6}$$

where y_{target} is the target waveform. The W^i represent the weight coefficients to be trained with maximum number of outputs (m = 16) at discrete time indices (t_n) over a total length (P) from n = 1 to 9000. To see whether the diverse dynamical regimes of ASNs may affect the efficiency of RC training, the input gain was varied to access the different characteristics generated of the higher harmonics. The weights were calculated independently using the output responses from the network at each input voltage amplitude. As the magnitude of the applied input voltage was increased, an abrupt onset of HHG was observed to influence the associated error for the waveform generation tasks. Specifically, the ratio of the second to higher harmonics (calculated with unweighted average of network outputs) dropped rapidly with increasing voltage (≈8 V) as seen in Figure 7-7(c). This bias dependent reduction in second harmonic

amplitude was found to correlate directly with the critical voltage where MSE increased dramatically in the task of generating a sine wave exhibiting frequency doubling of the input signal. As the second harmonic became less pronounced compared to the higher harmonics it became more difficult to isolate in a linear combination of the output signals through linear regression. An increased ratio of higher harmonics to the second harmonics resulted in better performance for the generation of waveforms containing higher harmonic components such as square and triangular waveforms. While HHG is not a universal parameter designed to indicate increased computational performance, it does faithfully explain computational performance on specific RC tasks.

The results clearly demonstrate that an ASN can be used as a pattern generating kernel in RC where it can be optimized by adjusting input gain and network connectivity. Training ASNs to carry out more complex tasks requiring multiple, simultaneous inputs/outputs as well as real-time feedback is currently under investigation [198].

7.5 Conclusions and outlook

Numerical modeling of atomic switch networks is essential for understanding the experimentally observed emergent phenomena, and the microscopic degrees of freedom for synaptic elements. A valid numerical simulation offers a controllable, convenient platform from which to study specific aspects of the device functionality, and permits identification of control parameters for network level behaviors as well as system optimization. By extracting the relevant dynamical components of the network, our model can be expanded to understand the functionalities of ASNs with respect to a larger theoretical framework.

The simulation, incorporating network stochasticity and filament dissolution into its state equation, shows ASNs as devices capable of forming feedforward subassemblies that utilize network plasticity. Simulation results also reveal the networks' nonlinear integration of local electrical responses. Specifically, individual atomic switch elements show changes in their power spectral density when embedded in a network, while HHG emerges in the ASN with external bias and connectivity as control parameters.

Our simulation results support the feasibility of utilizing nonlinear dynamics without needing to control or 'train' the connections in the reservoir, and have indicated how to best optimize physical device parameters to maximize RC efficiency for a given task. Future efforts will focus on implementing benchmark tasks in RC in both simulation and hardware to quantitatively assess the kernel quality and generalization rank [198] in relation to the changing parameters as compared to other software and hardware reservoirs. Note that the plasticity intrinsic to the ASN makes it a dynamical reservoir, which shows improved function for some RC tasks [203]. The dynamics of these devices during the training period may be further characterized by calculating the Lyapunov exponent and used to elicit the connections to increased computational power at the edge of chaos [176].

The results presented here also demonstrate the value of using synaptic elements within a biologically inspired connective architecture. Substantial efforts have been undertaken to characterize and comprehend the dynamical hierarchy of a functioning complex system such as the brain [193, 204-206]. The existence of a readily scalable, physical device exhibiting many of the same dynamics as biological neural assemblies underscores its potential as a tool to study complexity. The greatest potential of ASNs lies not only in the versatility of hardware design but also in their scalability. A strategy that scales up the hierarchical dimension, combined with

insights obtained by actual learning and task performance through RC could generate valuable new computational devices.

8. Programmable short- and long-term memory in atomic switch networks using a reinforcement learning scheme

Abstract

Training biological neural networks to perform a desired task is achieved through the modification of the synaptic strength between neurons, where modification is determined by inherent biochemical phenomena in response to global stimuli. Training in neuromorphic hardware should be accomplished through similar mechanisms, however hardware and software implementations use architectures which prevent local interactions from affecting plasticity, or artificially impose plasticity rules instead of relying on properties inherent to the system. In this work a training regimen is applied to a neuromorphic hardware device comprised of a densely interconnected network of resistive switches. Global stimuli in the form of voltage pulses are used to tune the network to predetermined resistance values by relying on the inherent interactions of switches in the network. This experiment demonstrates the feasibility of training neuromorphic hardware by allowing autonomous interactions within the system instead of micromanaging system behavior, with applications to hardware implementations of neural networks.

8.1 Introduction

Learning from experience is a central characteristic of biological neural networks (BNNs) and their simulated counterparts, artificial neural networks (ANNs), that is facilitated by their unique structure and function. Neurons, discrete information processing elements, are connected to each other via synapses to form an interconnected network. The transmission of action

potentials between any two neurons is mediated by synapses, which continually alter transmission probabilities as new behaviors are learned. This feature, known as synaptic plasticity, is affected by a wide range of neurological processes such as spike-timing dependent plasticity, Hebbian plasticity, and synaptic redistribution [21, 22]. When input into a subset of neurons, action potentials rapidly propagate through the network, resulting in intricate patterns of electrical activity that forms the essence of brain activity. Changes in synaptic transmission affect the flow of action potentials, brain activity, and ultimately, behavior. The conductivity of synapses thus encodes learned behavior and memories in BNNs and serves as a central descriptor of the state of the network at any given time.

While many variations of ANNs exist to emphasize different features of BNNS, the salient features are present in some fashion. Generally, neurons are replaced with 'nodes', synapses are replaces as links, and action potentials exist as discrete or continuous waveforms. Synaptic plasticity is replaced by any number of learning rules through which the connective strength of links is adjusted [21, 112, 140, 152, 168]. As with BNNs, learned behavior and memories are encoded in the connective strengths of links.

In BNNs learning is autonomous – inputs and feedback from previous outputs are all global signals which affect the entire system. Conductance modifications to individual synapses are strictly the result of its local interactions with neighboring units in accordance with the biochemical processes affecting plasticity. This contrasts with most ANN frameworks in which plasticity is determined by artificially introduced rule sets, and link conductivities are digitally adjusted one by one until a desired behavior is produced. .

Physical devices which operate similarly to BNNs are of great interest because they promise computing abilities associated with BNNs without the immense size, energy, and price of simulated ANNs using digital computers. A popular hardware approach incorporates a crossbar array of resistive switching elements that serve a similar purpose as synapses, connected to transistor-based artificial neurons [47, 57, 72, 207]. The crossbar array allows for precise control of connectivity between artificial neurons since the resistive switches can be addressable individually. This precise control limits or eliminates the local interaction between neurons, and establishes a fundamental difference between the hardware and the system it is intended to emulate.

Atomic Switch Networks (ASNs) were recently developed as a physical analogue to ANNs and BNNs in both structure and function. ASNs are comprised of millions of synaptic elements assembled into a complex, interconnected network [73, 77, 208]. The synaptic elements, known as atomic switches, are formed from a nanoscale $Ag|Ag_2S|Ag$ junction [39-41, 43]. Externally applied bias causes a phase change of the Ag_2S layer, facilitating electromigration of silver cations to the cathode. There they are reduced to form a conductive metal filament which bridges the insulating Ag_2S layer, resulting in a lower resistance. These filaments are thickened by additional bias, or can be destroyed by reversing the bias. The formation and destruction of conductive silver filaments enable individual atomic switches to have a multitude of resistance states of varying volatility. The minimum bias required to complete a filament yields a volatile resistance state akin to short term potentiation in synapses, while long term memory is accessed by allowing thicker filaments to form after additional bias is applied [38, 41]. Additionally, cessation of external bias causes the filament to dissolve to the more thermodynamically stable high resistance state. Since a recently completed filament will

experience a sudden drop in electric field, there exists an inherent instability as competing forces determine the lifespan of a filament. In the network setting, complex interactions between switches as a result of their connectivity produce emergent patterns of electrical activity such as metastability in network resistance, harmonic generation, and 1/f noise , even while the memory capabilities of individual switches are retained [73, 77, 115]. Both memory and emergent behaviors are dependent on the resistance states of atomic switches, so a central descriptor for the state of the network is a set of the resistance state of each atomic switch, defined as the global resistance. Training the global resistance of an ASN to a desired operational regime is thus analogous to adjustment of synaptic conductivities in BNNs to achieve a desired behavior.

In complex physical systems such as ASNs, training through the micromanagement of individual elements is neither feasible, as the number of links is prohibitively large, nor desirable since BNNs do not operate through micromanagement. We demonstrate a method of training the global resistance of the network state to specified target values ranging from $2x10^2$ Ω to $2x10^7$ Ω with less than 1% error by applying global network stimulation in the form of voltage pulses. Similar resistance training techniques known as 'write and verify' have been described and applied to individual synaptic devices that exhibit continuously adjustable or multistable resistance states [209-212]. Here we report resistance training in a network setting, in which voltage stimuli are applied to the entire network in order to train the global resistance state. Any modification of global resistance to the system is a result of properties inherent in any individual switch and propagation of interactions between switches and their nearest neighbors, as opposed to training individual elements. This experiment highlights the ability of using exclusively global training methods combined with complete autonomy of the system itself to reach a targeted state.

Resistance training can make ASNs useful for multilevel ReRAM applications, or as synaptic elements in neuromorphic hardware implementations of neural networks [213].

8.2 Experimental

Atomic Switch Network devices were fabricated on a SiO_2 substrate using standard photolithography techniques. A 150 nm layer of platinum was patterned onto the substrate to create electrical contact pads around the perimeter leading to a 4x4 grid of electrodes in the center. Next, a 500 nm layer of SU-8 polymer was patterned on top of the electrodes, such that the leads to these electrodes were insulated, leaving only the circular electrodes in direct electrical contact with the ASN. Electrode diameter varied from 30-50 um, and electrode pitch varied from 100-500 um. The ASN was fabricated on top of this electrode grid as described previously to yield a dense, randomly interconnected network of silver nanowires [208]. Exposing the nanowire network to sulfur gas results in $Ag|Ag_2S|Ag$ junctions in the regions where nanowires overlap, forming the basis of atomic switches. In analogy to ANNs, the platinum electrodes serve as input or output nodes of voltage signals, while atomic switches act as synaptic links, though due to the small number of electrodes relative to the network size a link between any two electrodes will be comprised of many atomic switches. The resulting devices have been shown to exhibit a wide variety of complex electrical behaviors including temporal metastability, fluctuations in resistance, pinched *I-V* hysteresis, and long term memory [73, 77].

The resistance training experiments were performed using a precision source measure unit (National Instruments 4132) and a high-speed switch matrix (National Instruments 2532) within a PXIe unit (National Instruments 8108), enabling rapid resistance measurements between any combination of the 16 electrodes. Resistance training was implemented through repetition of

a two-step process as shown in Figure 8-1. In the first step, an electrode *A* was selected randomly and the resistance between this reference and every other electrode was measured using a small (200 mV, 10 ms) bipolar pulse in order to minimize influence on network resistances, as shown in Figure 8-1a. The individual resistances of electrode *A* with each of the other 15 electrodes, R_{Aj}, defined the network state by calculating the total resistance between electrode *A* and the rest of the network as though the paths from electrode *A* to every other electrode were resistors in parallel:

$$R(i) = \left(\sum_{\substack{j=0 \\ j \neq A}}^{15} \frac{1}{R_{Aj}} \right)^{-1} \quad (1)$$

This quantity is hereafter referred to as the 'parallel resistance'. In the second step, a second electrode *B* was selected randomly, and a large unipolar training pulse (100 ms, > ±200 mV) was applied to influence the parallel resistance of electrode *A*, as shown in Figure 8-1b. Using the same electrode I/O scheme, the measure/training cycle was repeated until the parallel resistance of *A* reached the target resistance. For all trials the target resistance was predetermined, irrespective of the initial network resistance.

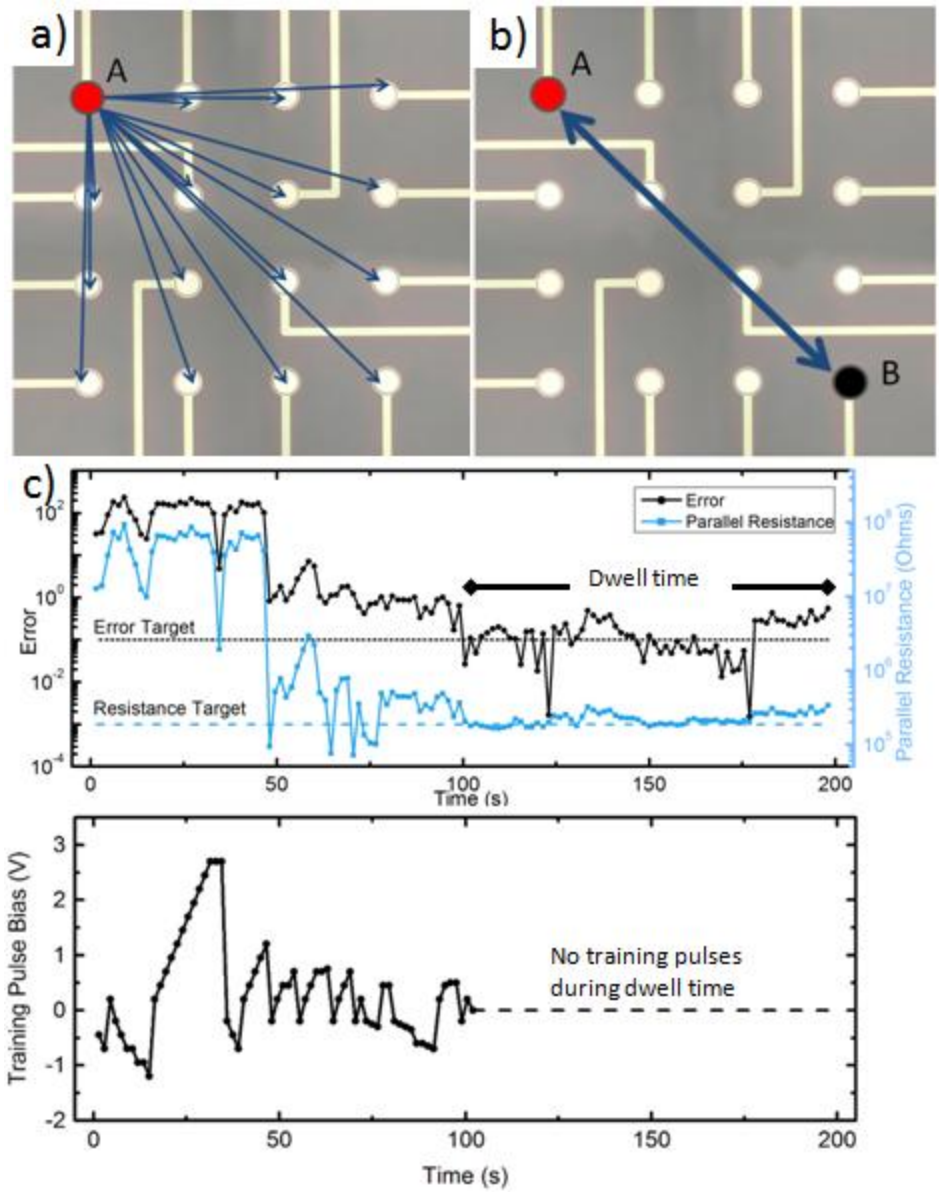

Figure 8-1. A schematic of the write and verify training scheme, and typical results for an individual training trial. **a)** Sub-threshold measurement pulses establish the parallel resistance of A, followed by **b)** a larger training/write pulse between A and B. **c)** The parallel resistance of a is recorded and compared to the target after each training pulse , when error is minimized the training ceases and the duration of the achieved target state is recorded as the dwell time.

In order to achieve training, an error function and rule set was devised. This system was designed to create sensible and consistent voltage adjustments even when both target resistance and parallel resistance error could vary by several orders of magnitude. The error function and

rule set also correctly accounted for events in which the parallel resistance overshot the target. Convergence of the parallel resistance to the target resistance was evaluated using an error function:

$$E(i) = \frac{1}{2}\left(\frac{R(i)}{R_g} - \frac{R_g}{R(i)}\right) \quad (2)$$

Where R_g was the target resistance, and *R(i)* was the parallel resistance. The error *E(i)* was calculated after each pulse/measure cycle, and adjustments to the training pulse bias were made by evaluating the relative change in error $C(i) = \frac{E(i)}{E(i-1)}$ from one cycle to the next using equations (3) and (4), which are described below.

Equation (3) concerned changes in the absolute magnitude of, *C(i)*, to evaluate changes in the absolute magnitude of the training pulse, *V(i)*. If the previous training pulse resulted in a large decrease in error |*C(i)*| would be less than 1. If significantly less than 1, as determined by an empirically determined threshold, C_m=0.6, then the training pulse *V(i)* was considered productive and no changes were made. If the previous pulse produced a significant increase in error, |*C(i)*|would be greater than 1. If |*C(i)*|was greater than $\frac{1}{C_m}$, the pulse was considered counterproductive and the training pulse magnitude was reset to a minimum value, V_{min}. If |*C(i)*| was between C_m and $\frac{1}{C_m}$ (i.e. approximately equal to 1) then the error had not significantly changed as a result of the previous pulse, indicating little influence on the parallel resistance. The pulse magnitude was then increased by V_{inc}.

$$V(i+1) = \begin{cases} V(i), & \text{if } |C(i)| < C_m \\ V_{min}, & \text{if } |C(i)| > \frac{1}{C_m} \\ V(i) + V_{inc}, & \text{if } C_m < |C(i)| < \frac{1}{C_m} \end{cases} \quad (3)$$

Next, equation (4) was used to determine the need for changes to the polarity of the training pulse. If *R(i)* and *R(i-1)* were both greater or both less than R_g then there was no overshoot and no need to reverse the bias, which is reflected by positive value for *C(i)*. However if *R(i)* changed enough with respect to *R(i-1)* that it overshot R_g, *C(i)* would be negative. In this case the training pulse voltage *V(i)* was reversed in sign, and its magnitude was automatically reset to the minimum pulse bias V_{min}.

$$sgn(V(i+1) = \begin{Bmatrix} sgn\big(V(i)\big), & if\ C(i) > 0 \\ -sgn\big(V(i)\big), & if\ C(i) < 0 \end{Bmatrix} \quad (4)$$

A single pulse/measurement cycle lasted 1.5 s, and the time required to reach the target resistance state was defined as the 'convergence time'. Upon reaching the target resistance, training pulses ceased and network resistances were measured every 0.5 s until the parallel resistance decayed away from the target and the error exceeded 0.5 (roughly equivalent to 50% error). This duration was defined as the 'dwell time.' The entire convergence/dwell time sequence constituted a single resistance training trial, an example of which is presented in Figure 8-1c. When a trial completed, new electrodes would be randomly selected and the training process was repeated after a 30 second delay.

8.3 Results

Thousands of trials of resistance training performed across many devices demonstrated that the parallel resistance can be tuned with less than 1% error, over a range of values from 200 Ω to 20 MΩ. Resistance training was successful when using training pulses of uniform bias (i.e. ± 500 mV), without the need for fine-tuning with smaller training pulses. As training pulses were applied to the network, the resistances R_{Aj} of different network pathways change (Figure 8-2) until the target resistance is achieved. The affects of a training pulse range from insignificant to profound, and identical pulses can produce dramatically different results. For example, the target resistance can be achieved either steadily or after several near misses and overshoots; it can be achieved either gradually after many pulses or immediately in response to a single pulse. This variability reflects the fact that a steady or linear approach to the target is not guaranteed when the possibility exists that even a single switch of too high or too low resistance could dictates the parallel resistance, obscuring the possibility that the rest of the network is very close to a configuration which yields the target resistance. Variability of convergence times and responses to training pulses indicates that network dynamics cannot be considered simply as a linear combination of elements. Rather, some interplay between the elements does not allow the network to be considered as additive elements

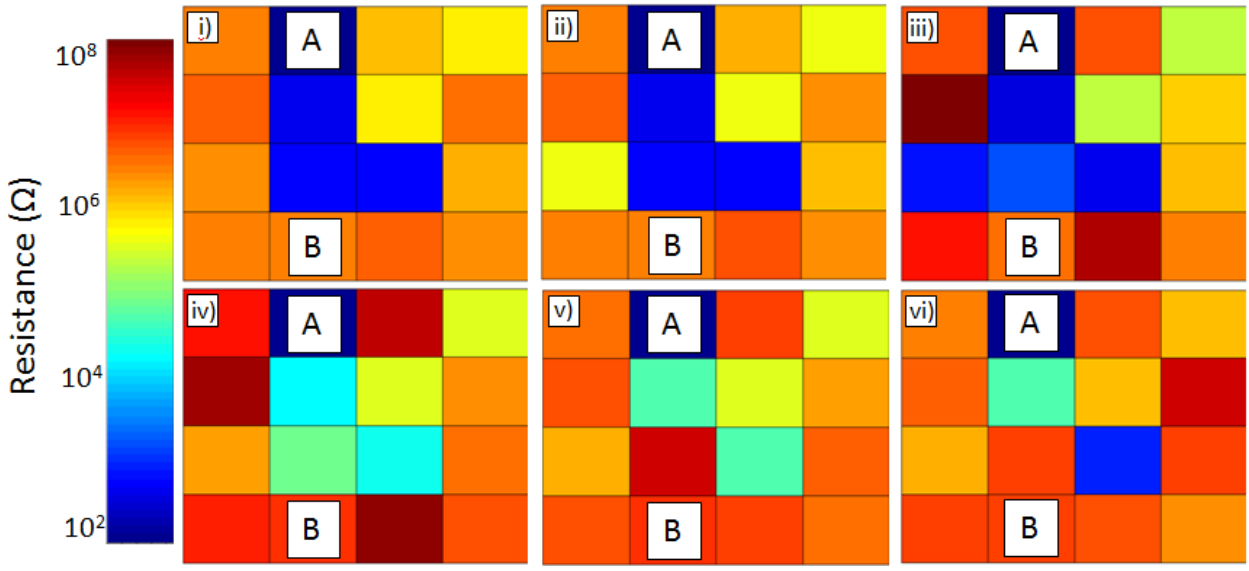

Figure 8-2. Training pulses caused resistance changes throughout the network. In this example 6 training pulses result in 6 unique network resistance configurations. The 4x4 grid of electrodes is represented by colored pixels for each of 6 (i-vi) consecutive training pulses between electrodes *A* and *B*. The resistance between *A* and each other electrode is measured and represented by a pixel placed where each electrode is physically located on the chip.

The success of the resistance training experiment contrasts the hypothetical case in which each training pulse causes a random parallel resistance value, allowing the target resistance to inevitably be achieved simply by random chance. In experiment, the statistical distribution of convergence times followed a power law. In contrast, a simple simulation of Bernoulli trials in which each pulse caused a random parallel resistance value resulted in a geometric distribution of convergence times. A variant simulation in which each training pulse resulted in individual resistances between electrode A and each other electrode resulted in training times that were effectively infinite. These simulation results contrast the experimental results and support the hypothesis that the training scheme harnesses memory in the ASN, allowing it to take a more direct path to the target resistance than would be possible by random chance.

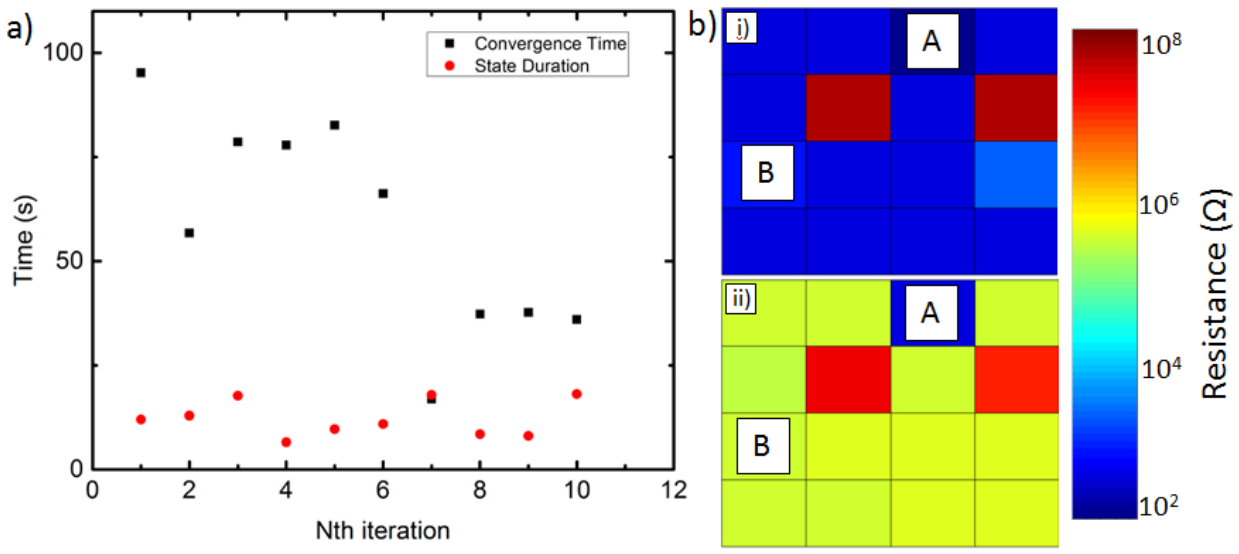

Figure 8-3. Changes in global resistance are presented in detail by showing each combinations' individual resistance. In **a)**, repeatedly training a single electrode pair to 20 kΩ resulted in progressively shorter training times, but the stability of the final state was not affected. Long term memory is exemplified in **b)**, in which a previously trained electrode pair reaches the target resistance (20 kΩ) in a single pulse. The resistances between electrode A and each other electrode is presented from two consecutive pulses (i-ii). While only *A* and *B* are directly pulsed, every single combination changes resistance, owing to the interdependencies of subregions of the network.

The resistance training scheme's leveraging of long term memory inherent in ASNs was most apparent when electrodes *A* and *B* were held constant and repeatedly trained to the same target. Figure 8-3a shows that the total training time decreases, suggesting that solutions to the target resistance become more established and easily accessed over time. In Figure 8-3b, individual resistances are plotted for two consecutive pulses: the initial state before the first training pulse and the final state after the first training pulse. This is one example of many trials in which only one pulse was needed to achieve the target resistance. Although the pulse was only between the two electrodes, every single value changed in concert, which shows that localized pulses on subregions of the network influence the global state of the system as well. Such rapid convergence also reveals that a large degree of error for the target resistance does not equate to a large degree of error in the phase space of the device – a few small changes to the state of the

network can result in a large change in resistance. Prior trainings establish pathways of fully formed conductive silver filaments among individual atomic switches, resulting in the correct parallel resistance, while divergence from the target resistance can theoretically result from just a few filaments dissolving in crucial locations, causing a large increase in error. Upon repeated trainings, these formed but incomplete pathways are undetected by resistance measurements until a sufficient training pulse reestablishes the conductive filaments, and the network appears to suddenly arrive at the target resistance.

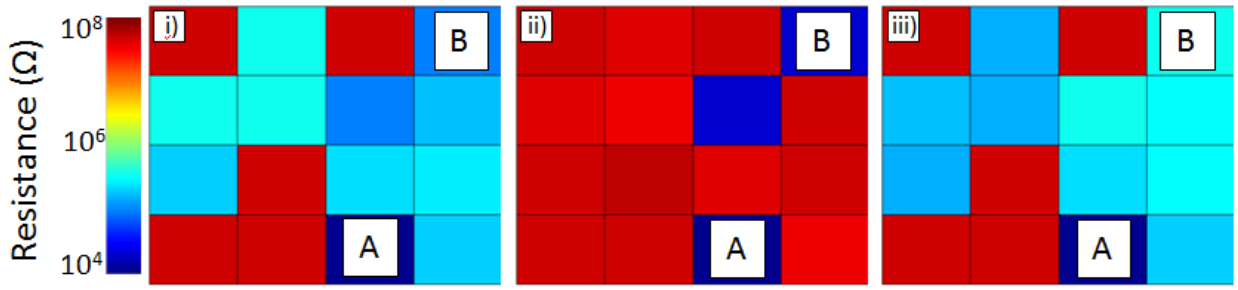

Figure 8-4. Electrodes *A* and *B* were held constant for several resistance training trials, and the final configurations of three consecutive trials (i-iii) are presented. The target resistance of 20 kΩ is precisely met three distinct ways, owing to the network's complex, plastic structure. Regardless of target resistance, the presence of multiple solutions meant a wide range in stability of the final configuration.

It is interesting that this memory effect coexists with the tendency of the device to achieve multiple degenerate solutions. Figure 8-4 presents the final configuration of the device after reaching the target resistance on three consecutive trainings. In the first trial, the target is reached when 10 different pathways reach resistances around 200 kΩ. In the next trial, the target is achieved by a different configuration such that one pathway is very close to 20 kΩ, and the rest are of very high resistance. In the third trial, a distinct third solution is found that bears resemblance to the first. These data show that there exists sufficient long term memory to easily recreate past solutions, yet the phase space of the network is rich enough that new solutions are

achieved even as previous ones are reinforced. Resistance training was also successful when the target resistance is defined as the resistance between only electrodes *A* and *B*, as opposed to the parallel resistance of A with every other electrode. Based on results of network training, it is likely that these achieving the same individual resistance multiple times are in fact different degenerate states that incorporate larger portions of the network than just one single pathway of completed filaments [115].

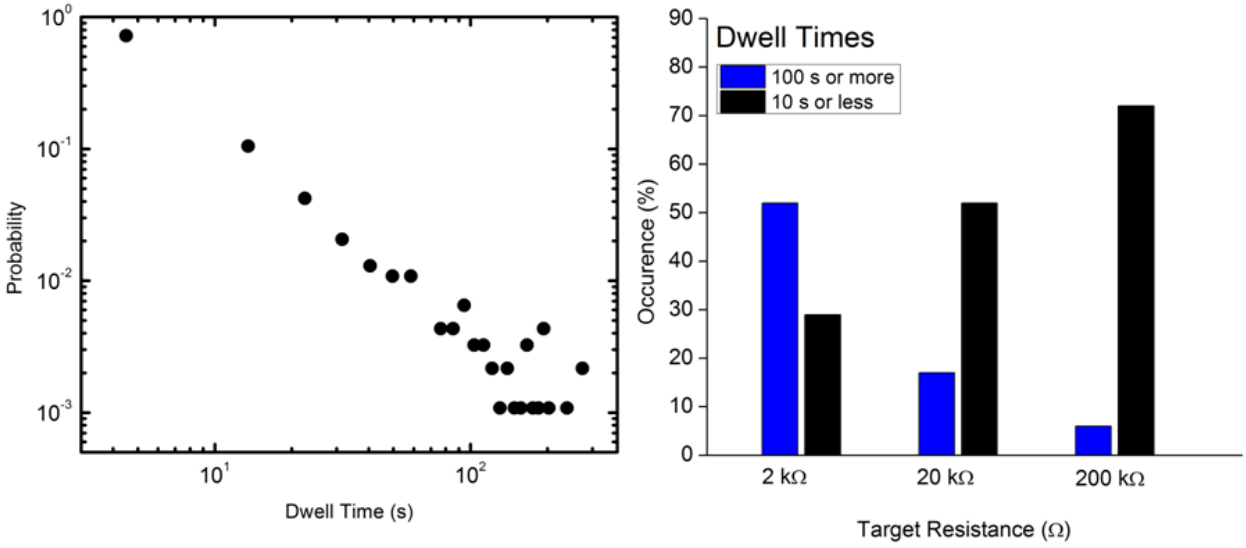

Figure 8-5. Dwell times vary widely, but depend on the target resistance. **a)** Networks are repeatedly trained to 200 kΩ and their dwell times are recorded. By repeating the training program many times on different networks, statistical distributions suggest that the probability *P(D)* of a dwell time lasting for duration *D* follows a power law relationship. Dwell times are generally 10 s or less, with occasional states lasting 100 s or more. **b)** At low target resistances, the final configurations are stable, with over 50% of trials resulting in a final state lifetime of 100 s or more. As target resistance increases, the final states are proportionately less stable.

Individual resistance states are the result of conductive silver filaments which bridge the Ag|Ag_2S|Ag gaps, and each filament is vulnerable to thermodynamically driven dissolution. Not surprisingly, a deterministic model of interacting thermodynamic variables is not available, and stability of target resistance is hard to predict. Figure 8-5a shows the distribution of dwell times for networks at the target resistance (R_g=200 kΩ). The distribution suggests a power law

dependency, with dwell times of less than 10 s being most common and occasional times lasting 10 times longer. This distribution was found to depend heavily on the target resistance value, as shown in Figure 8-3b. When R_g=200 kΩ, <10 s dwell times account for 72% of trials, but at 2 kΩ, dwell times of 100 s occur in more than 50% of trials. This is the expected result given the underlying operational mechanism of individual atomic switches. Lower resistances are achieved when an individual switch has a thicker conductive filament across the insulating layer, making them more resistant to thermodynamically driven dissolution. In the ASN, lower network resistances are more likely to have an abundance of parallel filamentary pathways, making the target state more resilient against changes from an individual filament. These factors of solved state stability outweigh any effects from repeatedly training the network, as Figure 8-2a shows no trend in the dwell time versus number of repeated trainings.

Resistance training was successfully conducted on a simulated ASN as well [114]. Due to computational demands the simulated network consisted only of a 5x5 array of nodes, with simulated atomic switches serving as links. Network connectivity was created by randomly distributing 105 connections, with 40 links in a nearest neighbor configuration.. Training pulses were administered between two nodes using the scheme described in equations 1-3. Resistance training in the simulated network proceeded as observed in the device, and could involve a direct approach to the target, or through a series of overshoots. The simulation allowed a complete analysis of every change in resistance in each link, and Figure 8-5b shows the net change that occurred in each link during the training process. The changes are widespread rather than localized along a single conductive pathway, which supports the hypothesis that network training is achieved by global interactions.

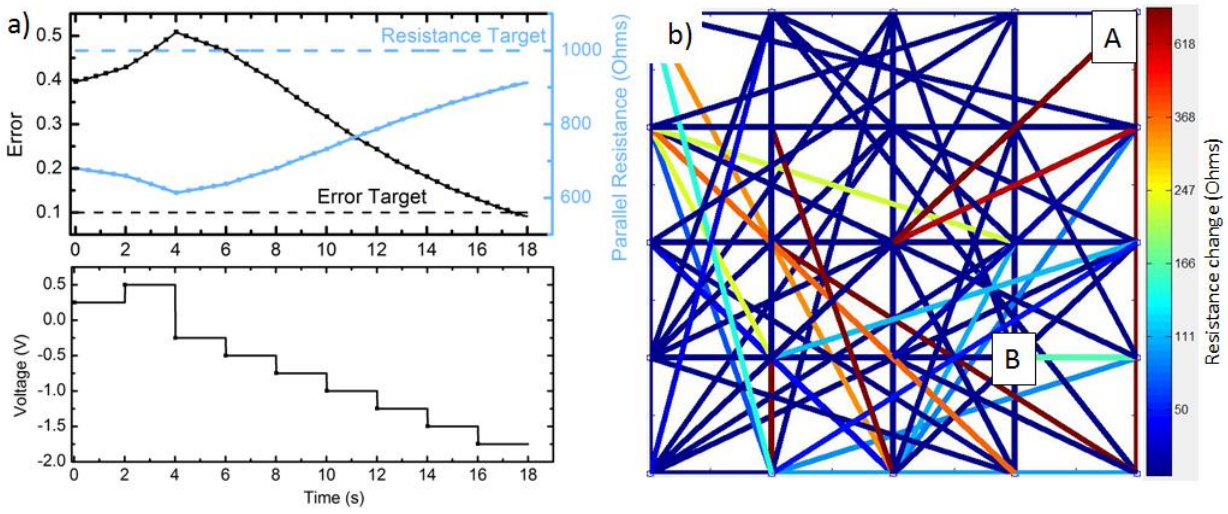

Figure 8-6. A simulated ASN is shows similar behavior in resistance training, and network-wide changes in resistance. A parallel resistance training program identical to the experimental one was used to successfully train parallel resistance. **a)** Target resistance was 1000 Ω, error target was 0.1, training pulses were 100 ms in 250 mV increments, measurement pulses are not necessary in simulation. The effects of resistance training are presented in **b)**, which shows the net resistance change in each link from start to finish. The simulation shows network-wide changes in resistance even though training pulses were applied exclusively from *A* to *B*.

8.4 Conclusions

Using a simple training algorithm, the network resistance state was accurately trained to different resistance states. This was achieved not through fine tuning or addressing individual memory elements, but by applying global signals which affect the entire system and permitting autonomous interactions between said elements. The resistance training experiment demonstrates that in a hardware setting that exhibits complex or unpredictable interactions, training is still possible. The intrinsic short and long term memory behaviors of individual switches are manifested in the form of long dwell times and progressively shorter training times, while the complex interactions allow a multitude of solutions or network resistance states to be explored. The ability to train a dynamic, complex system using global signals will undoubtedly be a

requirement for training physical systems where precise control is not possible, and the inherent adaptability of the system must be relied upon instead.

9. Outlook

In the preceding chapters, the conceptualization, fabrication, and characterization of neuromorphic hardware devices were presented. This research was motivated by the desire to explore whether or not the salient features of neuronal networks could be reproduced in a physical device which was intentionally fabricated to resemble such networks in structure.

Satisfactory device structures were realized through an inexpensive, scalable self-assembly process that produced complex, interconnected silver nanowire networks with large numbers of embedded atomic switches. Microscopic copper seeds lithographically patterned on top of pre-patterned electrode arrays served as nucleation sites for the electroless deposition of silver nitrate. The resultant silver network morphology could be qualitatively controlled through adjustments in the copper seed dimensions, allowing different types of networks to be fabricated.

Characterizations of these devices confirmed that the nanowire interfaces formed atomic switches, whose essential operating characteristics were found to exist in the devices, including bistable resistance switching, and short and long term memory. Additional characterizations revealed unique electronic behavior unreported in single atomic switches caused by complex, non-linear interactions between coupled switches in the device. A combination of I-V spectroscopy and IR imaging supported the hypothesis that electric current is distributed throughout the entire network, where the actions of atomic switches cause redistributions of electric potential and current flow, resulting in full, network-scale switching events cascading through the device. The emergent behaviors of ASNs constitute proof of principle, and support the continued development of physically complex device architectures which seek to produce neuromorphic behavior through the autonomous interactions of individual elements. These

successes warrant continued investigation of Atomic Switch Networks not only for the goal of computation, but as physical systems – microcosms – of the many complex interacting networks found throughout nature.

Future research regarding ASNs ought to focus primarily on two aspects: characterizations and applications. Characterization should focus on the nature of the emergent resistance fluctuations as there is incomplete understanding both in terms of their dynamics, and their fundamental origin. Worthwhile applications include attempting to perform computational tasks with the device, and establishing connections between ASN behaviors with those of other complex systems such that it may serve as an informative model. Both paths may serve each other if they are investigated concurrently: insights from behavioral analysis inform what conditions are optimal for computational tasks and modeling other systems, while successful applications will provide justification for continued study of ASNs.

Given that the large, complex network architecture displays the anticipated emergent behaviors, it is prudent to examine their origins. This could be accomplished by characterizing devices consisting of small numbers of atomic switches – beginning at two and scaling up to several hundred – the practical limits of computer simulated models which could be used to corroborate experimental data. Reports of the behaviors of two resistive switches in series and parallel have just begun to appear [214], and even in these cases device operation is non-trivial, and deviates significantly from computer simulations [215, 216]. While crossbar architectures were avoided in this study, the precise fabrication techniques would best serve the interest of understanding the relationship of mechanical properties in atomic switches such as gap width, metal composition, and stoichiometry with the emergent network behavior. The natural progression of these studies would lead to investigations of network-specific behavior in

crossbar-like architectures – it is well known that complex behaviors can exist in networks possessing only nearest neighbor connectivity, so these systems would provide commentary about whether or not highly interconnected, self-assembled networks are preferable.

More detailed studies into distributed resistance switching in ASNs are made possible by newly improved chip designs with up to 128 electrodes, as well as measurement I/O which can simultaneously sample electrical potential at each electrode's location [217]. Two notable analyses can be made owing to these improvements: functional connectivity, and avalanche dynamics.

Functional connectivity describes what level of correlation exists between different regions of a network regardless of the physical structure. In a complex system where an order parameter is measured at many locations, correlation coefficients are computed for every possible combination of said measurements. The resultant cross-correlation matrix is an accurate description of how the system is structured during operation. From this, basic quantities used in graph theory such as distance, clustering coefficients, and average degree may be calculated to infer fundamental characteristics of the system, such as whether it is a nearest neighbor or small world network, or even whether or not the system is critical. For example, functional connectivity of a human brain as measured through FMRI was compared with an Ising lattice model at different temperatures, revealing that networks reconstructed from brain activity were most similar to reconstructed networks from an Ising lattice at its critical temperature, supporting the theory that the brain operates in a critical regime [218]. A similar analysis could easily be performed on ASNs to scrutinize whether and when they operate at a critical state. Moreover, the resulting fundamental state descriptors could be used to identify and discriminate between different operational regimes such as the degree of soft/hard switches present in a network.

Analyses of avalanche dynamics clarify the manner in which switching events propagate through the network in time and space. In other words, detailed descriptions of the most striking yet least understood aspect of ASNs. In multielectrode array recordings of intrinsic activity in neuronal cultures and cortical slices, action potentials occur in synchronized bursts. Extracting statistics such the number of neurons involved in each burst and burst lifetimes resulted in a description of neuronal activity as occurring in a critical state, where a single action potential could be an isolated event, trigger a cascade of action potentials spanning the entire system, or result in semi-stable limit cycles [19, 23, 219]. In ASNs, the spatio-temporal fluctuations in voltage as recorded by the electrodes could determine where the statistical distribution of switching events is falls on the scale of order-criticality-disorder, and whether they are localized to a few distinct locations or distributed. While action potentials are known to travel on the order of 10^0 – 10^2 m/s, analysis of avalanche dynamics in ASNs could reveal how fast switching events propagate, which in turn could establish optimal system size with respect to sampling frequency.

Applications of the ASN towards computation must finally bridge the gap between indications that ASNs can compute, and actually performing a task. Experiments thus far have shown essential behaviors such as short and long term memory, higher harmonic generation, and nonlinear interactions between switches. But harnessing these behaviors to perform a task requires knowledge of how to implement them together and produce reliable results in the face of a constantly changing network. For example, from the perspective of reservoir computing, ASNs have demonstrated higher harmonic generation in the voltage time traces recorded at the electrodes. Linear combinations of these voltage readouts can be used to produce new waveforms. However, reservoir computing tasks are typically performed on static reservoirs –

systems that produce higher dimensional outputs that are consistent or at least similar from one trial to the next. Atomic switch networks, on the other hand, appear to be continually evolving. A linear combination of readouts used to fit a target function may require a completely combination on subsequent trials. This barrier can be overcome through the previously mentioned analysis techniques, where causal relationships between input signals and operational regimes become more obvious.

For all the experiments and analogies attempting to connect atomic switch networks with neuronal networks and reservoir computing, ASNs are ultimately a unique dynamical system that may not fit into any existing mold. It is the author's hope that future investigations of ASNs uncover new facets of dynamical systems' behavior, and pave the way for computational frameworks which lie outside the realm of digital or neural information processing.

10. References

[1] P.-M. Binder, "The edge of reductionism," *Nature*, vol. 459, pp. 332-334, 2009.

[2] P. W. Anderson, "More is Different," *Science*, vol. 177, pp. 393-396, 1972.

[3] G. Nicolis, "Physics of far-from-equilibrium systems and self-organization," *The new physics*, vol. 11, pp. 316-347, 1989.

[4] E. Bodenschatz, W. Pesch, and G. Ahlers, "Recent Developments in Rayleigh-Benard Convection," *Annu. Rev. Fluid Mech.*, vol. 32, pp. 709-778, 2000.

[5] P. Bak, *How Nature Works*. Heidelberg: Springer, 1999.

[6] H. Simons, "The Architecture of Complexity," *Proc. Am. Phil. Soc.*, vol. 106, pp. 467-482, 1962.

[7] J. Goldstein, "Emergence as a Construct: History and Issues," *Complexity*, vol. 1, 1999.

[8] D. Rickles, P. Hawe, and A. Shiell, "A simple guide to chaos and complexity," *Journal of epidemiology and community health*, vol. 61, pp. 933-7, 2007.

[9] J. D. Halley and D. A. Winkler, "Classification of Emergence and its Relation to Self-Organization," *Complexity*, vol. 13, 2008.

[10] V. Darley, "Emergent phenomena and complexity," *Artificial Life*, vol. 4, pp. 411-416, 1994.

[11] Bedau, "Weak emergence," *Nous*, vol. 11, pp. 375-399, 1997.

[12] H. E. Stanley, *Introduction to phase transitions and critical phenomena*: Oxford University Press, 1987.

[13] H. J. Jensen, *Self-organized criticality: emergent complex behavior in physical and biological systems*, vol. 10: Cambridge university press, 1998.

[14] S. N. Dorogovtsev, A. V. Goltsev, and J. F. F. Mendes, "Critical phenomena in complex networks," *Rev. Med. Phys.*, vol. 80, pp. 1275-1335, 2008.

[15] J. Crutchfield, "Between order and chaos," *Nat. Phys.*, vol. 8, pp. 17-24, 2011.

[16] J. M. Beggs and N. Timme, "Being critical of criticality in the brain," *Front. in physiol.*, vol. 3, pp. 1-14, 2012.

[17] M. Gell-Mann, "What is Complexity?," *Complexity*, vol. 1, pp. 16-19, 1995.

[18] J. D. Halley and D. A. Winkler, "Consistent concepts of self-organization and self-assembly," *Complexity*, vol. 14, 2008.

[19] D. R. Chialvo, "Emergent Complex Neural Dynamics," *Nat. Phys.*, vol. 6, pp. 744-750, 2010.

[20] O. Sporns, D. R. Chialvo, M. Kaiser, and C. C. Hilgetag, "Organization, Development and Function of Complex Brain Networks," *Trends in Cog. Sci.*, vol. 8, pp. 418–425, 2004.

[21] L. F. Abbott and S. B. Nelson, "Synaptic plasticity: taming the beast," *Nat. Neurosci.*, vol. 3, pp. 1178-1183, 2000.

[22] H. Markram and M. Tsodyks, "Redistribution of synaptic efficacy between neocortical pyramidal neurons," *Nature*, vol. 382, pp. 807-810, 1996.

[23] J. M. Beggs and D. Plenz, "Neuronal Avalanches in Neocortical Circuits," *J. Neurosci.*, vol. 23, pp. 11167-77, 2003.

[24] R. M. Douglas, M.; Mead, C., "Neuromorphic analogue VLSI," *Annu Rev Neurosci*, vol. 18, pp. 225-281, 1995.

[25] C. Mead, "Neuromorphic electronic systems," *Proc IEEE*, vol. 78, pp. 1629-1636, 1990.

[26] C. A. Mead and M. A. Mahowald, "A silicon model of early visual processing," *Neural Networks*, vol. 1, pp. 91-97, 1988.

[27] K. Likharev, A. Mayr, I. Muckra, and Ö. Turel, "CrossNets: High-Performance Neuromorphic Architectures for CMOL Circuits," *Ann. NY Acad. Sci.*, vol. 1006, pp. 146-163, 2003.

[28] K. K. Likharev and D. B. Strukov, "CMOL: Devices, circuits, and architectures," in *Introducing Molecular Electronics*, vol. 680, *Lecture Notes in Physics*: Springer Berlin Heidelberg, 2005, pp. 447-477.

[29] A. M. Turing, "Computing Machinery and Intelligence," *Mind: A Quarterly Review of Psychology and Philosophy*, vol. LIX, pp. 433, 1950.

[30] J. von Neumann, "The Principles of Large-Scale Computing Machines," *Annals Hist. Comput.*, vol. 10, pp. 243-256, 1989.

[31] R. Himeno and J. Wilkinson, "Largest neuronal network simulation achieved using K computer," 2013.

[32] O. Kavehei, A. Iqbal, Y. S. Kim, K. Eshraghian, S. F. Al-Sarawi, and D. Abbott, "The fourth element: characteristics, modelling and electromagnetic theory of the memristor." Proceedings of the Royal Society A: Mathematical, Physical and Engineering Science 466.2120 (2010): 2175-2202.," *Proceedings of the Royal Society A: Mathematical, Physical and Engineering Science*, vol. 466, pp. 2175-2202, 2010.

[33] L. Chua, "Memristor-The missing circuit element," *IEEE T. Circuits Syst.*, vol. 18, pp. 507-519, 1971.

[34] L. Chua, "Resistance switching memories are memristors," *Appl. Phys. A*, vol. 102, pp. 765-783, 2011.

[35] A. Chung, J. Deen, J.-S. Lee, and M. Meyyappan, "Nanoscale memory devices," *Nanotech.*, vol. 21, pp. 412001, 2010.

[36] D. B. Strukov, G. S. Snider, D. R. Stewart, and R. S. Williams, "The missing memristor found," *Nature*, vol. 453, pp. 80-83, 2008.

[37] R. Waser, R. Dittmann, G. Staikov, and K. Szot, "Redox-Based Resistive Switching Memories - Nanoionic Mechanisms, Prospects, and Challenges," *Advanced Materials*, vol. 21, pp. 2632-2663, 2009.

[38] T. Hasegawa, A. Nayak, T. Ohno, K. Terabe, T. Tsuruoka, J. K. Gimzewski, and M. Aono, "Memristive operations demonstrated by gap-type atomic switches," *Appl. Phys. A*, vol. 102, pp. 811-815, 2011.

[39] K. Terabe, T. Hasegawa, T. Nakayama, and M. Aono, "Quantized conductance atomic switch," *Nature*, vol. 433, pp. 47-50, 2005.

[40] Z. Xu, Y. Bando, W. Wang, X. Bai, and D. Golberg, "Real-Time In Situ HRTEM-Resolved Resistance Switching of Ag2S Nanoscale Ionic Conductor," *ACS Nano*, vol. 4, pp. 2515-2522, 2010.

[41] T. Hasegawa, T. Ohno, K. Terabe, T. Tsuruoka, T. Nakayama, J. K. Gimzewski, and M. Aono, "Learning Abilities Achieved by a Single Solid-State Atomic Switch," *Adv. Mater.*, vol. 22, pp. 1831-1834, 2010.

[42] T. Ohno, T. Hasegawa, A. Nayak, T. Tsuruoka, J. K. Gimzewski, and M. Aono, "Sensory and short-term memory formations observed in a Ag2S gap-type atomic switch," *Appl. Phys. Lett.*, vol. 99, pp. 203108, 2011.

[43] T. Ohno, T. Hasegawa, T. Tsuruoka, K. Terabe, J. K. Gimzewski, and M. Aono, "Short-term plasticity and long-term potentiation mimicked in single inorganic synapses," *Nat. Mater.*, vol. 10, pp. 591-595, 2011.

[44] J. Borghetti, Z. Li, J. Straznicky, X. Li, D. A. A. Ohlberg, W. Wu, D. R. Stewart, and R. S. Williams, "A hybrid nanomemristor/transistor logic circuit capable of self programming," *PNAS*, vol. 106, pp. 1699-1703, 2008.

[45] C. Kugeler, R. Rosezin, E. Linn, R. Bruchhaus, and R. Waser, "Materials, technologies, and circuit concepts for nanocrossbar-based bipolar RRAM," *Appl. Phys. A*, vol. 102, pp. 791-809, 2011.

[46] S. H. Jo, T. Chang, I. Ebong, B. B. Bhadviya, P. Mazumder, and W. Lu, "Nanoscale Memristor Device as Synapse in Neuromorphic Systems," *Nano Lett.*, vol. 10, pp. 1297-1301, 2010.

[47] K.-H. Kim, S. Gaba, D. Wheeler, J. M. Cruz-Albrecht, T. Hussain, N. Srinivasa, and W. Lu, "A Functional Hybrid Memristor Crossbar-Array/CMOS System for Data Storage and Neuromorphic Applications," *Nano Lett.*, vol. 12, pp. 389-395, 2012.

[48] B. S. Landman and R. L. Russo, "On a Pin Versus Block Relationship For Partitions of Logic Gates," *IEEE T. on Comput.*, vol. C-20, pp. 1469-1479, 1971.

[49] P. Christie and D. Stroobandt, "The interpretation and application of Rent's rule," *IEEE T. on Very Large Scale Integration (VLSI) Systems*, vol. 8, pp. 639-648, 2000.

[50] D. S. Bassett, D. L. Greenfield, A. Meyer-Lindenberg, D. R. Weinberger, S. W. Moore, and E. T. Bullmore, "Efficient Physical Embedding of Topologically Complex Information Processing Networks in Brains and Computer Circuits," *PLoS Comp. Biol.*, vol. 6, pp. e1000748, 2010.

[51] T. A. Witten and L. M. Sander, "Diffusion-Limited Aggregation, a Kinetic Critical Phenomenon," *Phys. Rev. Lett.*, vol. 47, pp. 1400-1403, 1981.

[52] A. Kuhn, F. Argoul, J. F. Muzy, A. Arneodo, and F. Argoul, "Diffusion-limited kinetics in thin-gap electroless deposition," *J. Electroanal. Chem.*, vol. 397, pp. 93-104, 1995.

[53] M. Kundu, K. Terabe, T. Hasegawa, and M. Aono, "Effect of sulfurization conditions and post-deposition annealing treatment on structural and electrical properties of silver sulfide films," *J. Appl. Phys.*, vol. 99, pp. 103501-9, 2006.

[54] W. Lu and C. M. Lieber, "Nanoelectronics from the bottom up," *Nature Materials*, vol. 6, pp. 841-50, 2007.

[55] T. Prodromakis, C. Toumazou, and L. Chua, "Two centuries of memristors," *Nature Materials*, vol. 11, pp. 478-81, 2012.

[56] Y. N. Joglekar and S. J. Wolf, "The elusive memristor: properties of basic electrical circuits," *European Journal of Physics*, vol. 30, pp. 661-675, 2009.

[57] Q. Xia, W. Robinett, M. W. Cumbie, N. Banerjee, T. J. Cardinali, J. J. Yang, W. Wu, X. Li, W. M. Tong, D. B. Strukov, G. S. Snider, G. Medeiros-Ribeiro, and R. S. Williams, "Memristor - CMOS Hybrid Integrated Circuits for Reconfigurable Logic," *Nano Lett.*, vol. 9, pp. 3640-3645, 2009.

[58] M. D. Pickett, G. Medeiros-Ribeiro, and R. S. Williams, "A scalable neuristor built with Mott memristors," *Nature Materials*, vol. 12, pp. 114-117, 2012.

[59] A. Chanthbouala, V. Garcia, R. O. Cherifi, K. Bouzehouane, S. Fusil, X. Moya, S. Xavier, H. Yamada, C. Deranlot, N. D. Mathur, M. Bibes, A. Barthélémy, and J. Grollier, "A ferroelectric memristor," *Nature Materials*, vol. 11, pp. 860-4, 2012.

[60] D. S. Jeong, R. Thomas, R. S. Katiyar, J. F. Scott, H. Kohlsedt, A. Petraru, and C. S. Hwang, "Emerging memories: resistive switching mechanisms and current status," *Nanotechnology*, vol. 75, pp. 1-31, 2012.

[61] R. L. Allen and W. J. Moore, "Diffusion of Silver in Silver Sulfide," *J. Phys. Chem.*, vol. 63, pp. 223-226, 1959.

[62] B. H. Grier, S. M. Shapiro, and R. J. Cava, "Inelastic neutron scattering measurements of the diffusion in b-Ag2S," *Phys. Rev. B*, vol. 29, pp. 3810-3814, 1984.

[63] A. Beck, J. G. Bednorz, C. Gerber, C. Rossel, and D. Widmer, "Reproducible switching effect in thin oxide films for memory applications," *Applied Physics Letters*, vol. 77, pp. 139, 2000.

[64] B. J. Choi, D. S. Jeong, S. K. Kim, C. Rohde, S. Choi, J. H. Oh, H. J. Kim, C. S. Hwang, K. Szot, R. Waser, B. Reichenberg, and S. Tiedke, "Resistive switching mechanism of TiO2 thin films grown by atomic-layer deposition," *Journal of Applied Physics*, vol. 98, pp. 033715, 2005.

[65] N. Gergel-Hackett, B. Hamadani, B. Dunlop, J. Suehle, C. Richter, C. Hacker, and D. Gundlach, "A flexible solution-processed memristor," *Electron Device Letters, IEEE*, vol. 30, pp. 706-708, 2009.

[66] K. Miller, K. S. Nalwa, A. Bergerud, N. M. Neihart, and S. Chaudhary, "Memristive Behavior in Thin Anodic Titania," *IEEE Electron Device Letters*, vol. 31, pp. 737-739, 2010.

[67] J. L. Tedesco, N. Gergel-Hackett, L. Stephey, A. A. Herzing, M. Hernandez-Mora, J. J. Kopanski, C. A. Hacker, and C. A. Richter, "Flexible Memristors Fabricated through Sol-Gel Hydrolysis," *ECS Transactions*, vol. 35, pp. 111-120, 2011.

[68] T. W. Hickmott and W. R. Hiatt, "Electrode Effects and Switching of Amorphous Nb2O5 Diodes," *Solid-State Electronics*, vol. 33, pp. 1033-1047, 1970.

[69] K. P. Biju, X. Liu, E. M. Bourim, I. Kim, S. Jung, J. Park, and H. Hwang, "Improved Resistive Switching Properties of Solution Processed TiO2 Thin Films," *Electrochemical and Solid-State Letters*, vol. 13, pp. 443, 2010.

[70] Z. J. Chew and L. Li, "A discrete memristor made of ZnO nanowires synthesized on printed circuit board," *Materials Letters*, vol. 91, pp. 298-300, 2013.

[71] K. H. Choi, M. Mustafa, K. Rahman, B. K. Jeong, and Y. H. Doh, "Cost-effective fabrication of memristive devices with ZnO thin film using printed electronics technologies," *Journal of The Electrochemical Society*, vol. 106, pp. 165-170, 2011.

[72] S. Park, J. Noh, M.-L. Choo, A. M. Sheri, M. Chang, Y.-B. Kim, C. J. Kim, M. Jeon, B.-G. Lee, B. H. Lee, and H. Hwang, "Nanoscale RRAM-based synaptic electronics: toward a neuromorphic computing device.," *Nanotechnology*, vol. 24, pp. 384009, 2013.

[73] A. V. Avizienis, H. O. Sillin, C. Martin-Olmos, H. H. Shieh, M. Aono, A. Z. Stieg, and J. K. Gimzewski, "Neuromorphic Atomic Switch Networks," *PloS one*, vol. 7, pp. e42772, 2012.

[74] S. Lv, H. Suo, T. Zhou, C. Wang, S. Jing, Q. Fu, Y. Xu, and C. Zhao, "Effect of synthesis route on the morphologies of silver nanostructures by galvanic displacement reaction," *Solid State Commun.*, vol. 149, pp. 227-230, 2009.

[75] X. Wen, Y.-T. Xie, W. C. Mak, K. Y. Cheung, X.-Y. Li, R. Renneberg, and S. Yang, "Dendritic Nanostructures of Silver: Facile Synthesis, Structural Characterizations, and Sensing Applications," *Langmuir*, vol. 22, pp. 4836-4842, 2006.

[76] A. V. Avizienis, C. Martin-Olmos, H. O. Sillin, M. Aono, J. K. Gimzewski, and A. Z. Stieg, "Morphological Transitions from Dendrites to Nanowires in the Electroless Deposition of Silver," *Crystal Growth & Design*, vol. 13, pp. 465-469, 2013.

[77] A. Z. Stieg, A. V. Avizienis, H. O. Sillin, C. Martin-Olmos, M. Aono, and J. K. Gimzewski, "Emergent Criticality in Complex Turing B-Type Atomic Switch Networks," *Adv. Mater.*, vol. 24, pp. 286-293, 2012.

[78] C. Liang, K. Terabe, T. Hasegawa, R. Negishi, T. Tamura, and M. Aono, "Ionic–Electronic Conductor Nanostructures: Template-Confined Growth and Nonlinear Electrical Transport," *Small*, vol. 1, pp. 971-975, 2005.

[79] E. N. Oskoee and M. Sahimi, "Electric currents in networks of interconnected memristors," *Phy. Rev. E*, vol. 83, pp. 031105, 2011.

[80] J. S. Langer, "Instabilities and pattern formation in crystal growth," *Rev. Mod. Phys.*, vol. 52, 1980.

[81] E. Ben-jacob, P. Garik, T. Meuller, and D. Grier, "Characterization of morphology transitions in diffusion-controlled systems," *Phys. Rev. A*, vol. 38, 1988.

[82] M. C. Cross and P. C. Hohenberg, "Pattern formation outside of equilibrium," *Rev. Mod. Phys.*, vol. 65, pp. 851-1112, 1993.

[83] V. Fleury, J. H. Kaufman, and D. B. Hibbert, "Mechanism of a morphology transition in ramified electrochemical growth," *Nature*, vol. 367, pp. 435-438, 1994.

[84] E. Ben-jacob and P. Garik, "The formation of patterns in non-equilibrium growth," *Nature*, vol. 343, pp. 523-530, 1990.

[85] I. Ohno, "Electrochemistry of electroless plating," *Materials Science and Engineering*, vol. 146, pp. 33-49, 1991.

[86] M. H. Rashid and T. K. Mandal, "Synthesis and Catalytic Application of Nanostructured Silver Dendrites," *J. Phys. Chem.*, vol. 111, pp. 16750-16760, 2007.

[87] M. Rai, A. Yadav, and A. Gade, "Silver nanoparticles as a new generation of antimicrobials," *Biotechnology Advances*, vol. 27, pp. 76-83, 2009.

[88] Y. Xia and N. J. Halas, "Shape-Controlled Synthesis and Surface Plasmonic Properties of Metallic Nanostructures," *MRS Bulletin*, vol. 30, pp. 338-348, 2005.

[89] S. M. Nie and S. R. Emery, "Probing Single Molecules and Single Nanoparticles by Surface-Enhanced Raman Scattering," *Science*, vol. 275, pp. 1102-1106, 1997.

[90] R. Ho, K. W. Mai, and M. A. Horowitz, "The future of wires," *Proc IEEE*, vol. 89, pp. 490-504, 2001.

[91] C. Teuscher, C. Grecu, T. Lu, and R. Weiss, "Challenges and Promises of Nano and Bio Communication Networks," presented at Networks on Chip (NoCS), Pittsburg, PA, 2011.

[92] B. Y. Park, R. Zaouk, C. Wang, and M. J. Madou, "A Case for Fractal Electrodes in Electrical Applications," *J. Electrochem. Soc.*, vol. 154, pp. 1-5, 2007.

[93] Y. Sawada, A. Dougherty, and J. P. Gollub, "Dendritic and Fractal Patterns in Electrolytic Metal Deposits," *Phys. Rev. Lett.*, vol. 56, pp. 1260-1263, 1986.

[94] D. Grier, E. Ben-Jacob, R. Clarke, and L. M. Sander, "Morphology and Microstructure in Electrochemical Deposition of Zinc," *Phys. Rev. Lett.*, vol. 56, pp. 1264-1267, 1986.

[95] M. Matsushita, M. Sano, Y. Hayakawa, H. Honjo, and Y. Sawada, "Fractal Structures of Zinc Metal Leaves Grown by Electrodeposition," *Phys. Rev. Lett.*, vol. 53, pp. 286-289, 1984.

[96] A. Kuhn, F. Argoul, J. F. Muzy, and A. Arneodo, "Structural Analysis of Electroless Deposits in the Diffusion-Limited Regime," *Phys. Rev. Lett.*, vol. 73, pp. 2998-3001, 1994.

[97] S. Miyashita, Y. Saito, and M. Uwaha, "Fractal aggregation growth and the surrounding diffusion field," *J. Cryst. Growth*, vol. 283, pp. 533-539, 2005.

[98] D. Ridgeway, H. Levine, and T. Yuhai, "Front stability in mean-field models of diffusion-limited growth," *Phys. Rev. E*, vol. 53, pp. 861-870, 1996.

[99] W. W. Mullins and R. F. Sekerka, "Stability of a Planar Interface During Solidification of a Dilute Binary Allow," *J. Appl. Phys.*, vol. 35, pp. 444-451, 1964.

[100] O. Shochet and E. Ben-jacob, "Coexistence of Morphologies in Diffusive Patterning," *Phys. Rev. E*, vol. 48, pp. 4168-R4171, 1993.

[101] S. Gohil, R. Banarjee, S. Bose, and P. Ayyub, "Influence of synthesis conditions on the nanostructure of immiscible copper-silver alloy thin films," *Scripta Materialia*, vol. 58, pp. 842-845, 2008.

[102] R. J. Chimentao, I. Kirm, F. Medina, X. Rodriguez, Y. Cesteros, P. Salagre, and J. E. Sueiras, "Different morphologies of silver nanoparticles as catalysts for the selective oxidation of styrene in the gas phase," *Chem. Commun.*, pp. 846-847, 2004.

[103] H. You, F. Chen, S. Yang, Z. Yang, B. Ding, S. Liang, and X. Song, "Size Effect on Nanoparticle-Mediated Silver Crystal Growth," *Cryst. Growth Des.*, vol. 11, pp. 5449-5456, 2011.

[104] R. Liu and A. Sen, "Unified Synthetic Approach to Silver Nanostructures by Galvanic Displacement Reaction on Copper: From Nanobelts to Nanoshells," *Chem. Mater.*, vol. 24, pp. 48-54, 2012.

[105] T. Nagatani, "Hydrodynamic instability and the structural phase transition in diffusion-limited aggregation with drift," *Phys. Rev. A*, vol. 40, pp. 5351-5355, 1989.

[106] K. K. Caswell, C. M. Bender, and C. J. Murphy, "Seedless, Surfactantless Wet Chemical Synthesis of Silver Nanowires," *Nano Lett.*, vol. 3, pp. 667-669, 2003.

[107] C. L. Luo and K. C. Hwang, "Nitrate Ion Promoted Formation of Ag Nanowires in Polyol Processes: A New Nanowire Growth Mechanism," *Langmuir*, vol. 28, pp. 3722-3729, 2012.

[108] S. Strogatz, "Exploring complex networks," *Nature*, vol. 410, pp. 268-276, 2001.

[109] S. Dorogovtsev and J. Mendes, "Evolution of networks," *Advances in physics*, vol. 51, pp. 1079-1187, 2002.

[110] M. E. J. Newman, "The Structure and Function of Complex Networks," *SIAM Review*, vol. 45, pp. 167-256, 2003.

[111] M. Kaiser, "Brain architecture: a design for natural computation," *Phil. Trans. R. Soc. A*, vol. 365, pp. 3033-3045, 2007.

[112] J. J. Hopfield, "Neural networks and physical systems with emergent collective computational abilities," *PNAS*, vol. 79, pp. 2554-2558, 1982.

[113] D. L. Turcotte, "Self-organized criticality," *Rep. Prog. Phys.*, vol. 62, pp. 1377-1429, 1999.

[114] H. Sillin, E. Sandouk, A. Avizienis, M. Aono, A. Z. Stieg, and J. K. Gimzewski, "Benchtop Fabrication of Memristive Atomic Switch Networks," *J. N*, 2013.

[115] H. O. Sillin, R. Aguilera, H.-H. H. Shieh, A. V. Avizienis, M. Aono, A. Z. Stieg, and J. K. Gimzewski, "A theoretical and experimental study of neuromorphic atomic switch networks for reservoir computing," *Nanotechnology*, vol. In press, 2013.

[116] A. Z. Stieg, A. V. Avizienis, H. O. Sillin, R. Aguilera, H. H. Shieh, C. Martin-Olmos, E. Sandouk, M. Aono, and J. K. Gimzewski, "Self-organization and Emergence of Dynamical Structures in Neuromorphic Atomic Switch Networks," in *Memristor Networks*, vol. XII. Heidelberg: Springer, 2014, pp. 761.

[117] O. Sporns and C. J. Honey, "Small worlds inside big brains," *PNAS*, vol. 103, pp. 19219-19220, 2006.

[118] X. F. Wang and G. Chen, "Complex networks: small-world, scale-free and beyond," *Circuits and systems Magazine, IEEE*, vol. 3, pp. 6-20, 2003.

[119] E. Bullmore and O. Sporns, "The economy of brain network organization," *Nat. Rev. Neurosci.*, vol. 13, pp. 336-349, 2012.

[120] F. Aurenhammer, "Voronoi Diagrams - A Survey of a Fundamental Geometric Data Structure," *ACM Computing Surveys*, vol. 23, pp. 345-405, 1991.

[121] C. Martin-Olmos, L. G. Villanueva, P. D. van der Wal, A. Llobera, N. F. de Rooij, J. Brugger, and F. Perez-Murano, "Conductivity of SU-8 Thin Films through Atomic Force Microscopy Nano-Patterning," *Adv. Funct. Mater.*, vol. 22, pp. 1482-1488, 2012.

[122] C. Martin, A. Llobera, G. Villanueva, A. Voigt, G. Gruetzner, J. Brugger, and F. Perez-Murano, "Stress and aging minimization in photoplastic AFM probes," *Microelectronic Engineering*, vol. 86, pp. 1226-1229, 2009.

[123] A. V. Avizienis, C. Martin-Olmos, H. O. Sillin, M. Aono, J. K. Gimzewski, and A. Z. Stieg, "Morphological Transitions from Dendrites to Nanowires in the Electroless Deposition of Silver," *Crystal Growth and Design*, vol. 13, pp. 465-9, 2013.

[124] R. Waser and M. Aono, "Nanoionics-based resistive switching memories," *Nat. Mater.*, vol. 6, pp. 833-840, 2007.

[125] J. J. Yang, D. B. Strukov, and D. R. Stewart, "Memristive devices for computing," *Nature Nanotechnology*, vol. 8, pp. 13-24, 2013.

[126] M. Aono and T. Hasegawa, "The Atomic Switch," *Proc IEEE*, vol. 98, pp. 2228-2236, 2010.

[127] D. Garlaschelli, A. Capocci, and G. Caldarelli, "Self-organized network evolution coupled to extremal dynamics," *Nat. Phys.*, vol. 3, pp. 813-817, 2007.

[128] W. J. Freeman, R. Kozma, and P. J. Werbos, "Biocomplexity: adaptive behavior in complex stochastic dynamical systems," *BioSystems*, vol. 59, pp. 109-123, 2001.

[129] G. Werner, "Metastability, criticality, and phase transitions in brain and its models," *BioSystems*, vol. 90, pp. 496-508, 2007.

[130] S. Ullman, "Object recognition and segmentation by a fragment-based hierarchy," *Trends Cogn Sci*, vol. 11, pp. 58-64, 2007.

[131] A. Torralba, R. Fergus, and W. T. Freeman, "80 Million Tiny Images: A Large Data Set for Nonparametric Object and Scene Recognition," *IEEE Pattern Anal.*, vol. 30, pp. 1958-1970, 2008.

[132] S. Thorpe, D. Fize, and C. Marlot, "Speed of processing in the human visual system," *Nature*, vol. 381, pp. 520-2, 1996.

[133] T. Serre, L. Wolf, S. Bileschi, M. Riesenhuber, and T. Poggio, "Robust Object Recognition with Cortex-Like Mechanisms," *IEEE Pattern Anal.*, vol. 29, pp. 411-426, 2007.

[134] R. J. Douglas and K. A. C. Martin, "Recurrent neuronal circuits in the neocortex," *Curr Biol*, vol. 17, pp. R496-R500, 2007.

[135] M. Abeles, *Corticonics*, First ed. Cambridge: Cambridge University Press, 1991.

[136] E. Bullmore and O. Sporns, "Complex brain networks:graph theoretical analysis of structural and functional systems," *Nat. Rev.Neurosci.*, vol. 10, pp. 187-198, 2009.

[137] M. S. Goldman, "Memory without Feedback in a Neural Network," *Neuron*, vol. 61, pp. 621-634, 2009.

[138] P. Tiesinga, J.-M. Fellous, and T. J. Sejnowski, "Regulation of spike timing in visual cortical circuits," *Nat. Rev. Neurosci.*, vol. 9, pp. 97-107, 2008.

[139] D. V. Buonomano and W. Maass, "State-dependent computations: spatiotemporal processing in cortical networks," *Nat. Rev. Neurosci.*, vol. 10, pp. 113-125, 2009.

[140] D. O. Hebb, *The Organization of Behavior; A Neuropsychological Theory*. New York: John Wiley and Sons, Inc, 1949.

[141] C. Teuscher and A. A. Hansson, "Non-traditional irregular interconnects for massive scale SoC," *Circuits and Systems, 2008. ISCAS 2008. IEEE International Symposium on*, pp. 2785-2788, 2008.

[142] M. Lukosevicius and H. Jaeger, "Reservoir computing approaches to recurrent neural network training," *Comp. Sci. Rev.*, vol. 3, pp. 127-149, 2009.

[143] R. Segev and E. Ben-Jacob, "Self-wiring of neural networks," *Phys. Lett. A*, vol. 237, pp. 307-313, 1998.

[144] N. C. Rowland and D. Jaeger, "Responses to Tactile Stimulation in Deep Cerebellar Nucleus Neurons Result From Recurrent Activation in Multiple Pathways," *J. Neurophys.*, vol. 99, pp. 704-717, 2008.

[145] B. K. Murphy and K. D. Miller, "Balanced Amplification: A New Mechanism of Selective Amplification of Neural Activity Patterns," *Neuron*, vol. 61, pp. 635-648, 2009.

[146] A. Kumar, S. Rotter, and A. Aertsen, "Spiking activity propagation in neuronal networks: reconciling different perspectives on neural coding," *Nat. Rev. Neurosci.*, vol. 11, pp. 615-627, 2010.

[147] S. Ganguli, D. Huh, and H. Sompolinsky, "Memory traces in dynamical systems," *PNAS*, vol. 105, pp. 18970-18975, 2008.

[148] Z. Wang, T. Kadohira, T. Tada, and S. Watanabe, "Nonequilibrium Quantum Transport Properties of a Silver Atomic Switch," *Nano Lett.*, vol. 7, pp. 2688-2692, 2007.

[149] J. M. Tour, W. L. Van Zandt, C. P. Husband, S. M. Husband, L. S. Wilson, P. D. Franzon, and D. P. Nackashi, "Nanocell logic gates for molecular computing," *IEEE. T. Nanotechnol.*, vol. 1, pp. 100-109, 2002.

[150] G. Indiveri, B. Linares-Barranco, T. Hamilton, A. van Schaik, R. Etienne-Cummings, T. Delbruck, S. Liu, P. Dudek, P. Hafliger, S. Renaud, J. Schemmel, G. Cauwenberghs, J. Arthur, K. Hynna, F. Folowosele, S. Saighi, T. Serrano-Gotarredona, J. Wijekoon, Y. Wang, and K. Boahen, "Neuromorphic silicon circuits," *Front. Neurosci.*, vol. 5, pp. 1-23, 2011.

[151] V. P. Roychowdhury, D. B. Janes, S. Bandyopadhyay, and W. Xiaodong, "Collective computational activity in self-assembled arrays of quantum dots: a novel neuromorphic architecture for nanoelectronics," *IEEE T Electron Dev.*, vol. 43, pp. 1688-1699, 1996.

[152] F. Rosenblatt, "The Perceptron: a probabalistic model for information storage and organization in the brain," *Psych. Rev.*, vol. 65, pp. 386-408 1958.

[153] J. R. Searle, "Minds, brains, and programs," *Behav. Brain Sci.*, vol. 3, pp. 417-424, 1980.

[154] G. Z. Cohen, Y. V. Pershin, and M. Di Ventra, "Second and Higher harmonics generation with memristive systems," *Appl. Phys. Lett.*, vol. 100, pp. 133109, 2012.

[155] K. S. Ralls and R. A. Buhrman, "Microscopic study of 1/f noise in metal nanobridges," *Phys. Rev. B*, vol. 44, pp. 5800-5817, 1991.

[156] M. S. Keshner, "1/f noise," *Proc. IEEE*, vol. 70, pp. 212-218, 1982.

[157] D. Ielmini, F. Nardi, and C. Cagli, "Resistance-dependent amplitude of random telegraph-signal noise in resistive switching memories," *Appl. Phys. Lett.*, vol. 96, pp. 053503-053503-3, 2010.

[158] S. Coombes and Y. Timofeeva, "Sparks and waves in a stochastic fire-diffuse-fire model of Ca^{2+} release," *Phys. Rev. E*, vol. 68, pp. 021915, 2003.

[159] D. S. Bassett, N. F. Wymbs, M. A. Porter, P. J. Mucha, J. M. Carlson, and S. T. Grafton, "Dynamic reconfiguration of human brain networks during learning," *PNAS*, vol. 108, pp. 7641-7646, 2011.

[160] K.-i. Funahashi and Y. Nakamura, "Approximation of dynamical systems by continuous time recurrent neural networks," *Neural Networks*, vol. 6, pp. 801-806, 1993.

[161] M. Campbell, A. J. Hoane, and F. H. Hsu, "Deep Blue," *Artificial Intelligence*, vol. 134, pp. 57-83, 2002.

[162] R. Ananthanarayanan, S. K. Esser, H. D. Simon, and D. Modha, "Anatomy of a Cortical Simulator," presented at Proc. of the Conference on High Performance Computing Networking, Portland, OR, 2007.

[163] A. Hashni, H. Berry, O. Temam, and M. H. Lipasti, "Proceedings of the Workshop on New Directions in Computer Architecture held in Conjunction with 42nd Annual IEEE/ACM International Symposium on Microarchitecture (MICRO-42)," 2009.

[164] J. Backus, "Can Programming Be Liberated from the von Neumann Style? A Functional Style and its Algebra of Programs.," *Communications of the ACM*, vol. 21, pp. 613-641, 1978.

[165] A. M. Turing, *Collected Works of A. M. Turing: Mechanical Intelligence*. New York: Elsevier Science Publishing Company, Inc., 1948.

[166] D. Verstraeten, B. Schrauwen, M. D'Haene, and D. Stroobandt, "2007 Special Issue: an Experimental Unification of Reservoir Computing Methods," *Neural Networks*, vol. 20, pp. 391–403, 2007.

[167] N. Bertschinger and T. Natschlager, "Real-Time Computation at the Edge of Chaos in Recurrent Neural Networks," *Neural Computation*, vol. 16, pp. 1413-1436, 2004.

[168] W. Maass, T. Natschlager, and H. Markram, "Real-Time Computing Without Stable States: A New Framework for Neural Computation Based on Perturbations," *Neural Computation*, vol. 14, pp. 2531-2560, 2002.

[169] D. V. Buonomano and M. M. Merzenich, "Temporal information transformed into a spatial code by a neural network with realistic properties," *Science*, vol. 267, pp. 1028-1030, 1995.

[170] D. H. Ackley, G. E. Hinton, and T. J. Sejnowski, "A Learning Algorithm for Boltzmann Machines," *Cog. Sci.*, vol. 9, pp. 147-169, 1985.

[171] C. Joachim, J. K. Gimzewski, and A. Aviram, "Electronics using hybrid-molecular and mono-molecular devices," *Nature*, vol. 408, pp. 541-548, 2000.

[172] C. Haldeman and J. M. Beggs, "Critical Branching Captures Activity in Living Neural Networks and Maximizes the Number of Metastable States," *Phys. Rev. Lett.*, vol. 94, pp. 058101-1, 2005.

[173] D. Millman, S. Milhalas, A. Kirkwood, and E. Niebur, "Self-organized criticality occurs in non-conservative neuronal networks during 'up' states," *Nat. Phys.*, vol. 6, pp. 801-805, 2010.

[174] A. Levina, J. M. Herrmann, and T. Geisel, "Dynamical Synapses Causing Self-Organized Criticality in Neural Networks," *Nat. Phys.*, vol. 3, pp. 857–860, 2007.

[175] A. Hashmi, H. Berry, O. Temam, and M. H. Lipasti, "Proceedings of the Workshop on New Directions in Computer Architecture held in Conjunction with 42nd Annual IEEE/ACM International Symposium on Microarchitecture (MICRO-42)," 2009.

[176] C. G. Langton, "Computation at the edge of chaos: Phase transitions and emergent computation," *Physica D: Nonlinear Phenomena*, vol. 42, pp. 12-37, 1990.

[177] Y. Chen, Q. X. Lai, L. Zhang, Z. Y. Li, W. F. Stickle, R. S. Williams, and Y. Chen, "Ionic/Electronic Hybrid Materials Integrated in a Synaptic Transistor with Signal Processing and Learning Functions," *Adv. Mater.*, vol. 22, pp. 2448-2453, 2010.

[178] Y. V. Pershin and M. Di Ventra, "Experimental demonstration of associative memory with memristive neural networks.," *Neural networks : the official journal of the International Neural Network Society*, vol. 23, pp. 881-6, 2010.

[179] D. S. Bassett, A. Meyer-Lindenberg, S. Achard, T. Duke, and E. Bullmore, "Adaptive reconfiguration of fractal small-world human brain functional networks," *PNAS*, vol. 103, pp. 19518-19523, 2006.

[180] M. G. Kitzbichler, M. L. Smith, S. R. Christensen, and E. Bullmore, "Broadband Criticality of Human Brain Network Synchronization," *PLoS Comp. Biol.*, vol. 5, pp. e1000314, 2009.

[181] L. de Arcangelis and H. J. Herrmann, "Learning as a phenomenon occurring in a critical state.," *PNAS*, vol. 107, pp. 3977-81, 2010.

[182] *International Technology Roadmap for Semiconductors: Emerging Research Devices*. San Jose: Semiconductor Industry Association, 2011.

[183] M. Mahowald and R. Douglas, "A silicon neuron," *Nature*, vol. 354, pp. 515-518, 1991.

[184] D. S. Jeong, I. Kim, M. Ziegler, and H. Kohlstedt, "Towards artificial neurons and synapses: materials point of view," *RSC Advances*, vol. 3, pp. 3169-83, 2013.

[185] W. S. Zhao, G. Agnus, V. Derycke, A. Filoramo, J.-P. Bourgoin, and C. Gamrat, "Nanotube devices based crossbar architecture: toward neuromorphic computing," *Nanotechnology*, vol. 21, pp. 175202, 2010.

[186] T. Chang, S.-H. Jo, K.-H. Kim, P. Sheridan, S. Gaba, and W. Lu, "Synaptic behaviors and modeling of a metal oxide memristive device," *Appl. Phys. A*, vol. 102, pp. 857-863, 2011.

[187] K. Seo, I. Kim, S. Jung, M. Jo, S. Park, J. Park, J. Shin, K. Biju, J. Kong, K. Lee, B. Lee, and H. Hwang, "Analog memory and spike-timing-dependent plasticity characteristics of a nanoscale titanium oxide bilayer resistive switching device," *Nanotechnology*, vol. 22, pp. 1-5, 2011.

[188] J. M. Cruz-Albrecht, M. W. Yung, and N. Srinivasa, "Energy-Efficient Neuron, Synapse and STDP Integrated Circuits," *IEEE T. on Biomedical Circuits and Systems*, vol. 6, pp. 246-256, 2012.

[189] D. Kuzum, R. Jeyasingh, S. Yu, and H. Wong, "Low-Energy Robust Neuromorphic Computation Using Synaptic Devices," *IEEE T. Elect. Dev.*, vol. 59, pp. 3489-3494, 2012.

[190] W. L. Shew, H. Yang, S. Yu, R. Roy, and D. Plenz, " Information Capacity and Transmission Are Maximized in Balanced Cortical Networks with Neuronal Avalanches," *J. Neurosci.*, vol. 31, pp. 55–63, 2011.

[191] W. J. Freeman, B. C. Burke, and M. D. Holmes, "Aperiodic phase re-setting in scalp EEG of beta–gamma oscillations by state transitions at alpha–theta rates," *Hum. Brain Mapp.*, vol. 19, pp. 248-272, 2003.

[192] D. B. Chklovskii, B. W. Mel, and K. Svoboda, "Cortical rewiring and information storage," *Nature*, vol. 431, pp. 782-788, 2004.

[193] R. Kozma, M. Puljic, P. Balister, B. Bollobas, and W. J. Freeman, "Phase transitions in the neuropercolation model of neural populations with mixed local and non-local interactions," *Biol. Cybern.*, vol. 92, pp. 367-379, 2005.

[194] R. Yang, K. Terabe, G. Liu, T. Tsuruoka, T. Hasegawa, J. K. Gimzewski, and M. Aono, "On-demand nanodevice with electrical and neuromorphic multifunction realized by local ion migration," *ACS Nano*, vol. 6, pp. 9515-9521, 2012.

[195] J. J. Hopfield and D. W. Tank, " "Neural" computation of decision in optimization problems," *Biol. Cybern.*, vol. 52, pp. 141-152, 1985.

[196] H. Jaeger, *Tutorial on training recurrent neural networks, covering BPPT, RTRL, EKF and the" echo state network" approach*: GMD-Forschungszentrum Informationstechnik, 2002.

[197] H. Jaeger, "The "echo state" approach to analysing and training recurrent neural networks," presented at GMD Report 148

German National Research Center for Information Technology, 2001.

[198] B. Schrauwen, D. Verstraeten, and J. Van Campenhout, "An overview of reservoir computing: theory, applications and implementations," *Proceedings of the 15th European Symposium on Artificial Neural Networks.* , pp. 471-482, 2007.

[199] L. Büsing, B. Schrauwen, and R. Legenstein, "Connectivity, dynamics, and memory in reservoir computing with binary and analog neurons," *Neural computation*, vol. 22, pp. 1272-1311, 2010.

[200] C. Fernando and S. Sojakka, "Pattern recognition in a bucket," *Advances in Artificial Life*, vol. 2801, pp. 588-597, 2003.

[201] F. Schürmann, K. Meier, and J. Schemmel, "Edge of chaos computation in mixed-mode VLSI-a hard liquid," *Advances in Neural Information Processing Systems*, vol. 17, pp. 1201-1208, 2004.

[202] Y. Paquot, F. Duport, A. Smerieri, J. Dambre, B. Schrauwen, M. Haelterman, and S. Massar, "Optoelectronic Reservoir Computing," *Scientific Reports*, vol. 2, pp. 1-6, 2012.

[203] A. Lazar, G. Pipa, and J. Triesch, "SORN: a self-organizing recurrent neural network," *Front. Comput. Neurosci.*, vol. 3, 2009.

[204] K. Friston, "Hierarchical Models in the Brain," *PLoS Comp. Biol.*, vol. 4, pp. e1000211, 2008.

[205] D. Meunier, R. Lambiotte, A. Fornito, K. D. Ersche, and E. T. Bullmore, "Hierarchical modularity in human brain functional networks," *Frontiers in Neuroinformatics*, vol. 3, pp. 1-12, 2009.

[206] P. M. Gleiser and V. I. Spoormaker, "Modelling heirarchical structure in functional brain networks," *Philos. Transact. A Math Phys Eng Sci.*, vol. 368, pp. 5633-44, 2010.

[207] J. M. Cruz-Albrecht, T. Derosier, and N. Srinivasa, "A scalable neural chip with synaptic electronics using CMOS integrated memristors," *Nanotechnology*, vol. 24, pp. 384001, 2013.

[208] A. Stieg, A. Avizienis, H. Sillin, C. Martin-Olmos, M.-L. Lam, M. Aono, and J. Gimzewski, "Self-organized atomic switch networks," *Japanese Journal of Applied Physics*, vol. 53, pp. 1-6, 2014.

[209] T. Nirschl, J. B. Philipp, T. D. Happ, G. W. Burr, B. Rajendran, M.-H. Lee, A. Schrott, M. Yang, M. Breitwisch, C.-F. Chen, E. Joseph, M. Lamorey, R. Cheek, S.-H. Chen, S. Zaidi, S. Raoux, Y. C. Chen, Y. Zhu, R. Bergmann, H.-L. Lung, and C. Lam, "Strategies for 2 and 4-bit Multi-Level Phase-Change Memory," presented at Electron Devices Meeting, 2007. IEEE Intl., Washington, DC, 2007.

[210] W. Yi, F. Perner, M. S. Qureshi, H. Abdalla, M. D. Pickett, J. J. Yang, M. M. Zhang, G. Medeiros-Ribeiro, and R. S. Williams, "Feedback write scheme for memristive switching devices," *Appl. Phys. A*, vol. 102, pp. 973-982, 2011.

[211] F. Alibart, L. Gao, B. D. Hoskins, and D. B. Strukov, "High precision tuning of state for memristive devices by adaptable variation-tolerant algorithm.," *Nanotechnology*, vol. 23, pp. 075201, 2012.

[212] N. Papandreou, H. Pozidis, A. Pantazi, A. Sebastian, M. Breitwisch, C. Lam, and E. Eleftheriou, "Programming Algorithms for Multilevel Phase-Change Memory," presented at IEEE Intl. Symposium on Circuits and Systems, Rio de Janeiro, 2011.

[213] J. Misra and I. Saha, "Artificial neural networks in hardware: A survey of two decades of progress," *Neurocomputing*, vol. 74, pp. 239-255, 2010.

[214] E. Gale, B. de Lacy Costello, and A. Adamatzky, "Emergent spiking in non-ideal memristor networks," *Microelectronics Journal*, pp. 1-15, 2014.

[215] R. Budhathoki, M. P. Sah, S. P. Adhikari, H. Kim, and L. Chua, "Composite behavior of multiple memristor circuits," *Circuits and systems I*, vol. 60, 2013.

[216] Y. V. Pershin, V. a. Slipko, and M. Di Ventra, "Complex dynamics and scale invariance of one-dimensional memristor networks," *Phys. Rev. E*, vol. 87, pp. 022116, 2013.

[217] E. C. Demis, R. Aguilera, H. O. Sillin, K. Scharnhorst, and E. J. Sandouk, "Atomic Switch Networks: Nanoarchitectonic Design of a Complex System for Natural Computing," *Nanotechnology*, 2015.

[218] D. Fraiman, P. Balenzuela, J. Foss, and D. R. Chialvo, "Ising-like dynamics in large-scale functional brain networks," *Phys. Rev. E*, vol. 79, pp. 061922, 2009.

[219] M. Shein Idelson, E. Ben-Jacob, and Y. Hanein, "Innate synchronous oscillations in freely-organized small neuronal circuits," *PloS one*, vol. 5, pp. e14443, 2010.